จุฬาลงกรณ์มหาวิทยาลัย
ทุนวิจัย
กองทุนรัชดาภิเษกสมโภช

รายงานวิจัย

การเชื่อมโยงของปรากฏการณ์เอลนินโญ และลานินญาต่อสิ่งแวดล้อมและทรัพยากร ของอ่าวบ้านดอนและสุราษฎร์ธานี

สถาบันวิทยบริการ
จุฬาลงกรณ์มหาวิทยาลัย

โดย

อัปสรสุดา ศิริพงศ์

CU
วท 15
013479

ตุลาคม 2546

Chulalongkorn University
Rajdapisaksompoj
Research Fund

Final Research Report

The Linkage of El Niño and La Niña on the Environment and Resources at Ban Don Bay and Surat Thani

สถาบันวิทยบริการ
จุฬาลงกรณ์มหาวิทยาลัย

Absornsuda Siripong
อัปสรสุดา ศิริพงศ์
Marine Science Department,
Faculty of Science,
Chulalongkorn University,
Bangkok, Thailand.

August 2007

Acknowledgments

I am grateful for the support given by Chulalongkorn University's Ratchadaphisek Somphoj Research Fund which made this study possible. I am also grateful to Geo-Informatics Center, Chulalongkorn University for equipment, infrastructural and other support. The GISTDA provided the LANDSAT-5 (TM) and LANDSAT-7 (ETM+) images. I thank Dr. Supichai Tangjaitrong for his advice during the writing of this manuscript. Mr. Narumitr Sawangphol analysed the Landsat data. The data on Meteorology are provided and analysed by Phuwieng Prakhammintara. The Fisheries statistics are provided by Chat Mongkolprasit and Mrs. Noppakhun Somesin kindly sent me the river runoff. The MSL data is managed by Dr. Pramot Sojisuporn.

สถาบันวิทยบริการ
จุฬาลงกรณ์มหาวิทยาลัย

ชื่อโครงการวิจัย การเชื่อมโยงของปรากฏการณ์เอลนินโญและลานินญาต่อสิ่งแวดล้อม และ ทรัพยากรของอ่าวบ้านดอนและสุราษฎร์ธานี

ชื่อผู้วิจัย ร.ศ. อัปสรสุดา ศิริพงศ์

เดือนและปีที่ทำวิจัยเสร็จ ตุลาคม 2546

แก้ไขปรับปรุง สิงหาคม 2550

บทคัดย่อ

ข้อมูลจากดาวเทียมแลนด์แสท ใน 3 ช่วงเวลา คือ ปีต่างๆที่เกิดเอลนินโญ (1993,1994,1997และ 2002) ปีที่เกิดลานินญา(1988, ,1998, และ 2000) และปีปกติ (1989,1996,และ 1999)ได้ถูกนำมาทำการจำแนกการใช้ประโยชน์ที่ดินและด้วย NDVI แล้วนำมาเปรียบเทียบผลกระทบของปรากฏการณ์ทั้งสอง เทียบกับปีปกติ ที่มีต่อการเจริญเติบโตของพืชพันธุ์ เราพบว่า ในช่วงเอลนินโญ ซึ่งฝนแล้งกว่าปกติ อุณหภูมิอากาศร้อนกว่าปกติ การไหลของแม่น้ำตาปีน้อยกว่าปกติ NDVI แสดงถึงการเจริญเติบโตของพืชพันธุ์มีน้อยกว่าปีปกติ ส่วนในปีที่เกิดลานินญา ฝนตกมากกว่าปกติ อุณหภูมิอากาศเย็นกว่าปกติ การไหลของแม่น้ำตาปีมากกว่าปกติ ค่า NDVI แสดงถึงการเจริญเติบโตที่มากกว่าปีปกติ สำหรับปี 1998 ครึ่งปีแรกเกิดเอลนินโญ ส่วนครึ่งปีหลังเกิดลานินญา แต่ข้อมูลใช้วันที่ 27 เมษายน 1998 ซึ่งอยู่ในช่วงของการเกิดเอลนินโญ จึงได้รับผลกระทบของเอลนินโญ

ในด้านการประมงและการเพาะเลี้ยง ระหว่างปีที่เกิด เอลนินโญ ปริมาณและผลผลิตของการเพาะเลี้ยงกุ้งและปลาสูงกว่าค่าเฉลี่ย ระหว่างปี ลานินญา มันมีค่าต่ำกว่าเฉลี่ย พื้นที่ของบ่อเลี้ยงกุ้งเพิ่มตามการเพิ่มของจำนวนประชากร ประชากรของสุราษฎร์ธานีเพิ่มขึ้นทุกปี ระหว่างปีเอลนินโญ พื้นที่ของป่าธรรมชาติและป่าชายเลนลดลง ในขณะที่ปีลานินญา พื้นที่เพิ่มขึ้น

เอลนินโญเพิ่มความถี่ของพายุหมุนเขตร้อน ส่วนลานินญาแสดงถึงการเชื่อมโยงกับพายุน้อยกว่าเอลนินโญ การเชื่อมโยงของเอลนินโญต่อระดับน้ำทะเลปานกลางไม่ชัดเจน เนื่องจากข้อมูลที่ได้มีเพียงไม่กี่ปี อย่างไรก็ตาม ระหว่างปีลานินญา ระดับน้ำทะเลแสดงออกทั้งค่าบวกและลบอย่างละค่าของปีเอลนินโญและลานินญา แต่เราอาจสรุปได้ว่า เอลนินโญทำให้ระดับน้ำทะเลสูงกว่าค่าเฉลี่ย เอลนินโญยังทำให้น้ำท่าของแม่น้ำตาปีน้อยกว่าปกติ ในขณะที่ในปีลานินญา มันมีค่าสูงกว่าปกติ

Project Title The Linkage of El Niño and La Niña on the Environment and Resources at Ban Don Bay and Surat Thani.
Name of Investigator Assoc. Prof. Absornsuda Siripong
Year October 2003
Revised August 2007

Abstract

The Landsat data in 3 periods: which are during the El Nino years (1993, 1994, 1997 and 2002); the La Nina years (1988,1998 and 2000); and Normal year (1989, 1996 and 1999), are classified for landuse types and by NDVI (Normalised Difference Vegetation Index). We found that during El Nino years, the rainfall anomalies are minus (less than normal), the air temperature anomalies are plus (hotter than normal), Tapi river discharge anomalies are minus, and NDVI's are lower than normal (less growing vegetations). During La Nina years, the rainfall anomalies are plus (higher than normal), the air temperature anomalies are minus (colder than normal), the Tapi river discharge anomalies are plus, and NDVI's are higher than normal (much growing vegetations). In 1998, first half of the year was El Nino, and last half of the year was La Nina. However, we used the data on 27 April 1998, which is in the El Nino period, so it received the impact of El Nino.

For fisheries statistics at Surat Thani during El Niño years, the quantity of fish catch and the yields of aquacultures (shrimp and fish) were higher than average. During the La Niña years the same parameters were lower than average The areas of shrimp ponds have been increased with the increasing population. The population of Surat Thani has been increased every year. During the El Niño years, the areas of natural and mangroves were decreased, while during the La Niña years, the areas were increased.

El Niño caused higher frequency of tropical cyclone. La Niña also caused tropical cyclone but lesser than El Niño linkage. The linkage of ENSO on MSL is not very clear owing to the small quantity of data. During La Niña years, MSLs show plus and minus anomalies for one of each year. However, we may conclude that El Niño causes higher MSL than mean value. El Niño caused lower river runoff than normal. La Niña caused higher runoff than normal.

Contents

สถาบันวิทยบริการ
จุฬาลงกรณ์มหาวิทยาลัย

สถาบันวิทยบริการ
จุฬาลงกรณ์มหาวิทยาลัย

List of Tables

สถาบันวิทยบริการ
จุฬาลงกรณ์มหาวิทยาลัย

List of Figures

สถาบันวิทยบริการ
จุฬาลงกรณ์มหาวิทยาลัย

Chapter 1
Introduction

1.1 ENSO The El Niño/Southern Oscillation (ENSO) phenomenon is a natural part of the global climate system and results from large-scale interactions between the oceans and the atmosphere that occur chiefly across its core region in the tropical-subtropical Pacific to Indian Ocean basins. As a consequence, the most direct climatic shifts and environmental impacts are found over, and in countries bordering, the Indo-Pacific sector of the planet. The importance of this phenomenon in the global climate system can be quantified to the extent that it is the next feature that explains a large amount of climatic variability after the seasonal cycle and the monsoon system (Allan, 2000).

ENSO is an irregular/aperiodic phenomenon that tends to reoccur in the range of 2-7 years and is manifest by alternations between its two phases or extremes, often called El Niño and La Niña events. Once it begins, the "average" event tends to last for 18-24 months and shows characteristics of being locked to the seasonal cycle. However, seasonal persistence is weakest in the boreal spring (austral autumn), the time of the so-called predictability barrier or spring frailty, when new events are likely to develop and existing conditions collapse.

Although composites of climatic patterns and impacts during El Niño and La Niña events tend to be of the opposite sign to one another, individual El Niño or La Niña events are never exactly the same and can vary in magnitude, spatial extent, onset, duration, cessation, etc. In reality, the phenomenon encompasses events that cover a wide range, or "family," of types and signatures.

During El Niño events, warming of tropical regions of the Pacific and Indian Oceans leads to the displacement of major rainfall-producing systems from the continents to over the previously mentioned oceanic areas, causing massive redistributions of climatic regimes. The opposite tendency with regard to continental and oceanic rainfall regimes occurs during La Niña episodes. As tropical regions are linked to mid- to high latitudes in both hemispheres via teleconnection patterns, any major variations in mass, energy, and momentum resulting from a redistribution of equatorial rainfall regimes are communicated into more temperate regions of the globe. This effect has the potential to extend ENSO influence beyond the tropics and cause near-global modulations of climate.

Within the tropical-subtropical regime, the ENSO phenomenon has shown a degree of interaction with the Indo-Asian monsoon system. This relationship is described as being "selectively interactive," in that during the boreal autumn to winter (austral spring to summer) ENSO is strong and the

Indo-Asian monsoon is weak, with the opposite situation in the boreal spring to summer (austral autumn to winter). Thus the nature of the Indo-Asian monsoon can influence ENSO and vice versa at various times of the year. In fact, it has been suggested that the "predictability barrier" may be a consequence of the nature of ENSO links with the Indo-Asian monsoon system.

Other features of the global climate system may also be coupled to ENSO at various space and time frames. Much remains to be unraveled concerning possible relationships between the phenomenon and climatic features such as the North Atlantic Oscillation (NAO), the Arctic Oscillation (AO), the North Pacific Oscillation (NPO), and the Antarctic Circumpolar Wave (ACW). A better understanding of ENSO links to the above features may shed light on questions about the extension of the phenomenon into Europe, the nature of the Pacific North American (PNA) teleconnection, and the apparent propagational structure of ocean-atmosphere variables as ENSO phases evolve.

Further complicating this current understanding of ENSO, however, is growing evidence that the phenomenon is not spatially or temporally stable in the longer term and responds on a number of timescales. This response appears to result from the influence of a range of patterns of natural decadal- to secular-scale variability that modulate ENSO and, as a consequence, global climate.

From Climate Change 2001, Synthesis Report (IPCC, 2001), confidence in projections of changes in future frequency, amplitude and spatial pattern of El Niño events in the tropical Pacific is tempered by some shortcoming in how well El Niño is simulated in complex models. Current projections show little change or a small increase in amplitude for El Niño events over the next 100 years. Even with little or no change in El Niño amplitude, global warming is likely to lead to greater extense of drying and heavy rainfall and increase the risk of droughts and floods that occur with El Niño events in many different regions.

1.2 ENSO with Rainfall and Global Temperature During El Nino, rainfall and thunderstorm activity diminishes over the western equatorial Pacific, and increases over the eastern half of the tropical Pacific. This area of increased rainfall occurs where the exceptionally warm ocean waters have reached about 28°C or 82°F. This overall pattern of rainfall departures spans nearly one-half the distance around the globe, and is responsible for many of the global weather impacts caused by El Niño.

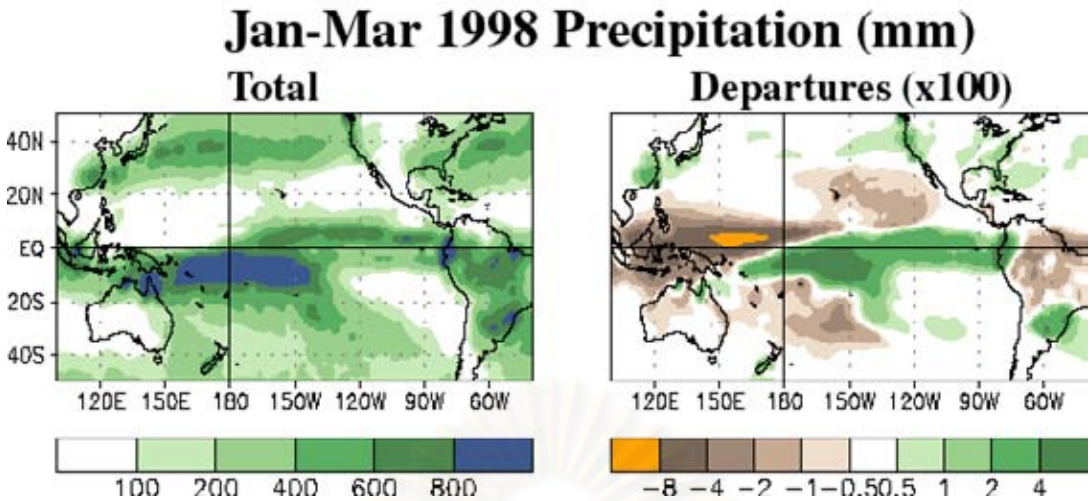

Fig.1. El Niño-related rainfall patterns over Tropical Pacific. (http://www.cpc.ncep.noaa.gov/products/analysis_monitoring/ensocycle/ensorain.html)

In the left-hand panel of Fig.1. the seasonal rainfall totals during the strong El Niño conditions of January-March 1998 are shown for over the Pacific Ocean, the United States, and South America. The heaviest rainfall [in millimeters (mm)] is shown by the darker green and blue colors, and lowest rainfall is shown by the lighter green colors. Since 25.4 mm is equal to one inch of rain, we see that the rainfall totals are more than 800 mm just south of the equator along the International Date Line (indicated by the 180 label), which is more than 31 ½ inches of rain. And nearly double the normal amount.

In the right-hand panel the January-March 1998 seasonal rainfall departures from average are shown. The areas with well above average rainfall are shown by darker green colors, and the areas with well below-average rainfall are shown by the darker brown and yellow colors. The rainfall departures are shown in units of 100 millimeters. We see that the seasonal rainfall totals were more than 400 mm above normal just south of the equator along the International Date Line (indicated by the 180 label), which is more than 15 ¾ inches above normal. Considerable rainfall also occurred farther north (near 40°N) over the central and eastern North Pacific, and across the western and southeastern United States. These areas lie along the main wintertime storm track, which brings above-average rainfall to the western and southeastern United States.

In contrast, the seasonal rainfall totals over the western Pacific just north of the equator were less than 100 mm during the season (see left-hand panel), which is more than 800 mm (or 31 1/2) inches) below normal. This extreme dryness led to a series of major uncontrolled wildfires in Indonesia.

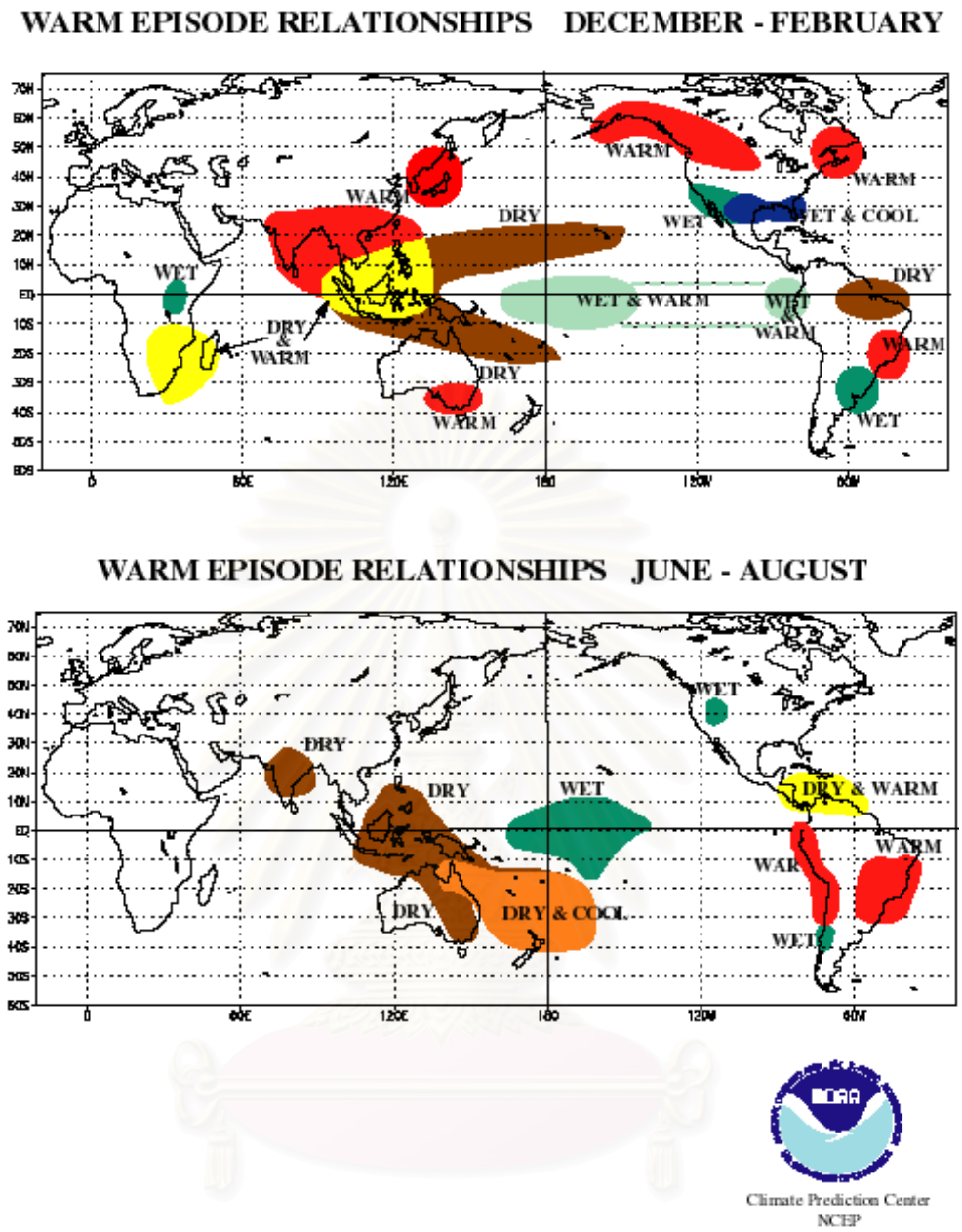

Fig.2. El Niño related global temperature and precipitation patterns(http://www.cpc.ncep.noaa.gov/products/analysis_monitoring/ensocycle/elninosfc.html).

In the Tropics, El Niño episodes are associated with increased rainfall across the east-central and eastern Pacific and with drier than normal conditions over northern Australia, Indonesia and the Philippines. Elsewhere, wetter than normal conditions tend to be observed 1) during December-February (DJF) along coastal Ecuador, northwestern Peru, southern Brazil, central Argentina, and equatorial eastern Africa, and 2) during June-August (JJA) in the intermountain regions of the United States and over central Chile. Drier than normal conditions generally observed over northern South America, Central America and southern Africa

during DJF, and over eastern Australia during JJA.

El Niño episodes also contribute to large-scale temperature departures throughout the world, with most of the affected regions experiencing abnormally warm conditions during December-February. Some of the most prominent temperature departures include: 1) warmer than normal conditions during December-February across southeastern Asia, southeastern Africa, Japan, southern Alaska and western/central Canada, southeastern Brazil and southeastern Australia; 2) warmer than normal conditions during June-August along the west coast of South America and across southeastern Brazil; and 3) cooler than normal conditions during December-February along the Gulf coast of the United States.

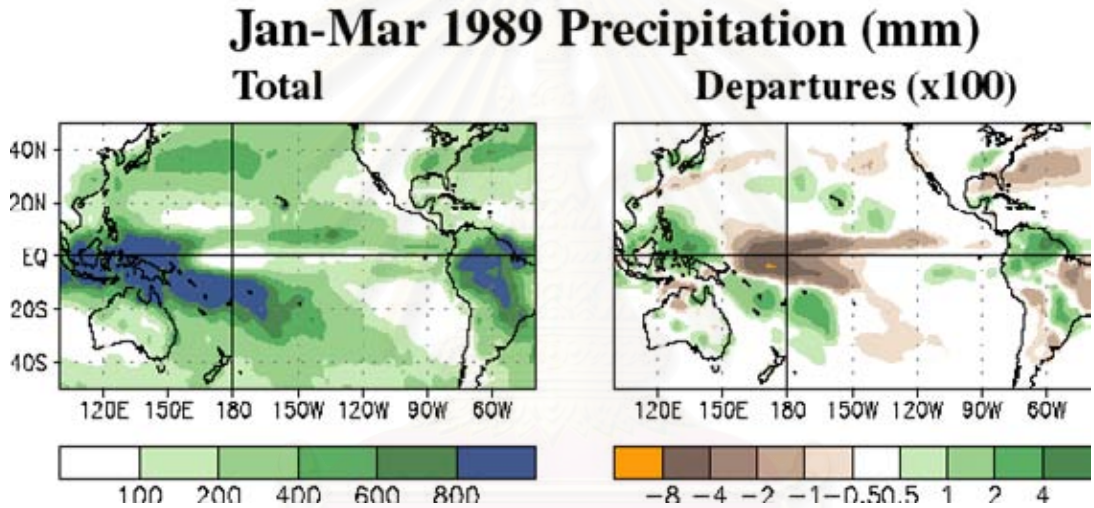

Fig.3. La Niña - related rainfall patterns over the Tropical Pacific (http://www.cpc.ncep.noaa.gov/products/analysis_monitoring/ensocycle/laninarain.html).

During La Niña, rainfall and thunderstorm activity diminishes over the central equatorial Pacific, and becomes confined to Indonesia and the western Pacific. The area experiencing a reduction in rainfall generally coincides quite well with the area of abnormally cold ocean surface temperatures. This overall pattern of rainfall departures spans nearly one-half the way around the globe, and is responsible for many of the global weather impacts caused by La Nina.

In the left-hand panel, Fig.3, you can see the seasonal rainfall totals over the Pacific Ocean, the United States, and South America during January-March 1989 when strong La Niña conditions were present. The heaviest rainfall is shown by the darker green and blue colors, and lowest rainfall is shown by the lighter green colors. The rainfall totals

are shown in units of millimeters (mm). Since 25.4 mm is equal to 1 inch of rain, we see that the rainfall totals are more than 800 mm over the western tropical Pacific and Indonesia, which is more than 31 ½ inches of rain.

In the right-hand panel you can see the January-March 1989 seasonal rainfall departures from average for strong La Nina conditions. The areas where the rainfall is well above average are shown by darker green colors, and the areas where the rainfall is most below average are shown by the darker brown and yellow colors. These rainfall departures are shown in units of 100 millimeters. We see that rainfall totals were more than 200-400 mm above normal over the western tropical Pacific and Indonesia during the season, which is roughly 8-16 inches above normal! We also see well below-average rainfall across the central tropical Pacific, where totals in some areas were more than 400 mm (15 ¾ inches) below normal.

During La Niña episodes rainfall is enhanced across the western equatorial Pacific, Indonesia and the Philippines and is nearly absent across the eastern equatorial Pacific. Elsewhere, wetter than normal conditions tend to be observed during December-February (DJF) over northern South America and southern Africa, and during June-August (JJA) over southeastern Australia. Drier than normal conditions are generally observed along coastal Ecuador, northwestern Peru and equatorial eastern Africa during DJF, and over southern Brazil and central Argentina during JJA.

La Niña episodes also contribute to large-scale temperature departures throughout the world, with most of the affected regions experiencing abnormally cool conditions. Some of the most prominent temperature departures include: 1) below-normal temperatures during December-February over southeastern Africa, Japan, southern Alaska and western/central Canada, and southeastern Brazil; 2) cooler than normal conditions during June-August across India and southeastern Asia, along the west coast of South America, across the Gulf of Guinea region, and across northern South America and portions of central America; and 3) warmer than normal conditions during December-February along the Gulf coast of the United States.

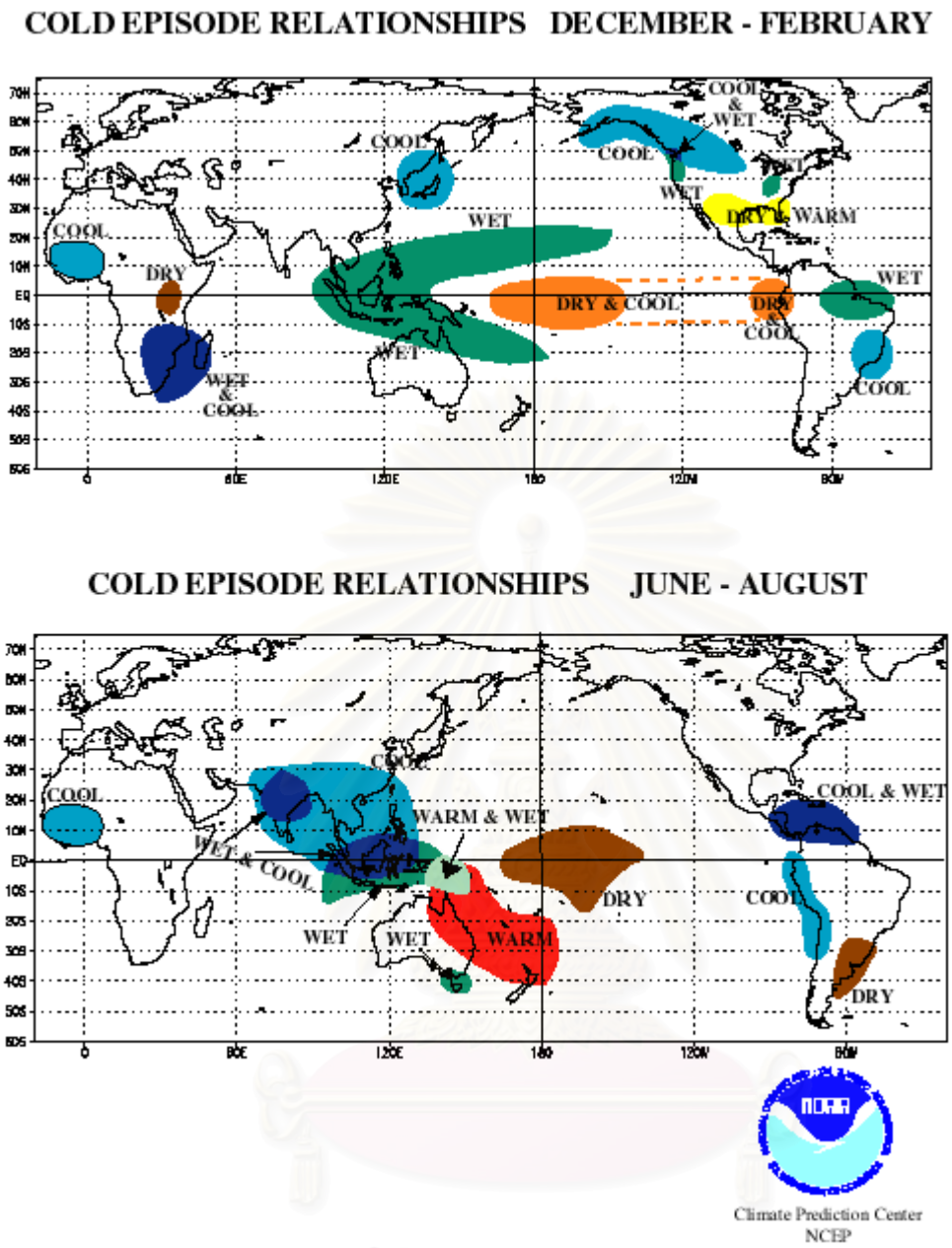

Fig.4. La Niña-related global surface temperature and precipitation patterns (http://www.cpc.ncep.noaa.gov/products/analysis_monitoring/ensocycle/lanainasfc.html)

During El Niño, the redistribution of heat resulting from the east-ward movement of warm Pacific water disrupts global weather patterns for several months, typically from about October through March. The most visible impacts of an ENSO result from the extreme patterns of precipitation that occur worldwide. Fig.5 summarizes the regions of flood and droughts and sea surface temperature anomalies during the El Niño.

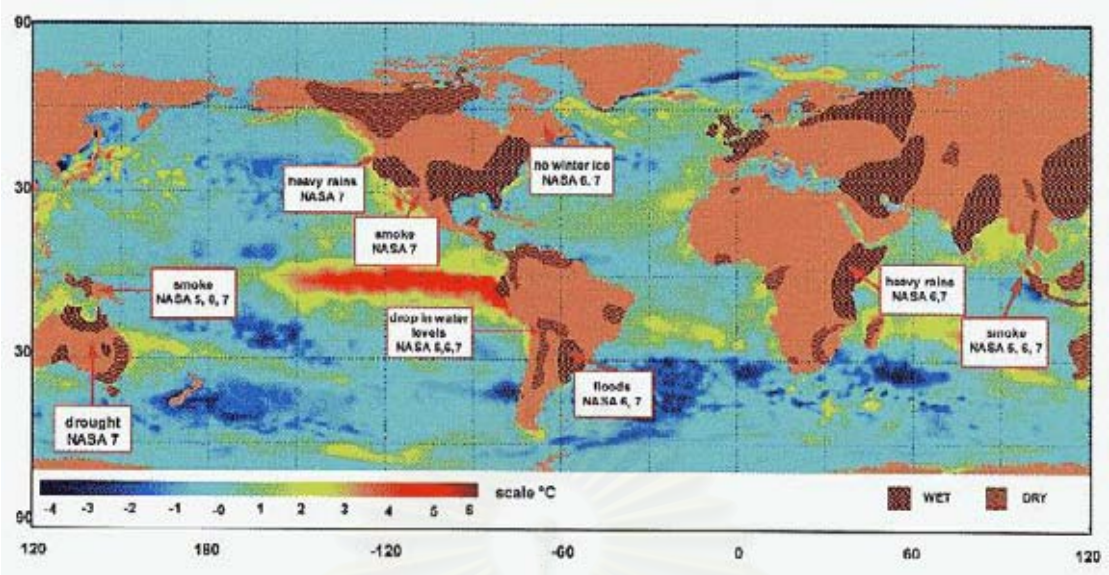

Fig.5. Sea surface temperature anomalies (SSTA) from early December 1997 with regions of flood and droughts from, November 1997 through January 1998 (Climatic Prediction Center in 1998).

For the first time, we had the opportunity to fully observe and document the global impact of an entire ENSO event as it developed and ebbed from satellite images and data. This continuum of imagery, which started in March 1996, included baseline pre- El Niño conditions (water levels and vegetation distribution) leading up to the record-breaking 1997-1998 El Niño. The data/images are rich visual portrayals of places that are classically effected by El Niño events. The 1996-1998 images have been correlated with imagery from the same regions taken during earlier missions to help define the spatial and temporal scale of well-known events such as droughts and fires in Australia, Indonesia and New Guinea; regional droughts and floods in various parts of South America; and the “greening” of the U.S. SW, coastal Peru and Ecuador, and northeastern Africa. Some of the best illustrations of the impact of the severe weather include water-level fluctuations (dropping water levels in lakes in Australia and the Andean Altiplano and drier than usual rivers in the Amazon, and rising water levels in the SW USA and NE African lakes) and large smoke palls from biomass burning in SE Asia, Australia, S. America and S. Africa. The images also help to explain the connection between the El Niño phenomenon and its major economic impacts, such as devastating droughts that result in large fires and crop failures, and equally devastating floods, which resulted in crop failures, landslides and the spread of waterborne diseases (Evans, et al., 2000).

Global Consequences of El Niño

http://www.pmel.noaa.gov/tao/elnino/impacts.html

The twists and turns in the ongoing dialogue between ocean and atmosphere in the Pacific can have a ripple effect on climatic conditions in far flung regions of the globe. This worldwide message is conveyed by shifts in tropical rainfall, which affect wind patterns over much of the globe. Imagine a rushing stream flowing over and around a series of large boulders. The boulders create a train of waves that extend downstream, with crests and troughs that show up in fixed positions. If one of the boulders were to shift, the shape of the wave train would also change and the crests and troughs might occur in different places (Fig.6).

Dense tropical rainclouds distort the air flow aloft (5-10 miles above sea level) much as rocks distort the flow of a stream, or islands distort the winds that blow over them, but on a horizontal scale of thousands of miles. The waves in the air flow, in turn, determine the positions of the monsoons, and the storm tracks and belts of strong winds aloft (commonly referred to as jet streams) which separate warm and cold regions at the Earth's surface. In El Niño years, when the rain area that is usually centered over Indonesia and the far western Pacific moves eastward into the central Pacific, as shown on Fig.7, the waves in the flow aloft are affected, causing unseasonable weather over many regions of the globe.

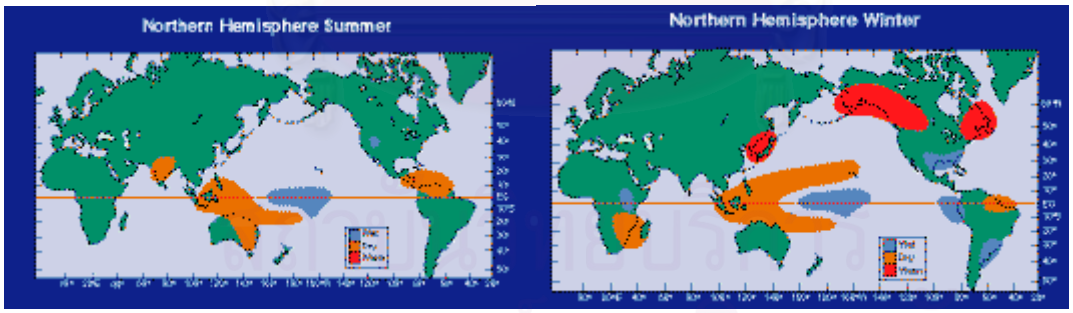

Fig.6 Precipitation anomalies during El Niño in (a) Summer and (b) Winter.

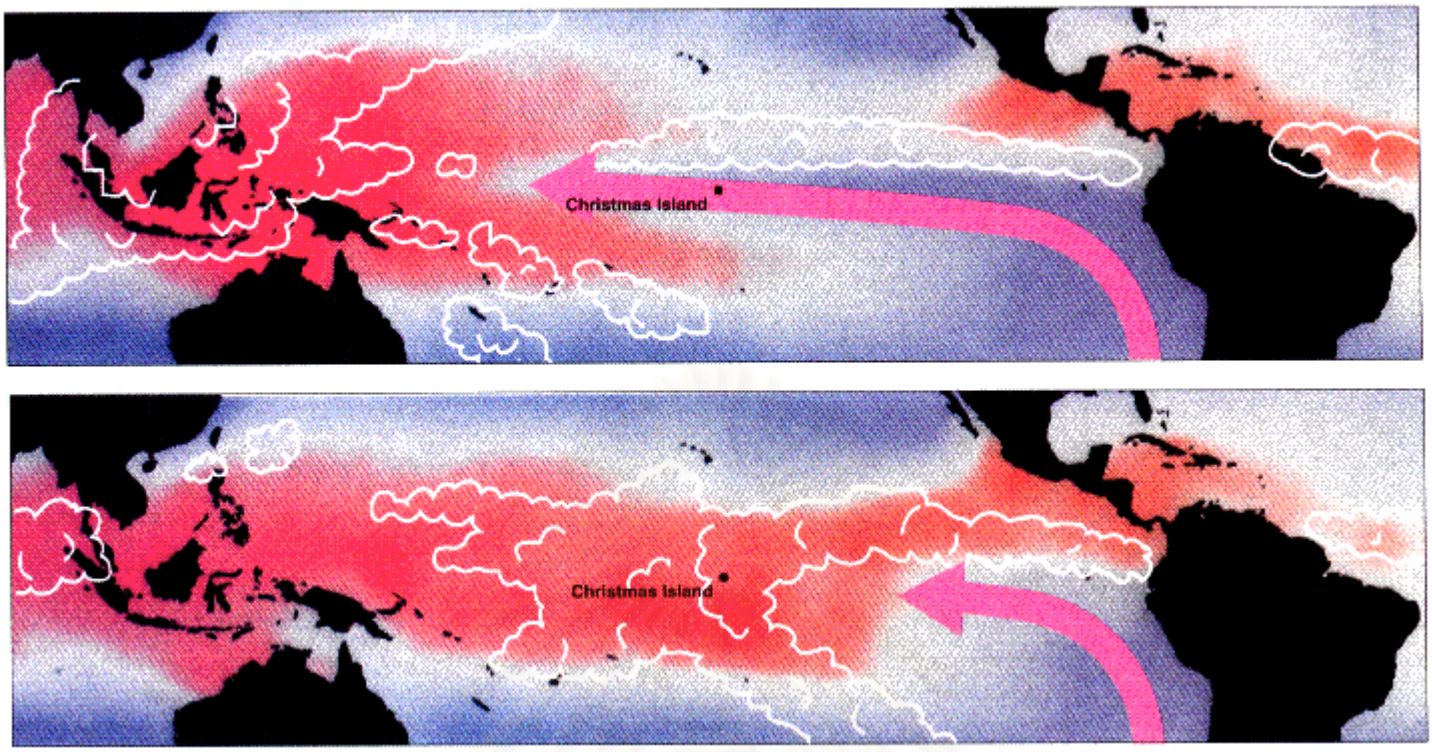

Fig. 7.Eastward movement of rain area during El Niño is indicated by clouds in the bottom figure below. The top figure is a non-El Niño pattern. http://www.pmel.noaa.gov/tao/elnino/report/figure17b.html

Above is a more detailed view of how El Niño rearranges the distribution of rainfall over the tropical Pacific. The colors indicate the distribution of sea-surface temperature for the cold month of November 1988 and the warm (El Niño) month of November 1982, the same months for which the pressure patterns are shown on Fig.8. Red indicates warmer water and blue indicates colder water. The regions of heavy rainfall as viewed by satellite are indicated by the clouds. The surface winds on the equator are indicated by the arrows. Note how tropical rainfall was suppressed wherever the sea-surface temperatures (SSTs) were lower than about 80^0 F (bluer colors).

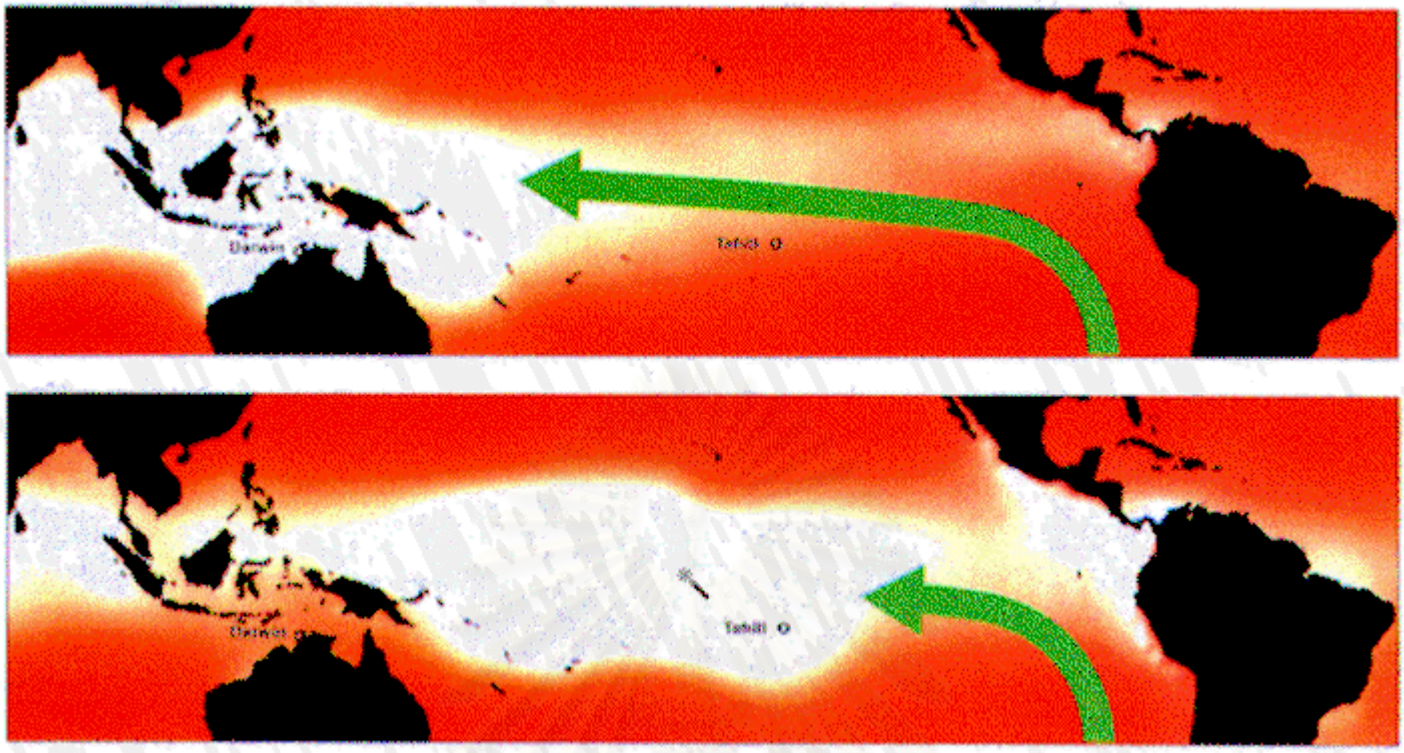

Fig.8. Pressure patterns

http://www.pmel.noaa.gov/tao/elnino/report/figure9.html

Sir Gilbert walker provided an important clue concerning El Nino when he discovered that air pressures at sea level in the South Pacific seesaw back and forth between two distinct patterns. In the "high index" phase of what Walker referred to as the "Southern Oscillation" (upper map for November 1988) pressure is higher (darker red) near and to the east of Tahiti than farther to the west near Darwin. The east-west pressure difference along the equator causes the surface air to flow westward, as indicated by the long arrow. When the atmosphere switches into the "low index" phase (lower map for November 1982) barometers rise in the west and fall in the east, signaling a reduction or even a reversal of the pressure difference between Darwin and Tahiti. The flattening of the seesaw causes the easterly surface winds to weaken and retreat eastward as shown. We now know that the "low index" phase is usually accompanied by El Nino conditions.

1.3 **ENSO and NDVI**

1.3.1 NDVI, MEI and ENSO relationships To test the idea that vegetation response could be used as a gauge of ongoing climate pulses to reveal links to ENSO, Taunton (2003) used NOAA/AVHRR bi-weekly composite images between 1989 and 2001. The study site is the SE corner of Arizona, with the San Pedro river running down the center.

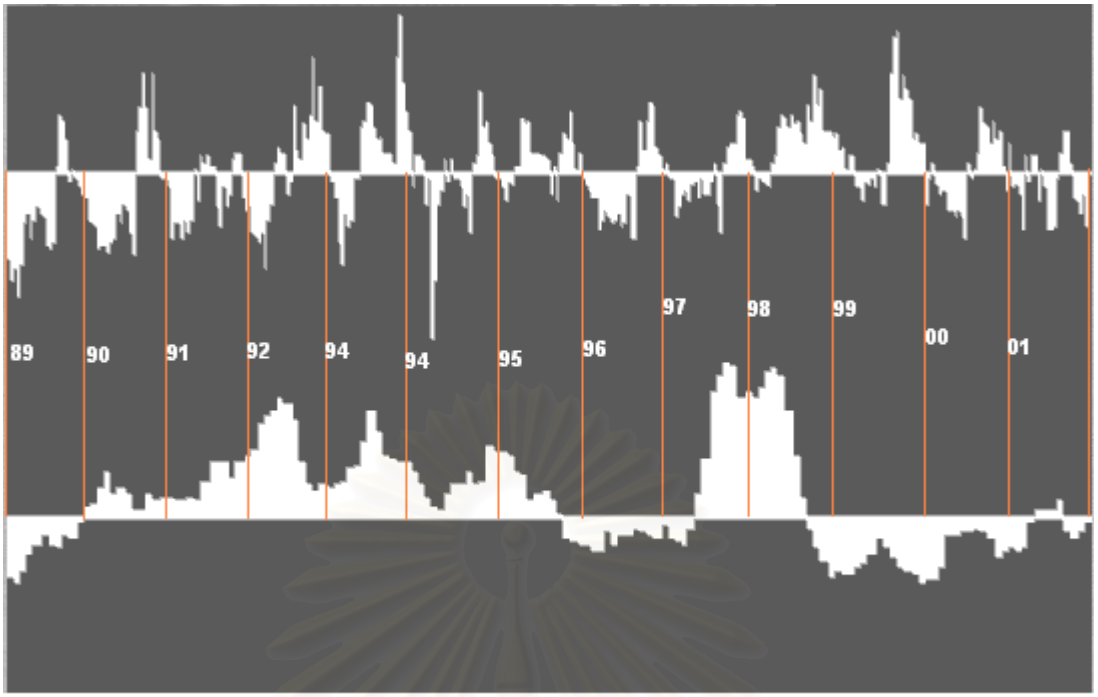

Fig.9. Comparing NDVI(above) and MEI (below) with ENSO signals in SE Arizona between 1989 and 2001.
(http://fp.arizona.edu/khirschboeck/climate/enso_rpt.htm)

These images were processed using Normalized Difference Vegetation Index (NDVI), which takes the ratio of the difference to the sum of the red and near infrared bands.

$$\textbf{NDVI} = \frac{\text{(Reflectance Channel 2 - Reflectance Channel 1)}}{\text{(Reflectance Channel 2 + Reflectance Channel 1)}}$$

The NDVI has been used as an indicator of vegetation health. The values plotted in Fig.9 are the z-scores of the sum of the NDVI values over the spatial extent (bi-weekly composite), over the temporal extent of the 13-year time frame (338 bi-weekly composites). The second plot is the MEI, which is an index that uses multiple measures to evaluate the strength of the ENSO signal.

The resulting two plots do not match cleanly, although after some study there are discernible temporal patterns. Years in the NDVI plots are often characterized by low or negative NDVI for the first 3/4ths of the year and then a burst of positive values. This pattern seems to very likely be reporting the annual dry spring early summer followed by heavy monsoon rains that characterize this region. The dry months would be characterized

by low or negative NDVI while just following the monsoon, a burst of NDVI can be expected. The riparian areas and other regions possibly associated with agriculture that darken (get bluer) and brighten (get greener) across the seasons, annually, like clockwise.

The MEI (Multivariate ENSO Index, http://www.cdc.noaa.gov/~kew/MEI/) seem to have the effect of complicating the dry spring early summer pattern with unexpected positive NDVI values. The large NDVI pulses along the top axis follow slightly to the right the large pulses in MEI that crop up along the lower axis as in, for example, the NDVI pulse following the mountainous cluster of positive MEI values centered on the year 1998.

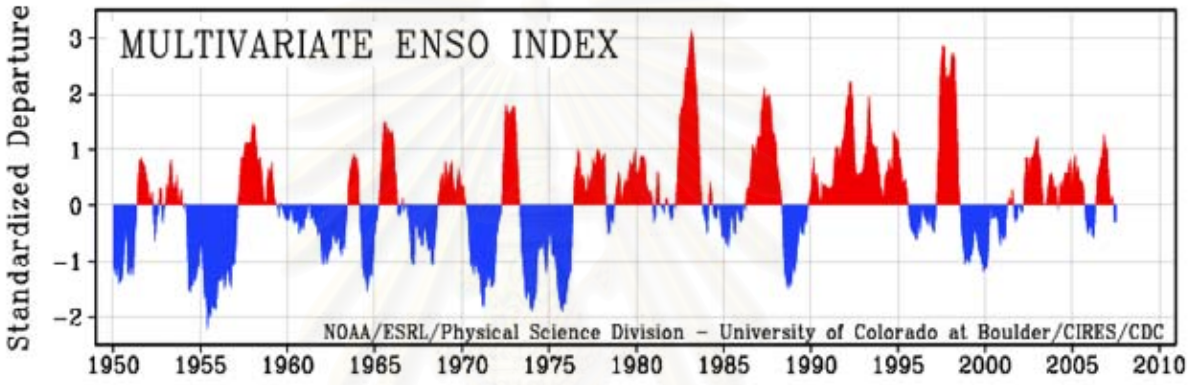

Fig. 10. MEI
http://www.cdc.noaa.gov/ENSO/enso.mei_index.html

Here we attempt to monitor ENSO by basing the Multivariate ENSO Index (MEI) on the six main observed variables over the tropical Pacific. These six variables are: sea-level pressure (P), zonal (U) and meridional (V) components of the surface wind, sea surface temperature (S), surface air temperature (A), and total cloudiness fraction of the sky (C). These observations have been collected and published in COADS for many years. The MEI is computed separately for each of twelve sliding bi-monthly seasons (Dec/Jan, Jan/Feb,..., Nov/Dec). After spatially filtering the individual fields into clusters (Wolter, 1987), the MEI is calculated as the first unrotated Principal Component (PC) of all six observed fields combined. This is accomplished by normalizing the total variance of each field first, and then performing the extraction of the first PC on the co-variance matrix of the combined fields (Wolter and Timlin, 1993). In order to keep the MEI comparable, all seasonal values are standardized with respect to each season and to the 1950-93 reference period. The MEI is extended during the first week of the following month based on near-real time marine ship and buoy observations (courtesy of R.W. Reynolds at NCEP) summarized into

COADS-compatible 2-degree monthly statistics at CDC. Caution should be exercised when interpreting the MEI on a month-to-month basis, since the input data for updates are not as reliable as COADS, and the MEI has been developed mainly for research purposes. Negative values of the MEI represent the cold ENSO phase (La Niña), while positive MEI values represent the warm ENSO phase (El Niño).

สถาบันวิทยบริการ
จุฬาลงกรณ์มหาวิทยาลัย

Table 1. Bimonthly MEI values (in 1/1000 of standard deviations), starting with Dec1949/Jan1950, thru last month. Missing values are left blank. Note that values can still change with each monthly update, even though such changes are typically smaller than +/-0.1. All values are normalized for each bimonthly season so that the 44 values from 1950 to 1993 have an average of zero and a standard deviation of "1".

http://www.cdc.noaa.gov/people/klaus.wolter/MEI/table.html

YEAR	DECJAN	JANFEB	FEBMAR	MARAPR	APRMAY	MAYJUN	JUNJUL	JULAUG	AUGSEP	SEPOCT	OCTNOV	NOCDEC
1950	-1.051	-1.145	-1.269	-1.039	-1.397	-1.373	-1.303	-1.057	-.644	-.411	-1.152	-1.248
1951	-1.055	-1.194	-1.237	-.521	-.233	.385	.769	.876	.807	.744	.724	.454
1952	.404	.151	.115	.262	-.294	-.668	-.191	-.153	.348	.333	-.312	-.104
1953	.038	.408	.249	.697	.829	.231	.433	.251	.547	.112	.083	.314
1954	-.023	-.05	.069	-.667	-1.483	-1.544	-1.406	-1.433	-1.19	-1.365	-1.1	-1.124
1955	-.763	-.664	-1.217	-1.652	-1.643	-2.247	-1.888	-1.986	-1.788	-1.776	-1.867	-1.876
1956	-1.433	-1.315	-1.383	-1.157	-1.35	-1.503	-1.182	-1.118	-1.345	-1.468	-1.087	-1.033
1957	-.981	-.419	.088	.386	.893	.761	.978	1.115	1.147	1.097	1.111	1.184
1958	1.474	1.454	1.288	.874	.754	.884	.679	.382	.077	.098	.428	.698
1959	.535	.79	.469	.133	.028	-.012	-.209	.071	-.015	-.1	-.188	-.25
1960	-.294	-.24	-.085	-.033	-.351	-.267	-.311	-.246	-.511	-.385	-.344	-.438
1961	-.215	-.235	-.014	.042	-.278	-.138	-.262	-.353	-.351	-.565	-.399	-.652
1962	-1.093	-.998	-.801	-1.056	-.928	-.812	-.801	-.55	-.517	-.667	-.667	-.517
1963	-.751	-.913	-.687	-.788	-.414	-.074	.379	.656	.752	.869	.938	.711
1964	.861	.5	-.334	-.672	-1.275	-1.124	-1.368	-1.539	-1.301	-1.2	-1.256	-.943
1965	-.548	-.331	-.238	.104	.541	.939	1.429	1.514	1.447	1.226	1.378	1.267
1966	1.334	1.189	.642	.438	-.145	-.178	-.118	.157	-.121	-.053	.024	-.171
1967	-.459	-.881	-1.053	-1.057	-.424	-.289	-.615	-.504	-.698	-.73	-.43	-.388
1968	-.65	-.842	-.717	-1.02	-1.07	-.769	-.495	-.15	.186	.423	.575	.349
1969	.661	.802	.391	.585	.731	.799	.419	.277	.222	.508	.672	.367
1970	.357	.364	.16	-.041	-.165	-.677	-1.1	-1.005	-1.237	-1.092	-1.076	-1.22
1971	-1.184	-1.5	-1.77	-1.815	-1.46	-1.465	-1.232	-1.26	-1.463	-1.443	-1.39	-1.03
1972	-.559	-.373	-.215	-.144	.545	1.117	1.814	1.764	1.582	1.637	1.723	1.766
1973	1.775	1.554	.888	.539	-.13	-.765	-1.076	-1.356	-1.693	-1.66	-1.478	-1.829
1974	-1.904	-1.786	-1.68	-1.578	-.999	-.652	-.784	-.703	-.622	-1.001	-1.209	-.88
1975	-.501	-.546	-.858	-.905	-.867	-1.179	-1.504	-1.678	-1.812	-1.924	-1.748	-1.778

1976	-1.598	-1.356	-1.238	-1.165	-.48	.278	.621	.724	1.024	.91	.443	.556
1977	.492	.285	.197	.56	.377	.489	.847	.698	.776	.986	.989	.894
1978	.773	.882	.944	.175	-.355	-.542	-.365	-.217	-.351	-.009	.231	.414
1979	.621	.396	.041	.322	.431	.467	.36	.622	.807	.698	.749	1.033
1980	.646	.52	.671	.869	.899	.878	.786	.369	.265	.2	.25	.096
1981	-.315	-.225	.412	.631	.063	-.03	-.045	-.152	.127	.119	-.005	-.143
1982	-.287	-.199	.07	-.094	.442	.99	1.6	1.749	1.794	2.031	2.458	2.444
1983	2.732	2.975	3.162	3.035	2.582	2.237	1.788	1.232	.527	.068	-.128	-.178
1984	-.355	-.507	.208	.461	.09	-.129	-.2	-.233	-.098	.021	-.307	-.578
1985	-.557	-.598	-.709	-.464	-.751	-.14	-.205	-.422	-.542	-.127	-.05	-.272
1986	-.304	-.242	.037	-.1	.311	.31	.384	.709	1.089	1.009	.855	1.187
1987	1.255	1.191	1.685	1.862	2.125	1.931	1.824	2.018	1.905	1.653	1.236	1.284
1988	1.128	.694	.504	.343	.06	-.647	-1.213	-1.307	-1.516	-1.365	-1.48	-1.329
1989	-1.093	-1.197	-.964	-.689	-.51	-.317	-.489	-.558	-.268	-.347	-.07	.156
1990	.223	.557	.868	.413	.549	.445	.094	.1	.421	.313	.358	.347
1991	.31	.275	.349	.322	.682	1.038	1.022	1.041	.748	1.003	1.165	1.249
1992	1.716	1.845	2.005	2.247	2.106	1.799	1.02	.596	.48	.586	.518	.617
1993	.637	.922	.959	1.357	1.966	1.561	1.117	1.056	1.006	1.045	.834	.593
1994	.388	.197	.139	.433	.608	.627	.814	.61	.658	1.324	1.22	1.176
1995	1.169	.862	.78	.319	.433	.468	.272	.055	-.341	-.428	-.481	-.495
1996	-.608	-.63	-.261	-.48	-.283	-.009	-.175	-.262	-.309	-.374	-.114	-.357
1997	-.427	-.496	-.166	.451	1.093	2.315	2.633	2.869	2.84	2.206	2.334	2.22
1998	2.421	2.704	2.74	2.639	1.979	1.146	.343	-.172	-.551	-.797	-1.078	-.943
1999	-1.007	-1.017	-.871	-.835	-.667	-.383	-.532	-.735	-.877	-.931	-1.048	-1.206
2000	-1.111	-1.127	-.902	-.298	-.008	-.264	-.226	-.165	-.232	-.336	-.726	-.622
2001	-.515	-.63	-.53	-.054	.127	.011	.133	.274	-.222	-.337	-.25	-.034
2002	-.012	-.146	-.068	.421	.855	.844	.544	.843	.787	.901	.983	1.151
2003	1.235	.91	.813	.387	.039	-.004	.039	.276	.469	.569	.548	.359
2004	.319	.374	-.082	.271	.442	.268	.457	.611	.58	.551	.831	.687
2005	.3	.742	.93	.556	.712	.464	.423	.443	.227	-.234	-.371	-.521
2006	-.362	-.402	-.553	-.593	-.011	.47	.639	.75	.892	1.027	1.293	.985
2007	1.037	.537	.133	.088	.179	-.307	-.291					

สถาบันวิทยบริการ
จุฬาลงกรณ์มหาวิทยาลัย

There are multiple reasons for the raggedness and fragmentedness in the NDVI signal. One reason is that the annual rhythms of higher frequency combine with and thus obscure the lower frequency ENSO rhythm. Another factor is that this region is populated by a large variety of plant species that demonstrate multiple survival strategies in this environment where moisture is the key limiting factor. Some plants may respond immediately to moisture such as grasses, while others may respond with longer lag times, such as Ponderosa Pine. Another complication is the variation in elevations across the region, producing multiple micro climates. Finally, the AVHRR data is very noisy.

1.3.2 NDVI-precipitation relationships Relation between the mean normalized difference vegetation index and mean annual precipitation for 1980-1994 for reporting stations in sub-Saharan Africa for 0-1200 mm/yr precipitation averaged over years. Every datum corresponds to a specific meteorological station location and the associated satellite data for an area of ~520 km^2 centered on the meteorological station in question (from Tucker and Nicholson, 1999). Similar highly correlated NDVI-precipitation relationships exist regionally within Africa although the functional form(s) may be slightly different. Precipitation and green vegetation dynamics are a major determinant of life cycles of animals and insects in semi-arid lands of Africa. Various research studies indicate a close relationship between the seasonal trace of green vegetation development (NDVI) with breeding and upsurge patterns of particular insect vectors including locusts and mosquitoes (Fig.10). Widespread heavy rains result in vegetation development, and provide a good environment for immature and adult mosquito vector populations to increase, significantly elevating the risk of RVF outbreaks. The life cycle of mosquitoes that carry the RVF virus is coupled to such rainfall events, with thousands of mosquitoes emerging from dambo environments following above normal rainfall. The close coupling between ENSO, rainfall, NDVI response patterns and mosquito life cycle dynamics, provides a basis for using NDVI time series measurements to map areas at risk from RVF.

สถาบันวิทยบริการ
จุฬาลงกรณ์มหาวิทยาลัย

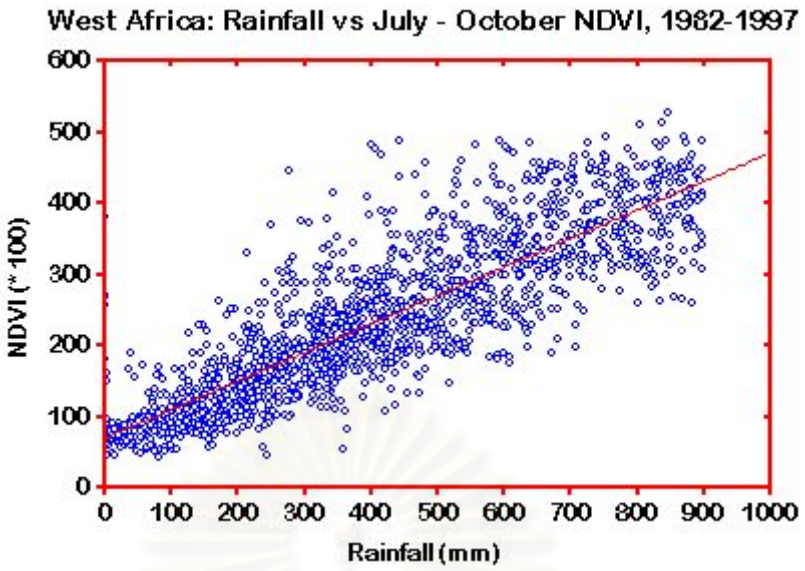

Fig.11. West African rainfall vs July-October NDVI, 1982 – 1997.

(http://www.geis.ha.osd.mil/GEIS/SurveillanceActivities/RVFWeb/infopages/climate.htm)

1.3.3 NDVI-ENSO linkages While SST, OLR (Outgoing Longwave Radiation) and pressure differences provide valuable information concerning the occurrence of ENSO, they do not provide adequate information about the geographic patterns of its effects over the land surface. NDVI from color sensor satellite such as NOAA is a means of mapping the spatial characteristics of ENSO events. Land surface reflectances in the visible and infrared portion of the spectrum as measured by AVHRR on NOAA satellites can be mathematically manipulated to form NDVI.

Because of the differential response of vegetation in the visible red (low reflectance) and near infrared (high reflectance), the derived index is used in general as an indicator of vegetation greenness and has been demonstrated to berelated to a number of climate-related vegetation characteristics such as Leaf Area index (LAI), Photosynthetically Active Radiation (PAR), biomass amongst others (Tucker, 1979; Justice et al, 1986; Cihlar et al, 1991). Taken in the form of time series measurements, NDVI is an effective proxy indicator of the time and space variability of rainfall over semi-arid areas (Nicholson et al, 1990; Tucker et al, 1991). More recently, it has been shown that NDVI time series measurements can be decomposed to yield time-space patterns of seasonal, annual and interannual variability associated with the ENSO phenomenon over Africa (Eastman and Fulk, 1991, Anyamba and Eastman, 1996, Anyamba, 1996). Similar ENSO related patterns have been identified in other tropical locations including Australia, and South America (Myneni et al, 1996). Furthermore, analysis of monthly departure patterns in NDVI during the last

four ENSO warm events illustrates that these events can have quite different and dramatic spatial manifestations over the Southern Africa region (Eastman et al, 1996). NDVI data therefore provide an appropriate base for understanding the dynamics of ENSO teleconnection patterns over the land surface, especially in areas with inadequate spatial coverage by conventional climate measurements.

1.4 **ENSO and Tropical Cyclone** Since ENSO produces large, wide-scale changes in tropical circulation, the tropical cyclones are strongly altered by ENSO. However, these changes are not uniform throughout the global tropics. In some regions, an El Niño would bring increases in tropical cyclone formation (e.g., the South Pacific and the North Pacific between 140^0W to 160^0E) while others would see decreases (e.g., the North Atlantic, the Northwest Pacific west of 160^0E, and the Australian region). La Niña typically brings opposite conditions. These alterations in tropical cyclone activity are due to a variety of ENSO effects: modulation of the intensity of the local monsoon trough, repositioning of the location of the monsoon trough, and alteration of the tropospheric vertical shear. Thus, based on the global nature of ENSO alone, assumptions of independence between different tropical cyclone basins would be incorrect.

In addition to ENSO, three basins (the Atlantic, SW Indian and NW Pacific) show systematic alterations of tropical cyclone frequency by the stratospheric Quasi-Biennial Oscillation (QBO). This intuitively is unexpected given that tropical cyclones are primarily a tropospheric phenomenon, but it may be due to alterations in the static stability and dynamics near the tropopause. When match the QBO phases, it appears unlikely that the association is purely a chance correlation.

Interannual tropical cyclone variations have also been linked to more localized, basin-specific features such as sea surface temperatures (SSTs), monsoon strength and rainfall, sea level pressures (SLPs), and tropospheric vertical changes. These regional factors can be as large as the forcing due to ENSO, though most are not. Together with ENSO and the QBO, these factors produce changes in the frequency, intensity, formation region and track of tropical cyclones in all basins. However, understanding how tropical cyclone variability relates to the surrounding environmental conditions is hampered because we have only a few decades worth of reliable tropical cyclone records (Landsea, 2000).

What is the relationship between hurricanes and El Niño?

http://www.pmel.noaa.gov/tao/elnino/faq.html#hurricanes

In general, warm ENSO episodes are characterized by an increased number of tropical storms and hurricanes in the eastern Pacific and a decrease in the Gulf of Mexico and the Caribbean Sea. A figure that shows tropical storm locations is available from the University of Washington. Tropical weather products pages are available on the Web from the University of Michigan and from the University of Hawaii. A Tropical Storm and Hurricane Watch Information web page is maintained by the Federal Emergency Management Agency (FEMA).

Pacific Ocean

El Niñotends to increase the numbers of tropical storms in the Pacific Ocean. For details, see the information about the location and numbers of tropical cyclones in the Eastern Pacific for El Niño and non-El Niño years from the Pacific ENSO Applications Center in Hawaii.

1.5 **SOI** The Southern Oscillation Index (SOI) is the most commonly used index for the ENSO phenomena (Glantz, 1991; Chagas and Puppi, 1986) and extends the history of ENSO back to the late 19th century. This index compares atmospheric pressure in Tahiti to that of Darwin, Australia, and is expressed as a standardized deviation from the norm. Strong negative anomalies are associated with an "El Niño" event (Cane, 1986; Rasmusson, 1991) and strong positive departures of the SOI are associated with "La Niña" conditions. Warm ENSO events are exemplified by above normal Sea Surface Temperatures (SSTs) in the Eastern Pacific (EP) and sometimes above normal SSTs in the Western Indian Ocean (WIO).Warm ENSOevents are known to increase precipitation in some regions of East Africa and result in droughts in southern Africa (Glantz, 1991; Ropelewski and Halpert, 1987). Such global scale precipitation anomalies can be inferred from Outgoing Longwave Radiation (OLR) data for example as shown in the OLR anomalies for December 1997.

สถาบันวิทยบริการ
จุฬาลงกรณ์มหาวิทยาลัย

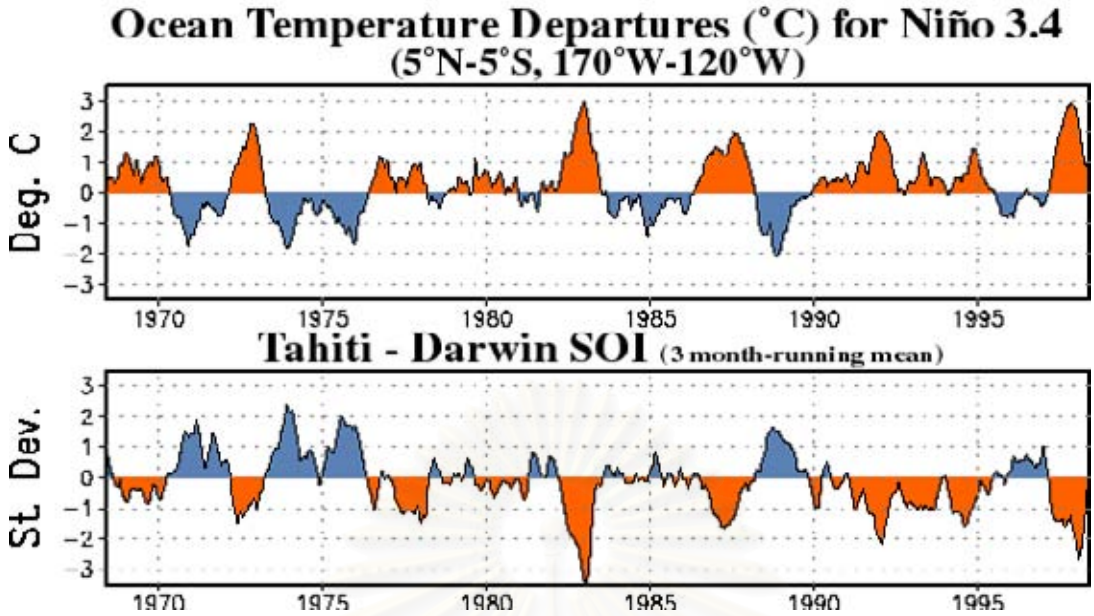

Fig.12. Ocean temperature departure for Niño 3,4 and SOI.

The Southern Oscillation Index (SOI) is one measure of the large-scale fluctuations in air pressure occurring between the western and eastern tropical Pacific (i.e., the state of the Southern Oscillation) during El Niño and La Niña episodes. Traditionally, this index has been calculated based on the differences in air pressure anomaly between Tahiti and Darwin, Australia. In general, smoothed time series of the SOI correspond very well with changes in ocean temperatures across the eastern tropical Pacific. The negative phase of the SOI represents below-normal air pressure at Tahiti and above-normal air pressure at Darwin. Prolonged periods of negative SOI values coincide with abnormally warm ocean waters across the eastern tropical Pacific typical of El Niño episodes. Prolonged periods of positive SOI values coincide with abnormally cold ocean waters across the eastern tropical Pacific typical of La Niña episodes.

The time series of the SOI and sea surface temperatures in the eastern equatorial Pacific indicates that the ENSO cycle has an average period of about four years, although in the historical record the period has varied between two and seven years. The 1980's and 1990's featured a very active ENSO cycle, with 5 El Niño episodes (1982/83, 1986/87, 1991-1993, 1994/95, and 1997/98) and 3 La Niña episodes (1984/85, 1988/89, 1995/96) occurring during the period. This period also featured two of the strongest El Niño episodes of the century (1982/83 and 1997/98), as well as two consecutive periods of El Niño conditions during 1991 - 1995 without an intervening cold episode.

Historically, there is considerable variability in the ENSO cycle from one decade to the next. For example, there are decades in which the

cycle was relatively inactive, and decades in which it was quite pronounced.

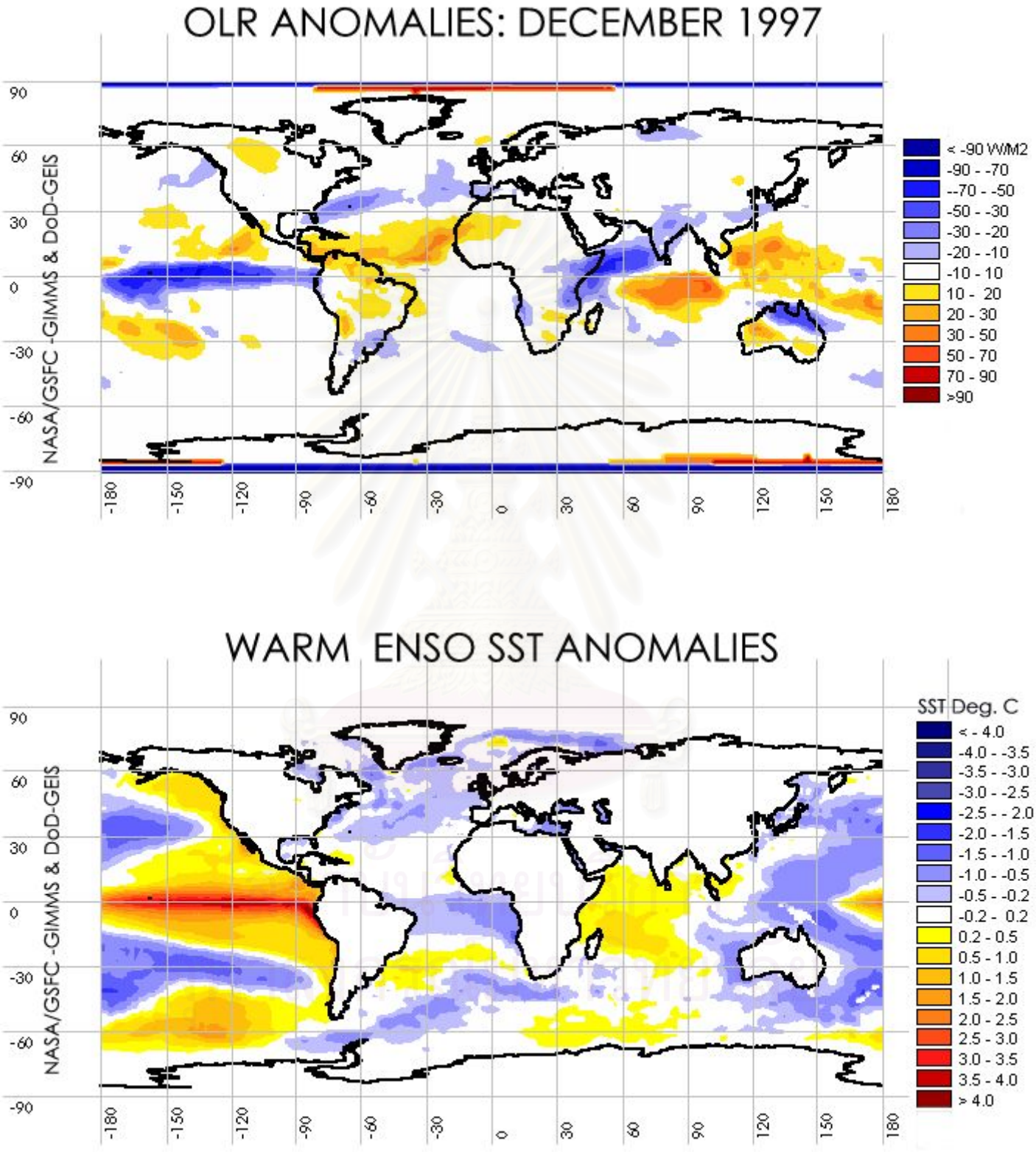

Fig.13. Outgoing Longwave Radiation (OLR) Dec. 1997 and Warm ENSO SST anomalies.

The Southern Oscillation

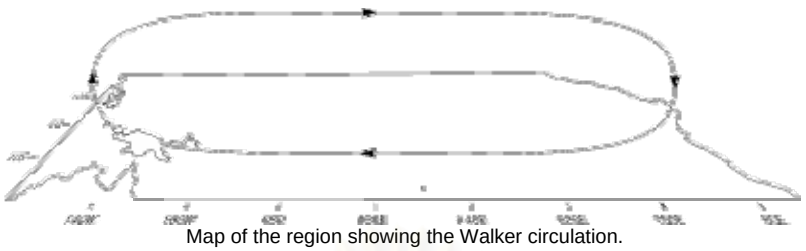

Fig. 14. Map of the region showing the Walker circulation.

The Walker circulation (Walker, 1924) is an east-west atmospheric circulation pattern characterised by rising air above Indonesia and the western Pacific and sinking air above the eastern Pacific, as shown in Fig. 14. Associated with the rise in air above Indonesia are heavy convective rains. The term "Southern Oscillation" refers to the variability of the strength of the Walker Circulation system and is quantified through the Southern Oscillation Index. During El Niño events there is a weakening of the Walker circulation, generally bringing drier conditions to the western Pacific region. During La Niña events the Walker circulation is especially strong, and rainfall may be unusually high over Indonesia. El Niño and the Southern Oscillation are two characteristics of the one large ocean-atmosphere event which we now refer to as ENSO (Rasmusson and Carpenter, 1982). The SOI is an index used to quantify the strength of an ENSO event. It is calculated from the difference between the sea level pressure (SLP) at Tahiti and Darwin. Although there are several methods of determining this relationship, a method often used, and shown in Fig. 15, was presented by Troup (1965):

$$SOI = 10.0 \times \frac{[\ SLPdiff - avSLPdiff\ ]}{StdDev(SLPdiff)}$$

where

SLPdiff = (mean Tahiti SLP for the month) - (mean Darwin SLP for the month),
avSLPdiff = long term mean of SLPdiff for the month in question, and
StdDev(SLPdiff) = standard deviation of SLPdiff for the month in question.

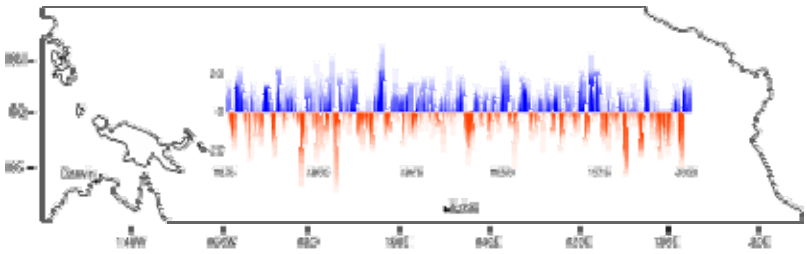

Fig. 15: Map of the region and the monthly Southern Oscillation Index. (http://www.cru.uea.ac.uk/cru/info/enso/)

In Fig 16, negative values (red) represent warmer than average conditions or El Niño events. Large positive values represent La Niña conditions. While the graph shows considerable variability in the SOI, the general pattern is for an ENSO event every four to seven years, with each event lasting between one and two years.

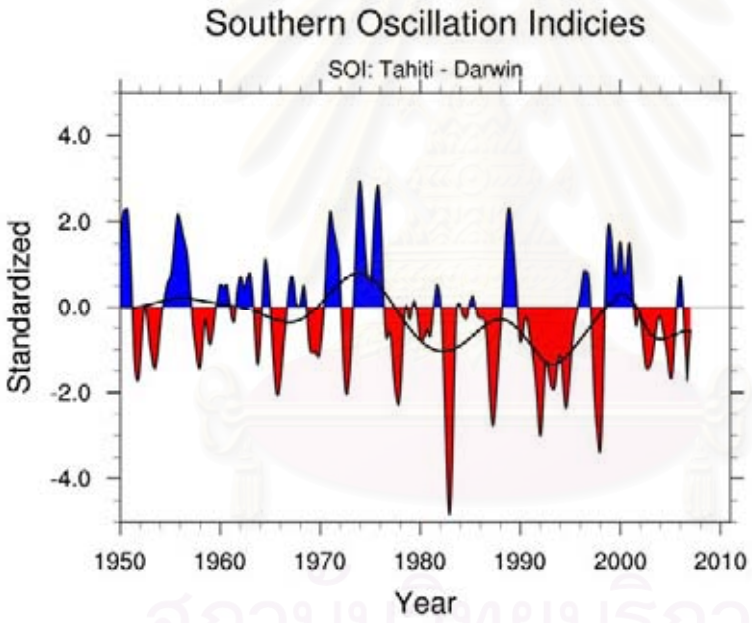

Fig.16. SOI 1950 to 2007.
http://www.cgd.ucar.edu/cas/catalog/climind/soi.html

It has been found that the cyclic warming and cooling of the eastern and central Pacific leaves it's distinctive fingerprint on sea level pressure. In particular, when the pressure measured at Darwin is compared with that measured at Tahiti, the difference between the two can be used to generate an "index" number. When there is a positive number, we have a La-Niña (or ocean cooling), but when the number is negative we have an El-Niño (or ocean warming).

Table 2. Monthly Southern Oscillation Index values as reported by Bureau of Meteorology, National Climate Centre, Climate Analysis Section. (ftp://ftp.bom.gov.au/anon/home/ncc/www/sco/soi/soiplaintext.html)

YEAR	JAN	FEB	MAR	APR	MAY	JUN	JUL	AUG	SEP	OCT	NOV	DEC
1950	5.1	17.6	17.6	16.8	7.6	26.9	21.1	12.3	6.9	17.1	12.5	23.0
1951	16.5	9.6	-1.4	-1.3	-6.6	5.0	-8.2	-0.5	-7.0	-8.0	-3.4	-3.0
1952	-9.2	-7.9	0.2	-8.8	6.0	7.4	3.5	-3.7	-3.4	1.8	-0.7	-12.6
1953	2.2	-6.0	-5.8	-0.5	-31.9	-2.3	-1.0	-17.2	-13.0	-0.1	-2.0	-4.0
1954	6.0	-3.6	-0.9	6.9	4.4	-1.5	4.2	10.4	4.5	1.8	3.9	12.8
1955	-5.4	15.2	2.9	-3.0	13.1	16.4	19.2	14.9	14.1	15.2	15.1	9.3
1956	11.3	12.4	9.4	11.1	17.9	12.3	12.6	11.0	0.2	18.3	1.9	10.3
1957	5.6	-2.2	-0.9	1.2	-12.2	-2.3	0.9	-9.5	-10.6	-1.3	-11.9	-3.5
1957	0.6	-0.5	-0.4	0.0	-1.0	-0.2	0.1	-1.0	-1.1	-0.2	-1.2	0.5
1958	-16.8	-6.9	-1.4	1.2	-8.2	0.2	2.2	7.8	-3.4	-1.9	-4.7	-6.5
1959	-8.7	-14.0	8.4	3.6	2.8	-6.3	-5.0	-5.0	0.2	4.2	11.1	8.2
1960	0.3	-2.2	5.6	7.8	5.2	-2.3	4.8	6.6	6.9	-0.7	7.2	6.7
1961	-2.5	6.3	-20.9	9.4	1.3	-3.1	2.2	0.1	0.8	-5.0	7.2	13.8
1962	17.0	5.3	-1.4	1.2	12.3	5.0	-0.4	4.6	5.1	10.3	5.2	0.6
1963	9.4	3.0	7.3	6.1	2.8	-9.6	-1.0	-2.4	-5.2	-12.9	-9.3	-11.6
1964	-4.0	-0.3	8.4	13.5	2.8	7.4	6.8	14.3	14.1	12.8	2.6	-3.0
1965	-4.0	1.6	2.9	-12.9	-0.3	-12.8	-22.6	-11.4	-14.2	-11.1	-17.9	1.6
1966	-12.0	-4.1	-13.9	-7.1	-9.0	1.0	-1.0	4.0	-2.2	-2.5	-0.1	-4.0
1967	14.6	12.9	7.8	-3.0	-3.5	6.6	1.6	5.9	5.1	-0.1	-4.0	-5.5
1968	4.1	9.6	-3.0	-3.0	14.7	12.3	7.4	0.1	-2.8	-1.9	-3.4	2.1
1969	-13.5	-6.9	1.8	-8.8	-6.6	-0.6	-6.9	-4.4	-10.6	-11.7	-0.1	3.7
1970	-10.1	-10.7	1.8	-4.6	2.1	9.9	-5.6	4.0	12.9	10.3	19.7	17.4
1971	2.7	15.7	19.2	22.6	9.2	2.6	1.6	14.9	15.9	17.7	7.2	2.1
1972	3.7	8.2	2.4	-5.5	-16.1	-12.0	-18.6	-8.9	-14.8	-11.1	-3.4	-12.1
1973	-3.0	-13.5	0.8	-2.1	2.8	12.3	6.1	12.3	13.5	9.7	31.6	16.9
1974	20.8	16.2	20.3	11.1	10.7	2.6	12.0	6.6	12.3	8.5	-1.4	-0.9
1975	-4.9	5.3	11.6	14.4	6.0	15.5	21.1	20.7	22.5	17.7	13.8	19.5
1976	11.8	12.9	13.2	1.2	2.1	0.2	-12.8	-12.1	-13.0	3.0	9.8	-3.0
1977	-4.0	7.7	-9.5	-9.6	-11.4	-17.7	-14.7	-12.1	-9.4	-12.9	-14.6	-10.6
1978	-3.0	-24.4	-5.8	-7.9	16.3	5.8	6.1	1.4	0.8	-6.2	-2.0	-0.9
1979	-4.0	6.7	-3.0	-5.5	3.6	5.8	-8.2	-5.0	1.4	-2.5	-4.7	-7.5
1980	3.2	1.1	-8.5	-12.9	-3.5	-4.7	-1.7	1.4	-5.2	-1.9	-3.4	-0.9
1981	2.7	-3.2	-16.6	-5.5	7.6	11.5	9.4	5.9	7.5	-5.0	2.6	4.7
1982	9.4	0.6	2.4	-3.8	-8.2	-20.1	-19.3	-23.6	-21.4	-20.2	-31.1	-21.3
1983	-30.6	-33.3	-28.0	-17.0	6.0	-3.1	-7.6	0.1	9.9	4.2	-0.7	0.1
1984	1.3	5.8	-5.8	2.0	-0.3	-8.7	2.2	2.7	2.0	-5.0	3.9	-1.4
1985	-3.5	6.7	-2.0	14.4	2.8	-9.6	-2.3	8.5	0.2	-5.6	-1.4	2.1
1986	8.0	-10.7	0.8	1.2	-6.6	10.7	2.2	-7.6	-5.2	6.1	-13.9	-13.6
1987	-6.3	-12.6	-16.6	-24.4	-21.6	-20.1	-18.6	-14.0	-11.2	-5.6	-1.4	-4.5
1988	-1.1	-5.0	2.4	-1.3	10.0	-3.9	11.3	14.9	20.1	14.6	21.0	10.8
1989	13.2	9.1	6.7	21.0	14.7	7.4	9.4	-6.3	5.7	7.3	-2.0	-5.0
1990	-1.1	-17.3	-8.5	-0.5	13.1	1.0	5.5	-5.0	-7.6	1.8	-5.3	-2.4
1991	5.1	0.6	-10.6	-12.9	-19.3	-5.5	-1.7	-7.6	-16.6	-12.9	-7.3	-16.7
1992	-25.4	-9.3	-24.2	-18.7	0.5	-12.8	-6.9	1.4	0.8	-17.2	-7.3	-5.5
1993	-8.2	-7.9	-8.5	-21.1	-8.2	-16.0	-10.8	-14.0	-7.6	-13.5	0.6	1.6
1994	-1.6	0.6	-10.6	-22.8	-13.0	-10.4	-18.0	-17.2	-17.2	-14.1	-7.3	-11.6
1995	-4.0	-2.7	3.5	-16.2	-9.0	-1.5	4.2	0.8	3.2	-1.3	1.3	-5.5
1996	8.4	1.1	6.2	7.8	1.3	13.9	6.8	4.6	6.9	4.2	-0.1	7.2
1997	4.1	13.3	-8.5	-16.2	-22.4	-24.1	-9.5	-19.8	-14.8	-17.8	-15.2	-9.1
1998	-23.5	-19.2	-28.5	-24.4	0.5	9.9	14.6	9.8	11.1	10.9	12.5	13.3

1999	15.6	8.6	8.9	18.5	1.3	1.0	4.8	2.1	-0.4	9.1	13.1	12.8
2000	5.1	12.9	9.4	16.8	3.6	-5.5	-3.7	5.3	9.9	9.7	22.4	7.7
2001	8.9	11.9	6.7	0.3	-9.0	1.8	-3.0	-8.9	1.4	-1.9	7.2	-9.1
2002	2.7	7.7	-5.2	-3.8	-14.5	-6.3	-7.6	-14.6	-7.6	-7.4	-6.0	-10.6
2003	-2.0	-7.4	-6.8	-5.5	-7.4	-12.0	2.9	-1.8	-2.2	-1.9	-3.4	9.8
2004	-11.6	8.6	0.2	-15.4	13.1	-14.4	-6.9	-7.6	-2.8	-3.7	-9.3	-8.0
2005	1.8	-29.1	0.2	-11.2	-14.5	2.6	0.9	-6.9	3.9	10.9	-2.7	0.6
2006	12.7	0.1	13.8	15.2	-9.8	-5.5	-8.9	-15.9	-5.1	-15.3	-1.4	-3.0
2007	-7.3	-2.7	-1.4	-3.0	-2.7	5.0	-4.3					

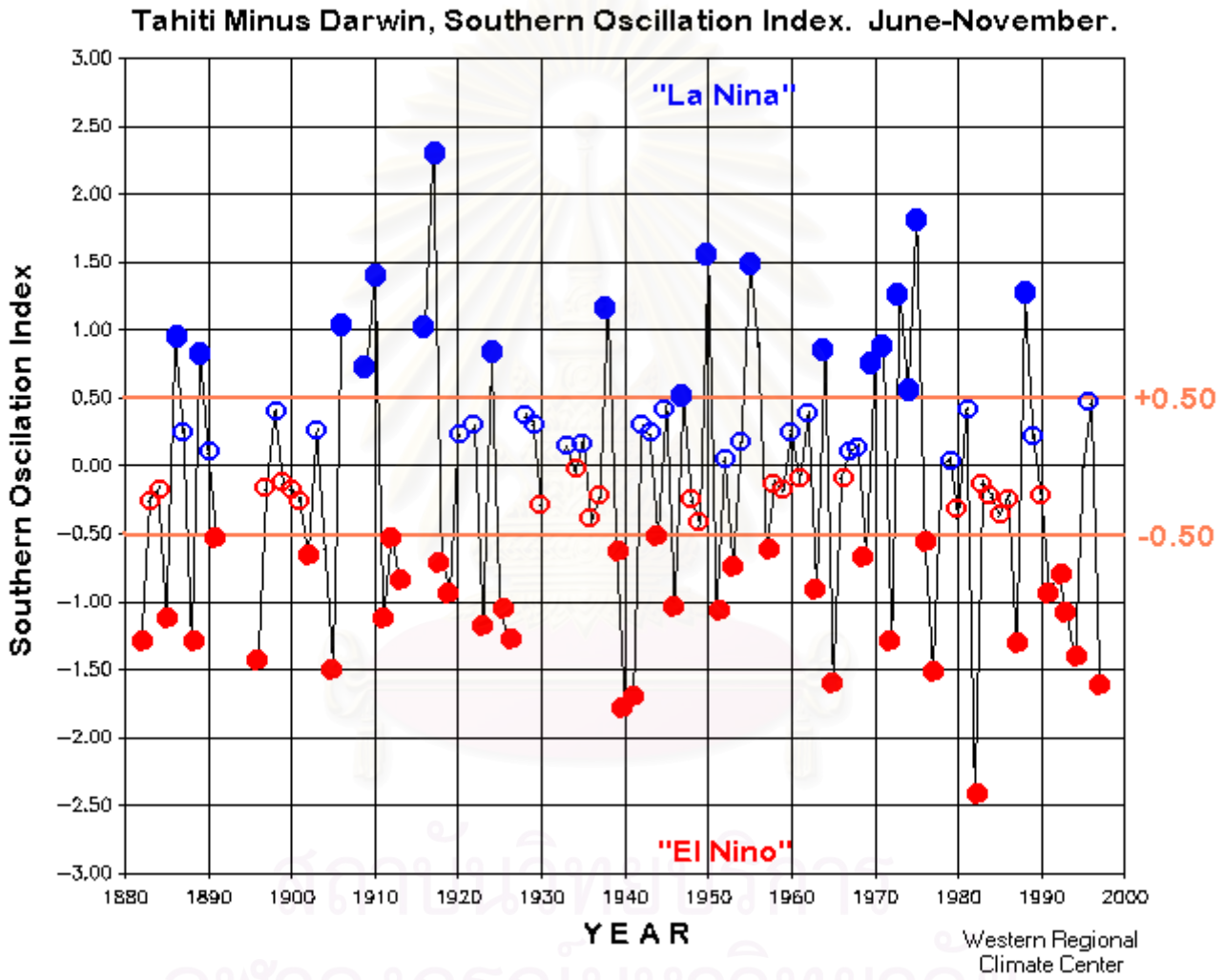

Fig.17. SOI, June-November, 1880-2000.
http://www.wrcc.dri.edu/enso/soiall.gif

Criteria for ENSO Classification What indices are used to see if an El Niño or La Niña is occurring?

A variety of indices are used to characterize ENSO because it effects so many elements of the atmosphere-ocean climate system. Probably the two principal indices are the Southern Oscillation Index (SOI), which is given by the

difference in sea-level pressure between Tahiti and Darwin, Australia, and the Nino 3 index, which referes to the anomalous SST within the region bounded by 5N-5S and 150W-90W. The measurements needed for these indices are straightforward, and we have long historical records, especially for the the SOI.

However, other indices are effective at characterizing other aspects of ENSO. For example, the anomalous 850 mb zonal winds show how the low-level atmospheric flow is responding to low-level pressure anomalies associated with ENSO and other mechanisms. Often the 850 mb flow (about 1.5 km above sea level) exhibits a "cleaner" signal than the winds at the surface, which are subject to local effects such as terrain. An index involving the 200 mb zonal flow is used to describe the upper tropospheric winds, whose anomalies tend to be opposite to those at 850 mb and below. The 200 mb flow is particularly important because it is changes at around this level in the tropics that tend to have the biggest consequences for the atmospheric circulation outside of the tropics. The 500 mb temperature represents a proxy for the anomalous heat content of the tropical troposphere. In an overall sense, there is greater heating of the troposphere, and more deep cumulus convection, than normal during warm ENSO events (El Ninos).

Finally, there is one more widely used index for the atmosphere and that relates to the outgoing longwave radiation or OLR. The deeper the cumulus convection, the colder the cloud tops, which means the thermal or infrared radiation to space is reduced. It is straightforward to monitor OLR via satellite; its value in the tropical Pacific near the dateline is an effective way to gauge the frequency and magnitude of the thunderstorm activity that changes with ENSO.

Current values of these indices provided on-line by the Climate Prediction Center

A number of WRCC ENSO tables and graphs are stratified by June-November Southern Oscillation Index (SOI), following the logic of Redmond & Koch (1991, 2381-2399, Water Resources Research). Slightly better relations are found between western climate and SOI than with SST (Sea Surface Temperatures). Also, better relations are often found when SOI leads winter climate (by about 4 months) rather than being concurrent with climate. And, whether better, similar, or even slightly worse, the predictive utility is retained with the earlier SOI period. Because the SOI is averaged over 6 months, the lead and lag periods are not completely separated (2 month overlap for Oct-Mar climate elements), but by early winter (Sept or Oct) the "ball park" value of the SOI is usually apparent.

Strictly speaking, with this approach ENSO phase is determined by atmospheric

quantities (SOI). "El Niño" and "La Niña" are usually defined solely by ocean temperatures (SST). The relationship between the two is strong enough that most moderately positive SOI years are also "La Niña" and most moderately negative SOI years are also "El Niño", and the terms are used interchangeably, at some risk of misinterpretation, to denote ENSO phase.

(Many El Niño, La Niña, Neither Niño categorization approaches use ocean criteria, such as Sea Surface Temperatures (SST), rather than atmospheric criteria, such as the Southern Oscillation Index (SOI). Most categorizations produce the same years; however, typically a few years are included with one approach that are not included in another, and vice versa.)

SE - Strongly Negative SOI (-1.00 or less) - "Stronger El Niño"
EN - Mildly Negative SOI (-0.50 or less) - "Moderate El Niño"
N - Neither (SOI between -0.50 and +0.50)- "Neither Niño" or "Nada Niño"
LN - Mildly Positive SOI (+0.50 or more) - "Moderate La Niña"
SL - Strongly Positive SOI (+1.00 or more) - "Stronger La Niña"

Unless stated otherwise, the term "El Niño" based on SOI usually includes EN and SE cases.
Unless stated otherwise, the term "La Nina" based on SOI usually includes LN and SL cases.

Table 3. Classification of winter as El Niño or La Niña years.
http://www.wrcc.dri.edu/enso/ensodef.html

Year	Jun-Nov Ave SOI	Following Winter -- -- - -- --	Label
1950	1.55	1950-51	SL
1951	-1.07	1951-52	SE
1952	0.05	1952-53	N
1953	-0.75	1953-54	EN
1954	0.18	1954-55	N
1955	1.50	1955-56	SL
1956	0.88	1956-57	LN
1957	-0.62	1957-58	EN
1958	-0.12	1958-59	N
1959	-0.18	1959-60	N
1960	0.27	1960-61	N
1961	-0.12	1961-62	N
1962	0.38	1962-63	N
1963	-0.92	1963-64	EN
1964	0.87	1964-65	LN
1965	-1.58	1965-66	SE
1966	-0.08	1966-67	N
1967	0.10	1967-68	N
1968	0.15	1968-69	N
1969	-0.67	1969-70	EN
1970	0.77	1970-71	LN
1971	0.92	1971-72	LN

1972	-1.28	1972-73	SE
1973	1.28	1973-74	SL
1974	0.55	1974-75	LN
1975	1.83	1975-76	SL
1976	-0.52	1976-77	EN
1977	-1.52	1977-78	SE
1978	0.00	1978-79	N
1979	0.05	1979-80	N
1980	-0.38	1980-81	N
1981	0.42	1981-82	N
1982	-2.42	1982-83	SE
1983	-0.12	1983-84	N
1984	-0.22	1984-85	N
1985	-0.37	1985-86	N
1986	-0.22	1986-87	N
1987	-1.35	1987-88	SE
1988	1.25	1988-89	SL
1989	0.22	1989-90	N
1990	-0.23	1990-91	N
1991	-0.95	1991-92	EN
1992	-0.80	1992-93	EN
1993	-1.08	1993-94	SE
1994	-1.43	1994-95	SE
1995	0.00	1995-96	N
1996	0.47	1996-97	N
1997	-1.67	1997-98	SE
1998	+1.05	1998-99	SL
1999	+0.40	1999-00	N (ocean temperatures definitely LN)
2000	+0.57	2000-01	LN
2001	-0.17	2001-02	N
2002	-0.83	2002-03	EN
2003	-0.33	2003-04	N
2004	-0.73	2004-05	EN (oc.T met EN criteria,too)
2005	0.08	2005-06	N (mild La Nina developed in mid-winter)
2006	-0.90	2006-2007	EN (oc.T moderately EN,too)

ENSO years are listed in Tables 3 and 4.

Table 4. ENSO warm and cold years 1949-1996.
http://www.geog.ucsb.edu/~joel/e206_w01/lect23/enso_table.html

El Nino/Southern Oscillation

Warm and Cold Years 1949-1996

Warm	Cold
1958	1950
1966	1951
1969	1955
1973	1956

1983	1971
1987	1974
1992	1976
1995	1987

Warm Events: 1877 1880 1884 1891 1896 1899 1902 1904 1911 1913 1918 1923 1925 1930 1932 1939 1951 1953 1963 1965 1969 1972 1976 1982 1986

Cold Events:1886 1889 1892 1903 1906 1908 1916 1920 1924 1928 1931 1938 1942 1949 1954 1964 1970 1973 1975 1988

Year 0 of a warm event is defined as the year when the SOI changes sign from positive to negative and when central and eastern equatorial Pacific SST anomalies become strongly positive. Year 0 of a cold event has the opposite characteristics.

From Kiladis, G. N., and H. F. Diaz, 1989: The following list of cold (La Niña) and warm (El Niño) episodes has been compiled to provide a season-by-season breakdown of conditions in the tropical Pacific. We have attempted to classify the intensity of each event by focusing on a key region of the tropical Pacific (along the equator from 150°W to the date line). The process of classification was primarily subjective using reanalyzed sea surface temperature analyses produced at the National Centers for Environmental Prediction/Climate Prediction Center and at the United Kingdom Meteorological Office. An objective procedure for classifying intensity is being explored at NCEP/CPC. In the following table, weak periods are designated as C- or W-, moderate strength periods as C or W, strong periods as W+ or C+, and neutral periods as N.

Table 5. Cold and warm episodes by season
http://www.cpc.noaa.gov/products/analysis_monitoring/ensostuff/ensoyears.shtml

Warm (red) and cold (blue) episodes based on a threshold of +/- 0.5^{o}C for the Oceanic Niño Index (ONI) [3 month running mean of ERSST.v2 SST anomalies in the Niño 3.4 region (5^{o}N-5^{o}S, 120^{o}-170^{o}W)], based on the 1971-2000 base period. For historical purposes cold and warm episodes (blue and red colored numbers) are defined when the threshold is met for a minimum of 5 consecutive over-lapping seasons.

Year	DJF	JFM	FMA	MAM	AMJ	MJJ	JJA	JAS	ASO	SON	OND	NDJ
1950	-1.8	-1.5	-1.4	-1.4	-1.4	-1.2	-0.9	-0.8	-0.8	-0.8	-0.9	-1.0
1951	-1.0	-0.8	-0.6	-0.4	-0.2	0.1	0.4	0.5	0.6	0.7	0.7	0.6
1952	0.3	0.1	0.1	0.1	0.0	-0.2	-0.3	-0.3	-0.1	-0.2	-0.2	-0.1
1953	0.1	0.3	0.4	0.5	0.5	0.4	0.4	0.4	0.4	0.4	0.3	0.3
1954	0.3	0.2	-0.1	-0.5	-0.7	-0.7	-0.8	-1.0	-1.1	-1.1	-1.0	-1.0
1955	-1.0	-0.9	-0.9	-1.0	-1.1	-1.0	-1.0	-1.0	-1.5	-1.8	-2.1	-1.7
1956	-1.2	-0.8	-0.7	-0.6	-0.6	-0.6	-0.7	-0.8	-0.9	-0.9	-0.9	-0.8
1957	-0.5	-0.1	0.2	0.6	0.7	0.8	0.9	0.9	0.8	0.9	1.2	1.5
1958	1.6	1.5	1.1	0.7	0.5	0.5	0.4	0.1	0.0	0.0	0.1	0.3
1959	0.4	0.4	0.3	0.2	0.0	-0.3	-0.4	-0.5	-0.4	-0.4	-0.3	-0.3
1960	-0.3	-0.3	-0.3	-0.2	-0.1	-0.1	0.0	0.0	-0.1	-0.2	-0.3	-0.2
1961	-0.2	-0.2	-0.2	-0.1	0.1	0.1	0.0	-0.3	-0.6	-0.6	-0.5	-0.5
1962	-0.5	-0.5	-0.5	-0.5	-0.4	-0.3	-0.2	-0.3	-0.4	-0.6	-0.7	-0.7
1963	-0.6	-0.3	0.0	0.1	0.1	0.3	0.6	0.8	0.8	0.9	1.0	1.0
1964	0.8	0.4	-0.1	-0.5	-0.7	-0.7	-0.8	-0.9	-1.0	-1.1	-1.1	-1.0
1965	-0.8	-0.5	-0.3	0.0	0.2	0.6	1.0	1.2	1.4	1.5	1.6	1.5
1966	1.2	1.1	0.8	0.5	0.2	0.1	0.1	0.0	-0.2	-0.3	-0.3	-0.4
1967	-0.4	-0.5	-0.6	-0.5	-0.3	0.0	0.0	-0.2	-0.4	-0.5	-0.5	-0.6
1968	-0.7	-0.9	-0.8	-0.8	-0.4	0.0	0.3	0.3	0.2	0.4	0.6	0.9
1969	1.0	1.0	0.9	0.7	0.6	0.4	0.4	0.4	0.6	0.7	0.7	0.6
1970	0.5	0.3	0.2	0.1	-0.1	-0.4	-0.6	-0.8	-0.8	-0.8	-0.9	-1.2
1971	-1.4	-1.4	-1.2	-1.0	-0.8	-0.8	-0.8	-0.8	-0.9	-0.9	-1.0	-0.9
1972	-0.7	-0.3	0.0	0.3	0.5	0.8	1.1	1.3	1.5	1.8	2.0	2.1
1973	1.8	1.2	0.5	-0.1	-0.5	-0.8	-1.1	-1.3	-1.4	-1.7	-1.9	-2.0
1974	-1.8	-1.6	-1.2	-1.1	-0.9	-0.7	-0.5	-0.4	-0.5	-0.7	-0.8	-0.7
1975	-0.6	-0.6	-0.7	-0.8	-1.0	-1.1	-1.3	-1.4	-1.6	-1.6	-1.7	-1.8
1976	-1.6	-1.2	-0.9	-0.7	-0.5	-0.2	0.1	0.3	0.5	0.7	0.8	0.8
1977	0.6	0.5	0.2	0.1	0.2	0.3	0.3	0.4	0.5	0.7	0.8	0.8
1978	0.7	0.4	0.0	-0.3	-0.4	-0.3	-0.4	-0.5	-0.5	-0.4	-0.2	-0.1
1979	-0.1	0.0	0.1	0.2	0.1	0.0	0.0	0.2	0.3	0.4	0.5	0.5
1980	0.5	0.3	0.2	0.2	0.3	0.3	0.2	0.0	-0.1	0.0	0.0	-0.1
1981	-0.3	-0.4	-0.4	-0.3	-0.3	-0.3	-0.4	-0.3	-0.2	-0.1	-0.1	-0.1
1982	0.0	0.1	0.2	0.4	0.6	0.7	0.8	1.0	1.5	1.9	2.2	2.3
1983	2.3	2.0	1.6	1.2	1.0	0.6	0.2	-0.2	-0.5	-0.8	-0.9	-0.8
1984	-0.5	-0.3	-0.2	-0.4	-0.5	-0.5	-0.3	-0.2	-0.3	-0.6	-1.0	-1.1
1985	-1.0	-0.8	-0.8	-0.8	-0.7	-0.5	-0.4	-0.4	-0.4	-0.3	-0.2	-0.3
1986	-0.4	-0.4	-0.3	-0.2	-0.1	0.0	0.2	0.5	0.7	0.9	1.1	1.2
1987	1.3	1.2	1.1	1.0	1.0	1.2	1.5	1.6	1.6	1.5	1.3	1.1
1988	0.8	0.5	0.1	-0.3	-0.8	-1.2	-1.2	-1.1	-1.3	-1.6	-1.9	-1.9
1989	-1.7	-1.5	-1.1	-0.9	-0.6	-0.4	-0.3	-0.3	-0.3	-0.3	-0.2	-0.1
1990	0.1	0.2	0.3	0.3	0.3	0.3	0.3	0.4	0.3	0.3	0.3	0.4
1991	0.5	0.4	0.4	0.4	0.6	0.8	0.9	0.9	0.8	1.0	1.4	1.7
1992	1.8	1.7	1.6	1.4	1.1	0.8	0.4	0.2	-0.1	-0.1	0.0	0.1
1993	0.3	0.4	0.6	0.8	0.8	0.7	0.5	0.4	0.4	0.3	0.2	0.2
1994	0.2	0.3	0.4	0.5	0.6	0.6	0.6	0.6	0.7	0.9	1.2	1.3
1995	1.2	0.9	0.7	0.4	0.2	0.1	0.0	-0.3	-0.5	-0.6	-0.7	-0.8
1996	-0.8	-0.7	-0.5	-0.3	-0.2	-0.2	-0.1	-0.2	-0.2	-0.2	-0.3	-0.4
1997	-0.4	-0.3	0.0	0.4	0.9	1.4	1.7	2.0	2.3	2.4	2.5	2.5

1998	**2.4**	**2.0**	**1.4**	**1.1**	0.4	-0.1	**-0.8**	**-1.0**	**-1.1**	**-1.1**	**-1.3**	**-1.5**
1999	**-1.6**	**-1.2**	**-0.9**	**-0.7**	**-0.8**	**-0.8**	**-0.9**	**-0.9**	**-1.0**	**-1.2**	**-1.4**	**-1.6**
2000	**-1.6**	**-1.5**	**-1.1**	**-0.9**	**-0.7**	**-0.6**	-0.4	-0.3	-0.4	**-0.5**	**-0.7**	**-0.7**
2001	**-0.7**	**-0.5**	-0.4	-0.2	-0.1	0.1	0.2	0.1	0.0	-0.1	-0.2	-0.2
2002	-0.1	0.1	0.3	0.4	**0.7**	**0.8**	**0.9**	**0.9**	**1.1**	**1.3**	**1.5**	**1.3**
2003	**1.1**	**0.8**	**0.6**	0.1	-0.1	0.0	0.3	0.4	0.5	0.5	0.6	0.5
2004	0.4	0.2	0.2	0.2	0.3	0.4	**0.7**	**0.8**	**0.9**	**0.9**	**0.9**	**0.8**
2005	**0.6**	**0.5**	0.3	0.4	0.5	0.3	0.2	0.0	0.0	-0.2	-0.4	-0.7
2006	-0.8	-0.7	-0.4	-0.2	0.0	0.1	0.3	0.4	**0.7**	**0.9**	**1.1**	**1.1**
2007	**0.8**	0.3	0.1	-0.1	0.0	-0.1						

1.6 Objectives

1) Landuse changes at Ban Don and Surat Thani in 11 times during El Niño, La Niña and non-ENSO years.

2) The linkage of ENSO (from 1951-2001) on the environments in the study area such as rainfall, air temperature, tropical cyclone, sea level fluctuation, Tapi river runoff.

3) The linkage of ENSO (from 1951-2001) on the natural resources in the study area such as fish catch, aquaculture, landuse and population.

4) Recommendation for environment and resources management if the ENSO occur in the future.

สถาบันวิทยบริการ
จุฬาลงกรณ์มหาวิทยาลัย

Chapter 2
Study Impact of ENSO by Remote Sensing

2.1 Study Area.

Bandon Bay (9.20 ^{0}N and 99.67 ^{0}E) is located in Surat Thani Province, southern Thailand. The watershed of the bay is 12,220 km^2, of which an important part consists of agricultural lands and aquaculture. The population living within the watershed numbers approximately 830,000 with fisheries, aquaculture and tourism as their main activities. In the coastal area, there are several socio-economic activities such as fisheries, oyster culture and shrimp farming that represent an income for the people living in the area. Mangroves (*Rhizophora spp, Sonneratia alba, Xylocarpus spp, Avicennia alba* and *Bruguiera spp*.) cover the shores of the bay and the upland area (Fig. 18a).

Fig. 18a. ETM+ imagery of Bandon Bay, Surat Thani Province uses bands 5, 4, 3 to differentiate features (January 6, 2002).

Ban Don Bay is an inlet of the biggest river on the east coast of the Southern Peninsula, which is the Tapi-Phumduang river to the Gulf of Thailand, which lies to the east of Surat Thani province. Mangrove forest plays an important role in the economies of Ban Don Bay, particularly as a

source of energy and food protein. However, population and economic development pressures have been responsible in part for the conversion of mangroves to various land uses in the past years, i.e., agricultural, residential and industrial sites, salt ponds, ports and harbors, and aquaculture (Fig.18b).

Fig. 18b Ban Don Bay - A historical port, center of economy and fishing

http://www.st.ac.th/ep/TheProvince/AoBanDon.htm

Ao Ban Don (Fig.18c) lies deep inside the land, naturally protected from the tide by various islands. Once an important port, Ao Ban Don today is a land and sea transportation hub. The fertile mangrove forest around the bay coastline makes Amphoe Muang, Kanchanadit and Don Sak appropriate for aquatic animal nurseries and fishing industries.

Fig. 18c. Ao Ban Don

http://www.travelthailand.com/south/suratthani/bandon/bandon_map2.html

Fig.19. The South of Thailand.

http://www.tourismthailand.org/about_thailand/south.php

Surat Thani (Fig.19) is southern Thailand's largest province, covers some 12,800 square kilometres, and has an extensive coastline lapped by Thai Gulf waters. The provincial capital is 685 kilometres south of Bangkok. Surat Thani boasts some of Thailand's loveliest islands namely the Penang-sized Ko Samui, Thailand's third largest island, palm-fringed jewel of a sparkling archipelago that includes the stunning 250-square-kilometre Ang Thong Marine National Park.

Surat Thani once formed part, and may have been the centre, of the Mahayana Buddhist Srivijaya Empire which steeped in legend and mystery, dominated the Malay peninsula and much of Java some 1,500 years ago. Srivijaya was best described by the itinerant Chinese monk I Ching after a pilgrimage he made to India during the late 600s. Archaeological discoveries at Chaiya district indicate the former empire's splendour.

The primary objective of this study is to classify land cover/land use pattern in the Ban Don Bay coastal area by using remote sensing techniques, and to estimate the rate of mangrove area depletion and effects of ENSO on land cover along the coast of Ban Don Bay.

2.2 Methods

1) Compile various historical data up to 2001 of:

- Years that ENSO occurred from internet.
- Data and informations from internet.
- Order Landsat data for 11 times.
- SOI from internet.
- Variations of Mangrove areas from Royal Forestry Department.
- Fisheries statistics from Department of Fisheries.
- Meteorological data from Meteorological Department, analysed by mean and anomaly methods.
- Runoff data from Royal Irrigation Department, analysed by mean and anomaly methods.
- Sea level data from Harbour Department, analysed by mean and anomaly methods.
- Landuse map from Agriculture Ministry.
- Population statistics from Institute of Population.
- Ground truth data to validate (geo-reference) satellite data.

2) Design the data base of the above data.

3) Analyse the data statistically for the mean, 3-years running mean, anomaly and correlation methods. Plot the data and compare to SOI in order to see the linkage of ENSO events and data.

4) For satellite digital data: Perform preprocessing analyses such as image restoration, warping with ground control points with field data and rectified. Processing procedures are enhancing, supervised classification for landuse change with maximum likelihood decision. To see the linkage of ENSO with vegetation using NDVI classification.

5) Find the relation from results of the classifications and physical data. Estimate the linkage of ENSO on the landuse and NDVI changes.

6) For Fisheries, using statistical analyses to see the linkage of ENSO on fisheries data. Find the relationship between mangrove deforestation and aquaculture with population.

7) For Meteorological data, using statistical analyses and compare SOI and Monsoon Index on meteorological data.

8) For runoff data also using the statistical analyses for comparison of ENSO and runoff data.

9) Conclusion and recommendation. Submit the final report.

2.3. NDVI and Landuse Classifications

1) Supervised classify the landuse into 12 classes such as:
- Shrimp farm
- Rubber plantation
- Paddy field
- Town
- Natural water resource and wetland
- Mangrove
- Palm and Coconut plantations
- Other areas.

2) Compute NDVI value for estimation the vegetation health using

$$NDVI = \frac{Band4 - Band3}{Band4 + Band3} * 128 + 127.5$$

3) Cut only 1 pixel (Plot only x-value)

4) Export from ERDAS Imagine to Surfer by choosing Surfer GRID.

5) Save from Surfer GRID to Surfer Binary $\rightarrow$Excel.

6) Change Y value by substitute the Count date.

7) Cut only 1 line by choosing Y = 1011890.

8) Plot for comparison the variation of NDVI at different dates.

Table 6. Count date from first date of satellite data.

Date	Count Date from first date
March 30, 1988	1
March 17, 1989	353
March 28, 1993	1825
December 12, 1994	2449
February 17, 1996	2881
June 11, 1997	3361
April 27, 1998	3681
January 8, 1999	3937
April 12, 2000	4397
December 4, 2000	4633

9) Plots by Surfer.

2.4 Remote Sensing Data Processing

Classification of land cover/land use pattern in Ban Don Bay coastal area (Fig. 18a.) was carried out using high altitude satellite imaging technique. Sources of data using for this study describe in Table 7.

Table 7 Source of data use in this study.

Data Sources	Acquisition Date	Sensor
1. **Remotely sensed data**	March 30, 1988 (LN)	Landsat 5-TM
	March 17, 1989 (Normal)	Landsat 5-TM
	March 28, 1993 (EN)	Landsat 5-TM
	December 12, 1994 (EN)	Landsat 5-TM
	February 17, 1996 (Normal)	Landsat 5-TM
	June 11, 1997 (EN)	Landsat 5-TM
	April 27, 1998 (LN)	Landsat 5-TM
	January 8, 1999 (Normal)	Landsat 5-TM
	April 12, 2000 (LN)	Landsat 5-TM
	December 4, 2000 (LN)	Landsat 7-ETM+
	January 6, 2002 (EN)	Landsat 7-ETM+

2. **Hard copy Maps** (Digitized to GIS coverage)
2.1 Topographic maps at a scale of 1:50,000 produced by the Royal Thai Survey Department in 1975
2.2 Topographic maps at a scale of 1:250,000 produced by the Royal Thai Survey Department in 1975
2.3 Land-use map at a scale of 1:50,000, produced by the Royal Forestry Department in 1993
2.4 Land-use map at a scale of 1:50,000, produced by the Land Development Department in 1984
2.5 Land-use map at a scale of 1:50,000, produced by the Land Development Department in 2000
2.6 Land-use map at a scale of 1:50,000, produced by the National Mangrove Committee, National Research Council of Thailand in 1993

Note: EN means El Niño,

LN means La Niña

Normal is the normal year, no El Niño nor La Niña.

Satellite imagery was analyzed using the PCI Easi+, version 7.0, Erdas Imagine version 8.5 , IDRISI 32 for Windows and Golden Software Surfer version 7.0 to obtain the results for land-use classification and grid interpolation and results plot. This study use ArcView GIS version 3.2a for analysis previous secondary data and classified results in this study. Digital data analysis techniques employed in this study involved the following steps:

2.4.1 Image rectification and restoration

Since a large amount of data sets were involved, pre-processing of the data in the most efficient way is the prime concern. It is necessary to geometrically correct LANDSAT images to remove image distortion caused by variations of orbital parameters of the satellite and by imperfections of the sensor. The precise geometric correction could be applied by using the known ground control points (GCPs) from maps with a standard cartographic projection such as the Universal Transverse Mercator Projection (UTM). After taking known GCPs from the topographic map (scale 1:50,000), the LANDSAT satellite imageries were geo-rectified by using the first order nearest neighbor methods. The pixel size of the rectified image is 25 m x 25 m.

Transformation matrices containing the coefficients for converting coordinates were calculated from the GCPs by the least square regression methods. The best GCPs were selected and adjust until the total RMS (Root

Means Square) error was less than the tolerance level (0.5 of pixel size). The first-order transformation was applied which yields adequate result because of flat terrain of the study area. Nearest neighbor interpolation was followed during resampling. Table 8 shows number of GCPs for transformation input.

$$X = X_0 + a_1 (x - x_0) + a_2 (y - y_0) \quad \text{(Eq. 1)}$$

$$Y = Y_0 + b_1 (x - x_0) + b_2 (y - y_0) \quad \text{(Eq. 2)}$$

Where

x, y	are the satellite image coordinates
X, Y	are the map coordinates
x_0, y_0	are the coordinate of the center (arithmetic mean) of the GCPs from satellite image
X_0, Y_0	are the coordinate of the center (arithmetic mean) of the GCPs from map
a_t, b_t	are the model constants

Values of x_0, y_0 , X_0, Y_0 are dependent on the subset image and the positions of the ground control points. The model constants (a_t and b_t) are dependent on the relative orientation between the two coordinate systems. Table 9 show rectification formulae for each LANDSAT satellite imageries.

These formulae were used to rectify the satellite image so that its geographical reference was the same as the other layers in the GIS.

There were two field trips in order to check the ground control point and for validate the supervised classification on

a) 12-13 October 2002 and

b) 26-27 March 2003.

Some of the photos from the ground surveys are shown from Figs.21 to 28.

Table 8 Number of Ground Control Points (GCPs) used to created transformation model

Acquisition Date	Number of GCPs
March 30, 1988	74
March 17, 1989	70
March 28, 1993	71
December 12, 1994	70
February 17, 1996	74
June 11, 1997	67
April 27, 1998	72
January 8, 1999	75
April 12, 2000	79
December 4, 2000	77
January 6, 2002	71

Table 9 Rectification formulae

Date	Rectification formulae
March 30, 1988	$X = 370.84 + 2.55x10^{-2} (x - 462459.54) - 2.44x10^{-4} (y - 474487.46)$
	$Y = 545.22 - 2.37x10^{-4} (x + 631978.49) - 4.27x10^{-2} (y + 468952.65)$
March 17, 1989	$X = 210.46 + 2.41x10^{-2} (x - 452657.78) - 1.98x10^{-4} (y - 474077.87)$
	$Y = 870.45 + 2.94x10^{-4} (x + 64847.49) - 4.27x10^{-2} (y + 418890.85)$
March 28, 1993	$X = 279.30 + 2.67x10^{-2} (x - 442184.27) - 2.43x10^{-4} (y - 476589.57)$
	$Y = 425.09 + 1.98x10^{-4} (x - 65759.29) - 4.27x10^{-2} (y - 434227.75)$
December 12, 1994	$X = 254.15 + 2.42x10^{-2} (x - 492134.11) - 2.50x10^{-4} (y - 487177.87)$
	$Y = 675.18 + 2.63x10^{-4} (x - 621334.49) - 4.27x10^{-2} (y - 476548.51)$
February 17, 1996	$X = 244.42 + 2.36x10^{-2} (x - 454667.18) - 2.39x10^{-4} (y - 412556.91)$
	$Y = 745.64 + 2.84x10^{-4} (x - 62859.09) - 4.27x10^{-2} (y - 445611.19)$
June 11, 1997	$X = 246.07 + 2.76x10^{-2} (x + 462859.08) + 2.11x10^{-4} (y + 482977.97)$
	$Y = 786.27 + 2.48x10^{-4} (x - 62859.09) - 4.27x10^{-2} (y - 445009.65)$
April 27, 1998	$X = 237.53 + 2.46x10^{-2} (x - 46519.64) - 2.43x10^{-4} (y - 481231.10)$
	$Y = 755.12 + 2.43x10^{-4} (x - 69919.59) - 4.27x10^{-2} (y - 413446.75)$
January 8, 1999	$X = 251.44 + 2.32x10^{-2} (x - 412159.08) - 2.14x10^{-4} (y - 410322.27)$
	$Y = 709.98 + 2.89x10^{-4} (x - 66849.11) - 4.43x10^{-2} (y - 441676.81)$
April 12, 2000	$X = 301.11 + 2.35x10^{-2} (x - 461819.01) - 2.73x10^{-4} (y - 406547.12)$
	$Y = 771.75 + 2.49x10^{-4} (x - 61851.49) - 4.61x10^{-2} (y - 434204.55)$
December 4, 2000	$X = 294.58 + 2.71x10^{-2} (x - 432853.58) - 2.33x10^{-4} (y - 482977.27)$
	$Y = 798.45 + 2.40x10^{-4} (x - 62454.71) - 4.77x10^{-2} (y - 440972.55)$
January 6, 2002	$X = 235.57 + 2.72x10^{-2} (x - 412810.18) - 2.62x10^{-4} (y - 402977.20)$
	$Y = 812.54 + 2.49x10^{-4} (x - 65829.79) - 4.17x10^{-2} (y - 448072.55)$

2.4.2 Reduction of noise and image enhancement Noise is a digital image that can manifest itself as either inaccurate gray level readings or missing data altogether. Noise is the result of sensor malfunctions

during the recording or transmittal of information. Unlike geometric distortions and other radiometric degradation, noise is readily identifiable, even to those unfamiliar with the scene of the image. Noise was removed by using Furrier method; the image was then enhanced to encompass a variety of operation design to improve the visual interpretability of an image, by increasing the apparent distinction between features in a scene.

All the spectral bands excluding Thermal Infrared Channel of TM (band 6) and ETM+ (band 6L and 6H), were used. To minimize the effect of illumination difference, spectral band were normalized by the total intensity as follows:

$$NB_i = 255 (OB_i / \Sigma OB_i) \qquad i = 1 \text{ to } n \qquad \text{(Eq 3)}$$

Where

NB_i is the band normalized by total intensity
OB_i is the original spectral band

The constant (255) is used to fit the data in a byte range of 0-255. The resulting bands have the poverty that the sum of any pixel values is 255 due to normalization. In figure 2a, the hypothetical location of water, vegetation and soil is shown in a two-dimensional feature space. After normalization, the location of these objects is projected onto a diagonal line of uniform intensity (Fig 20b), indicating that the objects are free from intensity variation.

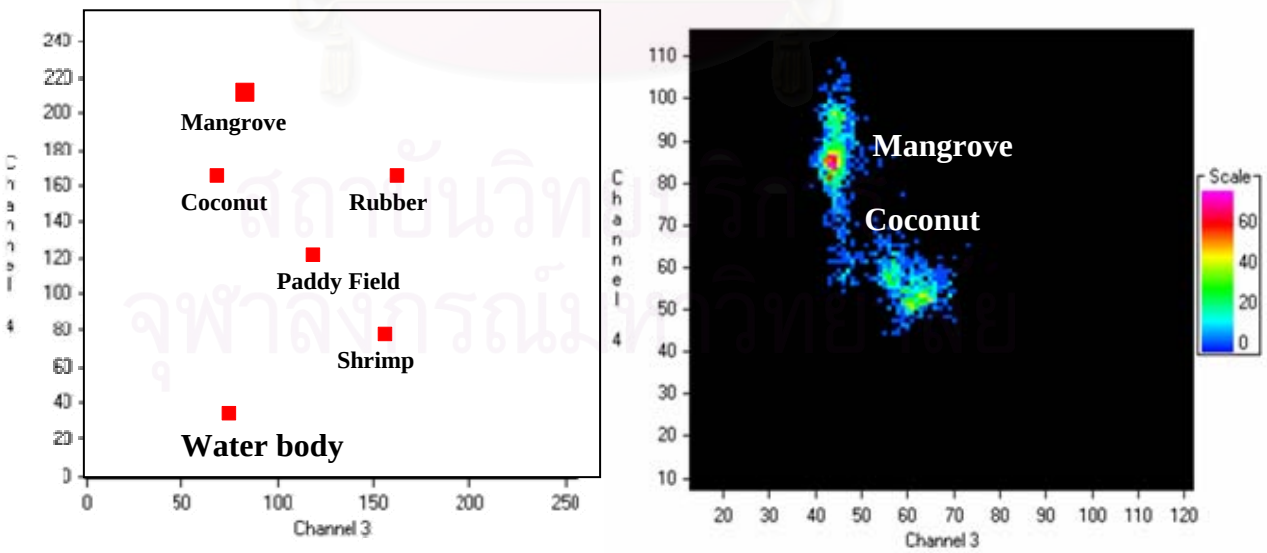

20a) Hypothetical plot **20b) Feature space plot**

Fig 20 Hypothetical and feature space plot of classification categories.

2.4.3 Masking of cloud and shadow areas

The LANDSAT images cloud-covered and cloud shadowed areas, the latter enlarged because of the South of Thailand climate in tropical rain forest (always cover by cloud). As no information could be extracted from these areas, they were masked and classified as cloud area (merge cloud and shadows together).

2.4.4 Image classification

The intent of the classification process is to categorize all pixels in a digital image into one of several land cover classes or themes. This categorized data set will then be used to produce thematic maps of land cover present in an image. Thematic map provides an easily interpretable summary with which the eventual end user can make informed decisions.

In conventional classification of multi spectral data, the maximum likelihood classifier is considered to provide the best results since it takes into account the shape, size and orientation of a cluster. Based on the class mean and the variance-covariance matrix, an unknown pixel is assign to the most likely class.

Maximum likelihood classification (MLC) technique was employed to perform the classification of an unknown pixel. This technique has been found to be the most accurate procedure in quantitatively evaluate both the variance and correlation of the category spectral reflectance patterns. The land cover/land use was classified into twelve categories, based on vegetative characteristics.

This technique calculates the distance from each feature vector (pixel to be classified) to class means. The within-class variability is taken care of by adding a factor, which is a function of the variance-covariance matrix of that class. The formula used (Mather, 1987) reads:

$$D_i (x) = \ln |V_i| + (X-M_i)^T V_i^{-1} (X-M_i) \qquad \text{(Eq 4)}$$

In which; D_i (X) = distance between pixel vector X and a class means based on probabilities; X mea pixel vector X; M_i = mean vector of the class considered; V_i = the variance-covariance matrix of the class considered; V_i^{-1} = the inverse of Vi; |Vi| = determinant of the variance-covariance matrix Vi; (X- Mi) = the distance towards a class means' and $(X-M_i)$ = the transportation of $(X-M_i)$

During classification, the shortest distance to a class mean we founded and the pixel is class-labeled if the distance is smaller than the threshold value. The reasons for using this classification system for land cover/land use were as follows:

The major land use on this study area was rubber plantations and paddy fields. Rubber trees were planted in rows and usually had areas under their canopies cleared. This is different from natural forest where multi-levels of plant structures are usual. Forest in this study area is very complex. Although different plant species have different signature, classification of natural forest at the species level is not possible.

Therefore areas mostly cover with natural trees were simply classified as forests. Areas mostly cleared of vegetation can be considered as barren land or bare soil. In this, areas which are sparsely covered by trees (woody plants more than 2 m tall, with a single stem, or branches well above the base), shrubs (woody plants generally multi-stemmed at the base, and less than 2 m tall) and grasses (herbaceous plants, generally less than 2 m tall).

2.4.5 Post-processing

Following the classification process, the "island themes" may then be discovered. These are single pixel themes that are most likely classification errors. These island themes can be assigned the same gray level as their phenomenon-surrounding theme using a mode filter. The mode filter is a filter algorithm that replaces a pixel gray value with the mode of the gray levels within the filter windows surrounding the pixel. This research applied mode filter with 5x5 windows size to reduce the island themes.

2.5 Groundtruth Data

The field surveys were conducted on October 12-13 2002 and March 26-27, 2003 to observe and collect information on land cover/land use classes. These groundtruth data were shown in Figs. 21 to 28.

สถาบันวิทยบริการ
จุฬาลงกรณ์มหาวิทยาลัย

Fig.21 Mangrove at Kradae River Mouth on 26 March 2003.

Fig.22 Shrimp pond on 26 March 2003.

Fig.23 Coconut plantation on 26 March 2003.

Fig.24 Barren and inundated area on 26 March 2003.

Fig. 25 Urban area on 26 March 2003.

Fig 26 Rubber plantation on 13 October 2002.

Fig. 27 Oil Palm plantation on 13 October 2002.

Fig.28 Paddy Field on 13 October 2002.

Chapter 3
Results and Discussions

3.1 Results from Remote Sensing Data

3.1.1 Classification Results from Landsat Data.

The land cover/land use classification of Ban Don Bay coastal area is presented in Tables 10 and 11 and Figs. 29. Land cover/land use pattern can be classified into 12 categories.

Land use in 1998 was largely agricultural land which is mainly land for rubber, coconut and oil palm plantations and paddy fields. Small amounts of land have been used for residential, commercial and industry. Mangrove forest occupies an area of 17 km^2 and shrimp farm area is 109.5 km^2.

Coastal development is a major force for the loss of mangrove area. The total population of Surat Thani has grown steadily over the years from 588,400 in 1980 to 816,400 in 1990, and to 920,283 in the year 2002 (Department of Provincial Administration). The coastal resources of Ban Don Bay are heavily utilized for economic development, particularly land reclamation and development for agriculture, aquaculture and human settlement. In the past five years, a lot of the mangrove forest and inundated area in the coastal zone has been converted to both shrimp farms and/or other uses. Land for rubber and oil palm plantations, as well as rice fields have been found to increase whereas that for coconut plantations (or mixed orchards) was decreased in area.

Mangrove forest depletion, as well as shrimp farm expansion can be determined by comparison of data from the present study with the previous mangrove forest studies (Siripong et al., 1996; Charuppat and Charuppat, 1997; Havanond, 1997). However, since our study area, which covered an area from Chaiya to Karnchanadit, is smaller than that of Charuppat and Charuppat (1997) but larger than that of Siripong et al. (1996), it is not that straight forward in trying to compare the data. It is possible, however, to compare the two sets of data namely Surat Thani and Ban Don Bay separately. The rate of mangrove depletion in Surat Thani from the period of 1979 to 1989 was 31.4% or 172 ha/year. The rate of depletion was less (16.8%) during the period of 1989 -1996, being 10-150 ha/year.

Land use in 1998 was largely agricultural land which is mainly land for rubber, coconut and oil palm plantations and paddy fields (Table 12).

For Ban Don Bay, it was found that during 1973 to 1984 mangrove depletion rate was 45.8% or at a rate of 210 ha/year (Siripong et al, 1993).

The depletion was lower (15%) between the year 1984 to 1993; being 45 ha/year. However, the rate of depletion was increased again to 31% (or 145

Table 10 Classification of land cover/land use in Ban Don Bay coastal area from 1988-2002 (in frequency and %).

Categories	**March 30, 1988**		**March 17, 1989**		**March 28, 1993**		**December 12, 1994**	
	Frequency	**%**	**Frequency**	%	**Frequency**	**%**	**Frequency**	**%**
Forest	24,124.12	0.60	20,103.44	0.50	20,103.44	0.50	18,093.09	0.45
Mangrove	28,144.81	0.70	30,155.15	0.75	23,319.98	0.58	23,319.98	0.58
Rubber	482,482.44	12.00	510,627.25	12.70	593,855.47	14.77	648,134.74	16.12
Coconut	201,034.35	5.00	241,241.22	6.00	180,930.92	4.50	176,910.23	4.40
Oil palm	120,620.61	3.00	128,661.98	3.20	140,724.05	3.50	136,703.36	3.40
Paddy field	321,654.96	8.00	329,696.33	8.20	414,532.83	10.31	402,068.70	10.00
Shrimp	96,496.49	2.40	98,104.76	2.44	152,786.11	3.80	140,724.05	3.50
Urban area	40,608.94	1.01	44,227.56	1.10	50,258.59	1.25	52,268.93	1.30
Water	40,206.87	1.00	120,620.61	3.00	24,124.12	0.60	28,144.81	0.70
Cloud	60,310.31	1.50	80,413.74	2.00	52,268.93	1.30	160,827.48	4.00
Barren land	71,970.30	1.79	486,905.20	12.11	799,714.64	19.89	665,423.70	16.55
Others	1,527,861.06	38.00	1,527,861.06	38.00				
Total	***4,020,687***	***100.00***	***4,020,687***	***100.00***	***4,020,687***	***100.00***	***4,020,687***	***100.00***

Categories	**February 17, 1996**		**June 11, 1997**		**April 27, 1998**		**January 8, 1999**	
	Frequency	**%**	**Frequency**	**%**	**Frequency**	**%**	**Frequency**	**%**
Forest	18,093.09	0.45	17,288.95	0.43	19,299	0.48	18,495.16	0.46
Mangrove	22,515.85	0.56	21,711.71	0.54	23,320	0.58	22,917.92	0.57
Rubber	339,748.05	8.45	589,030.65	14.65	998,337	14.84	620,794.07	15.44
Coconut	166,858.51	4.15	171,683.33	4.27	177,312	4.41	178,920.57	4.45
Oil palm	112,579.24	2.8	138,713.70	3.45	138,312	3.44	137,105.43	3.41
Paddy field	258,530.17	6.43	484,090.71	12.04	366,285	9.11	412,924.55	10.27
Shrimp	119,816.47	2.98	141,528.18	3.52	149,570	3.72	151,579.90	3.77
Urban area	46,237.90	1.15	53,877.21	1.34	48,650	1.21	49,454.45	1.23
Water	17,288.95	0.43	32,165.50	0.8	21,712	0.54	18,897.23	0.47
Cloud	42,217.21	1.05	126,249.57	3.14	49,052	1.22	46,237.90	1.15
Barren land	199,828.14	4.97	571,339.62	14.21	294,716	17.32	140,724.05	3.5
Others	1,573,696.89	39.14	1,572,490.69	39.11	1,529,067	38.03	1,573,696.89	39.14
Total	***4,020,687***	***100.00***	***4,020,687***	***100.00***	***4,020,687***	***100.00***	***4,020,687***	***100.00***

Categories	**April 12, 2000**		**December 4, 2000**		**January 6, 2002**	
	Frequency	**%**	**Frequency**	**%**	**Frequency**	**%**
Forest	17,288.95	0.43	18,495.16	0.46	16,484.82	0.41
Mangrove	21,711.71	0.54	22,515.85	0.56	22,113.78	0.55
Rubber	580,989.27	14.45	609,536.15	15.16	488,111.40	12.14
Coconut	174,497.82	4.34	178,920.57	4.45	170,879.20	4.25
Oil palm	139,115.77	3.46	156,404.72	3.89	156,002.66	3.88
Paddy field	395,635.60	9.84	368,294.93	9.16	385,985.95	9.6
Shrimp	155,600.59	3.87	155,198.52	3.86	156,404.72	3.89
Urban area	49,856.52	1.24	50,660.66	1.26	52,671.00	1.31
Water	20,505.50	0.51	24,124.12	0.6	26,134.47	0.65
Cloud	46,237.90	1.15	45,835.83	1.14	51,062.72	1.27
Barren land	240,839.15	5.99	254,509.49	6.33	823,436.70	20.48
Others	1,565,655.52	38.94	1,567,263.79	38.98	1,572,490.69	39.11
Total	***4,020,687***	***100.00***	***4,020,687***	***100.00***	***4,020,687***	***100.00***

Table 11 Classification of land cover/land use in Ban Don Bay coastal area from 1988-2002 (in km^2 and Rai).

Categories	March 30, 1988		March 17, 1989		March 28, 1993		December 12, 1994	
	area (km^2)	area (rai) *	area (km^2)	area (rai)	area (km^2)	area (rai)	area (km^2)	area (rai)
Forest	15.08	9,423	12.56	7,853	12.56	7,853	11.31	7,068
Mangrove	17.59	10,994	18.85	11,779	14.57	9,109	14.57	9,109
Rubber	287.73	179,832	319.14	199,464	371.16	231,975	405.08	253,178
Coconut	125.65	78,529	150.78	94,235	113.08	70,676	110.57	69,106
Oil palm	79.16	49,473	80.41	50,259	87.95	54,970	85.44	53,400
Paddy field	201.03	125,646	206.06	128,788	259.08	161,927	251.29	157,058
Shrimp	60.31	37,694	61.32	38,322	95.49	59,682	87.95	54,970
Urban area	25.38	15,863	27.64	17,276	31.41	19,632	32.67	20,418
Water	35.43	22,145	75.39	47,117	15.08	9,423	17.59	10,994
Cloud	37.69	23,559	50.26	31,412	32.67	20,418	100.52	62,823
Barren land	44.73	27,956	304.32	190,197	499.82	312,389	415.89	259,931
Others	954.91	596,821	954.91	596,821				
Total	***2,512.93***	***1,570,581***	***2,512.93***	***1,570,581***	***2,512.93***	***1,570,581***	***2,512.93***	***1,570,581***

Categories	February17, 1996		June 11,1997		April 27,1998		January8,1999	
	area (km^2)	area (rai)	area (km^2)	area (rai)	area (km^2)	area (rai)	area (km^2)	area (rai)
Forest	11.31	7,068	10.81	6,753	15.08	9,423	11.56	7,225
Mangrove	14.07	8,795	13.57	8,481	17.59	10,994	14.32	8,952
Rubber	212.34	132,714	368.14	230,090	287.73	179,832	388.00	242,498
Coconut	104.29	65,179	107.30	67,064	125.65	78,529	111.83	69,891
Oil palm	70.36	43,976	86.70	54,185	79.16	49,473	85.69	53,557
Paddy field	161.58	100,988	302.56	189,098	201.03	125,646	258.08	161,299
Shrimp	74.89	46,803	88.46	55,284	60.31	37,694	94.74	59,211
Urban area	28.90	18,062	33.67	21,046	25.38	15,863	30.91	19,318
Water	10.81	6,753	20.10	12,565	35.43	22,145	11.81	7,382
Cloud	26.39	16,491	78.91	49,316	37.69	23,559	28.90	18,062
Barren land	124.89	78,058	357.09	223,180	44.73	27,956	87.95	54,970
Others	983.56	614,725	982.81	614,254	954.91	596,821	983.56	614,725
Total	***2,512.93***	***1,570,581***	***2,512.93***	***1,570,581***	***2,512.93***	***1,570,581***	***2,512.93***	***1,570,581***

Categories	April 12, 2000		December 4, 2000		January 6, 2002	
	area (km^2)	area (rai)	area (km^2)	area (rai)	area (km^2)	area (rai)
Forest	10.81	6,753	11.56	7,225	10.30	6,439
Mangrove	13.57	8,481	14.07	8,795	13.82	8,638
Rubber	363.12	226,949	380.96	238,100	305.07	190,669
Coconut	109.06	68,163	111.83	69,891	106.80	66,750
Oil palm	86.95	54,342	97.75	61,096	97.50	60,939
Paddy field	247.27	154,545	230.18	143,865	241.24	150,776
Shrimp	97.25	60,781	97.00	60,624	97.75	61,096
Urban area	31.16	19,475	31.66	19,789	32.92	20,575
Water	12.82	8,010	15.08	9,423	16.33	10,209
Cloud	28.90	18,062	28.65	17,905	31.91	19,946
Barren land	150.52	94,078	159.07	99,418	514.65	321,655
Others	978.53	611,584	979.54	612,212	982.81	614,254
Total	***2,512.93***	***1,570,581***	***2,512.93***	***1,570,581***	***2,512.93***	***1,570,581***

Note: 6.25 rai equals 1 hectare

Table 12 Classification of land cover/land use in Ban Don Bay from previous studies.

Categories	1993 ✞		1998 ✡	
	area (km^2)	area (rai)	area (km^2)	area (rai)
Forest	6.86	4,287.50	5.83	3,643.75
Mangrove	23.32	14,575.0	16.07	10,043.75
Rubber	168.04	105,025.0	363.35	227,093.7
Coconut	161.14□	100,712.5	110.31	68,943.75
Oil palm	0.65	406.25	42.10	26,312.5
Paddy field	140.82	88,012.50	188.30	117,687.5
Shrimp	64.56	40,350.0	80.88	50,550.0
Urban area	19.10	11,937.50	26.77	16,731.25
Water				
Cloud				
Barren land	61.47□□	38,418.75	20.50	12,812.5
Others				

Note: ✞. from Siripong et al.(1996)
✡. from Sawangphol and Watayakorn (1999)
□ classified as mixed orchards
□□ classified as Inundated areas.

The area of 6.25 Rai equals 1 hectare.

ha/year) during the last five years (1993 -1998), this probably is due to the booming of the "Shrimp-culture Fever" in Thailand as a whole. Hence, the mangrove forest area of Ban Don Bay has been deteriorated by 68% (or 3,452 ha) in the last 25 years (1973 - 1998), with the average rate of depletion of 138 ha per year (Siripong et al., 1996; Charuppat and Charuppat, 1997; Havanond, 1997).

Since mangrove forest is one of the most valuable resources of Ban Don Bay, the need to maintain the mangrove forest as nursery ground for marine life has to be balanced against the use of the area for shrimp farming. Shrimp farms can be sustainable, but need to be highly managed. The mangrove areas need to be preserved or replanted to support its various ecological functions.

The El Niño years caused some less agricultural land areas due to the longer dry season and Laña years caused some more productive land areas due to more wetter season.

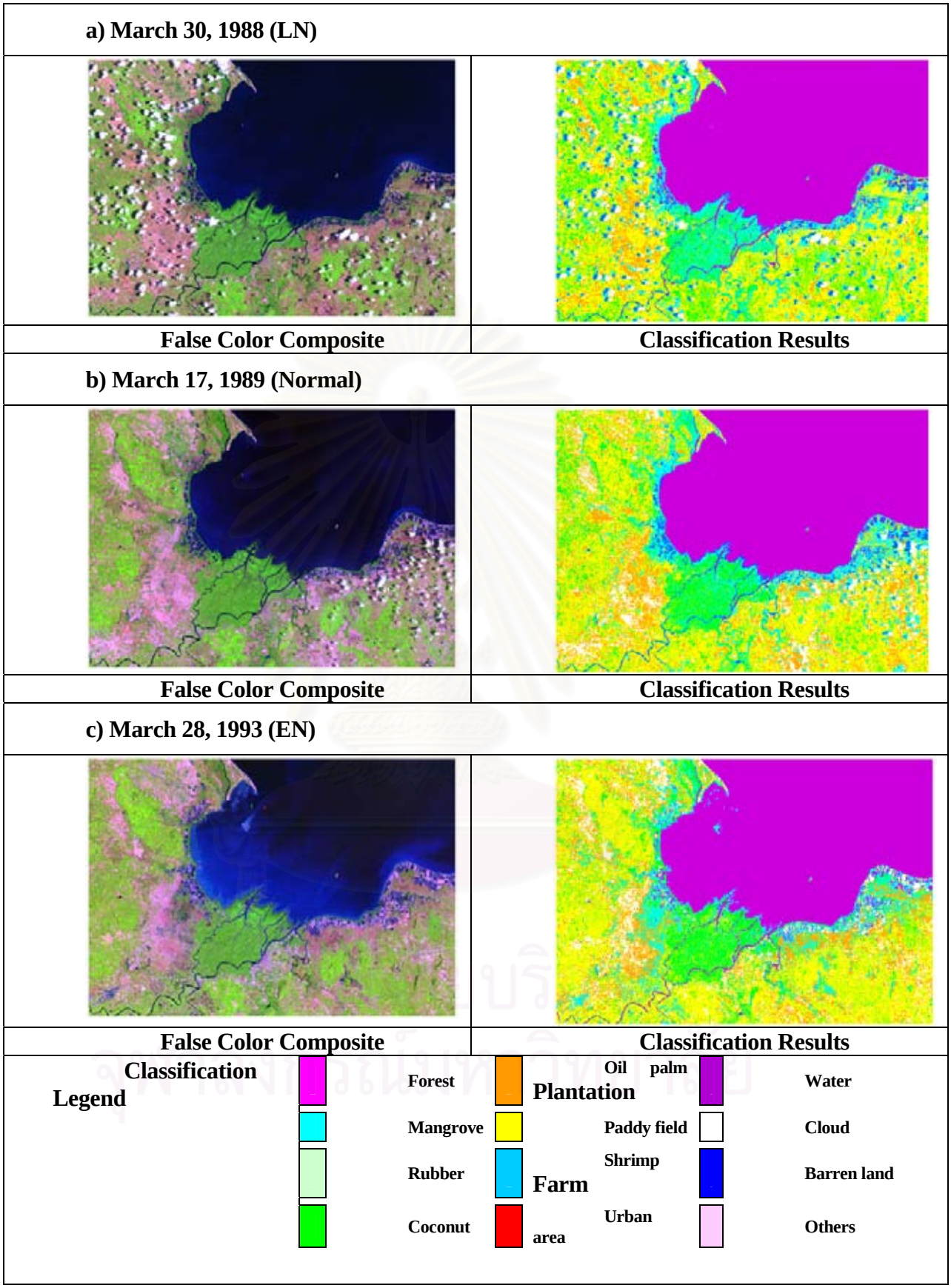

Fig. 29 Comparison between false color composite (Left) of Landsat imageries (RGB = 543) and land use classification results (Right).

d) December 12, 1994 (EN)

False Color Composite

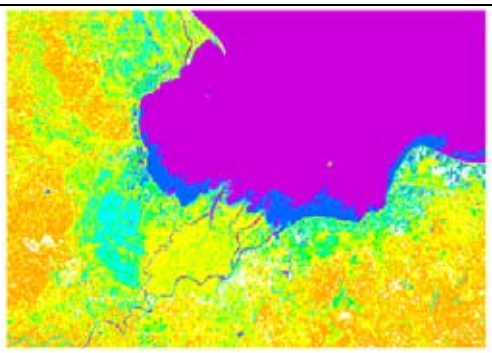

Classification Results

e) February17, 1996 (Normal)

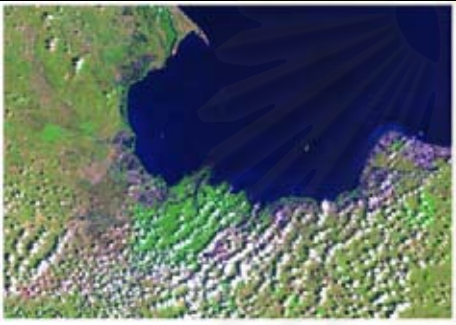

False Color Composite

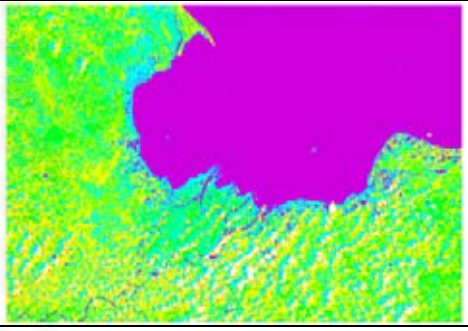

Classification Results

f) June 11,1997 (EN)

False Color Composite

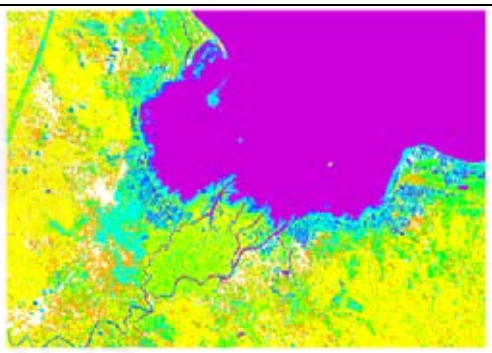

Classification Results

Classification Legend

- Forest
- Mangrove
- Rubber
- Coconut
- Oil palm Plantation
- Paddy field
- Shrimp Farm
- Urban area
- Water
- Cloud
- Barren land
- Others

Fig. 29 (cont'd) Comparison between false color composite (Left) of Landsat imageries (RGB = 543) and land use classification results (Right)

g) April 27,1998 (LN)

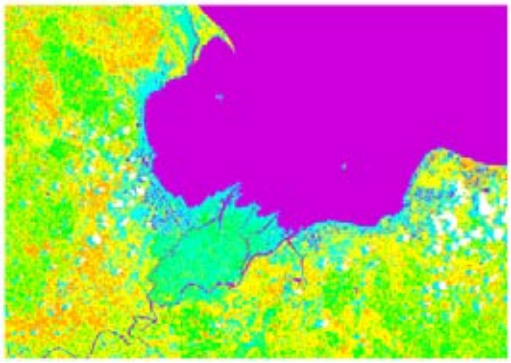

False Color Composite | **Classification Results**

h) January 8,1999 (Normal)

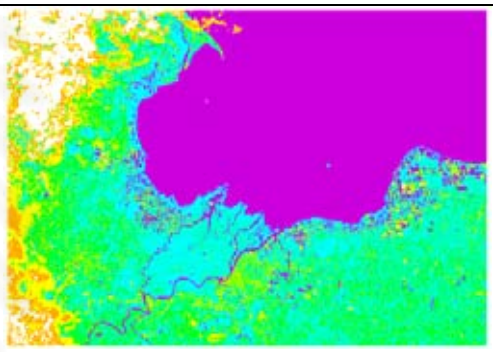

False Color Composite | **Classification Results**

i) April 12, 2000)

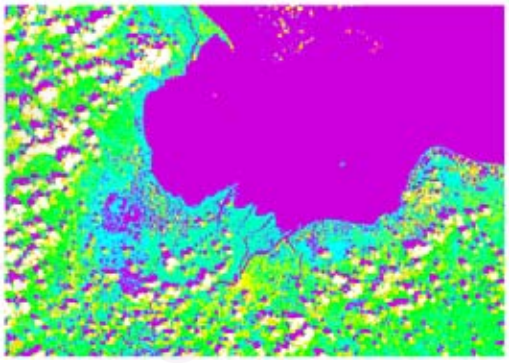

False Color Composite | **Classification Results**

Classification Legend

Forest	Oil palm Plantation	Water
Mangrove	Paddy field	Cloud
Rubber	Shrimp Farm	Barren land
Coconut	Urban area	Others

Fig. 29 (Cont'd) Comparison between false color composite (Left) of Landsat imageries (RGB = 543) and land use classification results (Right)

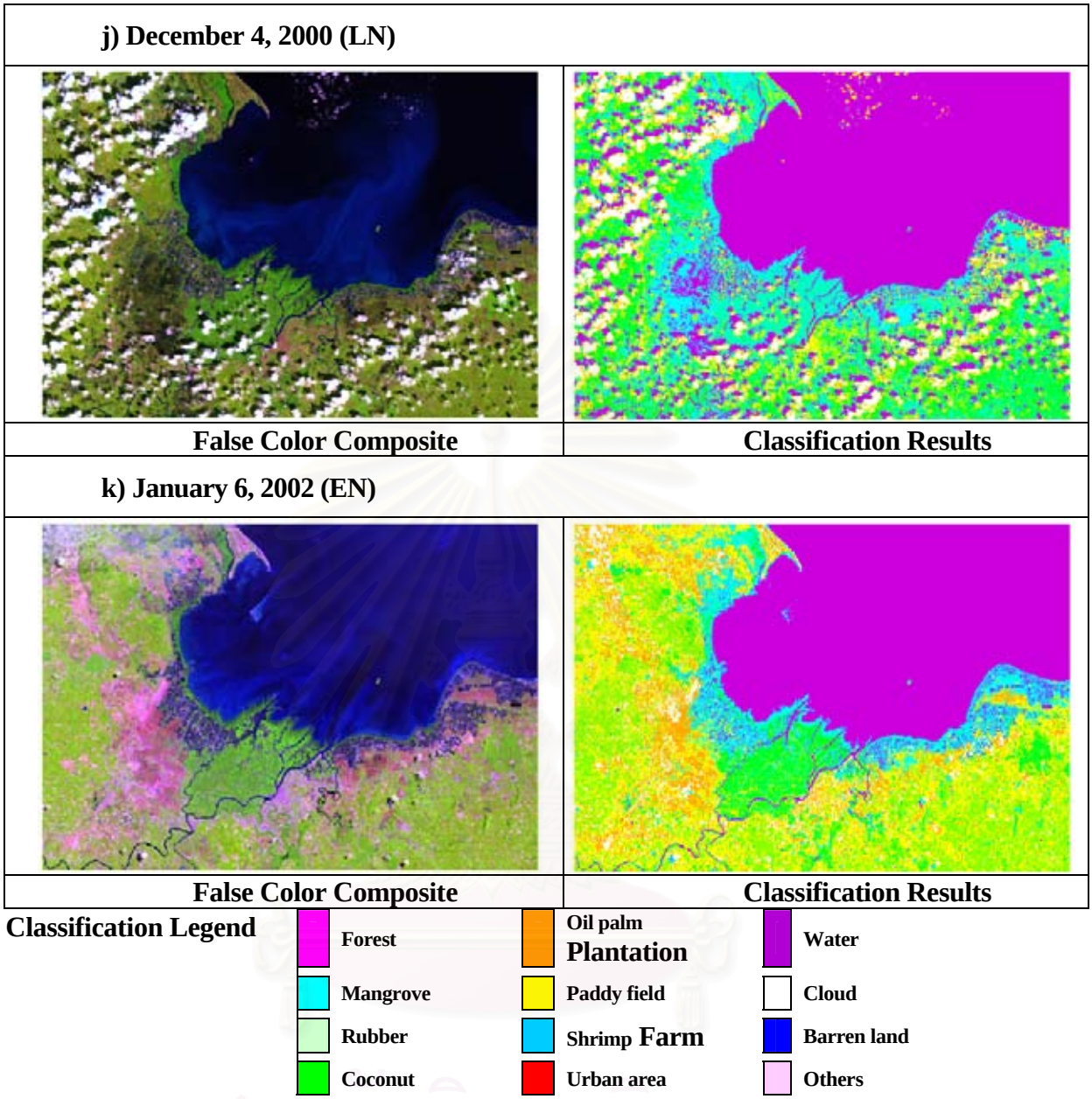

Fig. 29 (Cont'd) Comparison between false color composite (Left) of Landsat imageries (RGB = 543) and land use classification results (Right)

3.1.2 NDVI

Over the past few decades, a number of vegetation indices have been developed and used for monitoring of vegetation structured and function (Xiao et al , 2003). To determine the density of green on a patch of land, researchers must observe the distinct colors (wavelengths) of visible and near-infrared sunlight reflected by the plants. As can be seen through a prism, many different wavelengths make up the spectrum of sunlight. When sunlight strikes

objects, certain wavelengths of this spectrum are absorbed and other wavelengths are reflected. The pigment in plant leaves, chlorophyll, strongly absorbs visible light (from 0.4 to 0.7 μm) for use in photosynthesis. The cell structure of the leaves, on the other hand, strongly reflects near-infrared light (from 0.7 to 1.1 μm). The more leaves a plant has, the more these wavelengths of light are affected, respectively.

Among these, Normalized Different Vegetation Index (NDVI), which uses spectral information in red and near infrared bands, is the most widely used, Case studies of NDVI as a remote sensing proxy for various characteristics of terrestrial vegetation include net primary production (Tucker and Sellers, 1986), growing season length (Myneni et al, 1997), fire, land use and land cover change (Potter et al, 1993), and biogeochemical modeling.

Nearly all satellite Vegetation Indices employ this difference formula to quantify the density of plant growth on the Earth — near-infrared radiation minus visible radiation divided by near-infrared radiation plus visible radiation. The result of this formula is called the Normalized Difference Vegetation Index (NDVI). Written mathematically, the formula is:

$$NDVI = \frac{NIR - VIS}{NIR + VIS} \qquad \text{(Eq. 5)}$$

NDVI is calculated from the visible and near-infrared light reflected by vegetation. Healthy vegetation (left) absorbs most of the visible light that hits it, and reflects a large portion of the near-infrared light. Unhealthy or sparse vegetation (right) reflects more visible light and less near-infrared light. The numbers on the figure above are representative of actual values, but real vegetation is much more varied. (Fig 30). Calculations of NDVI for a given pixel always result in a number that ranges from minus one (-1) to plus one (+1); however, no green leaves gives a value close to zero. A zero means no vegetation and close to +1 (0.8 – 0.9) indicates the highest possible density of green leaves.

According to the IPCC (2001), the atmospheric concentration of CO_2 has increased by 31% since 1750 (Fig 31). Accompanied by a 0.6ºC increase in temperature over the past century (IPCC, 2001), these two factors alter the pattern, rate, and type of global vegetation growth. This has agricultural implications on the types of crops that can be grown in an area as well as their condition due to temperature and moisture fluctuations. Ecologically, while boreal forests have a simpler biodiversity than rainforests, they also fluctuate due to changes in vegetation. The vegetation

affects climate via its albedo, surface roughness, transpiration, and respiration. Because climate affects vegetation, and vegetation affects climate, it is important to monitor vegetation other than the rainforest; this can be done by means of the normalized difference vegetation index (NDVI), a measure of the greenness of the Earth due to photosynthetic activity.

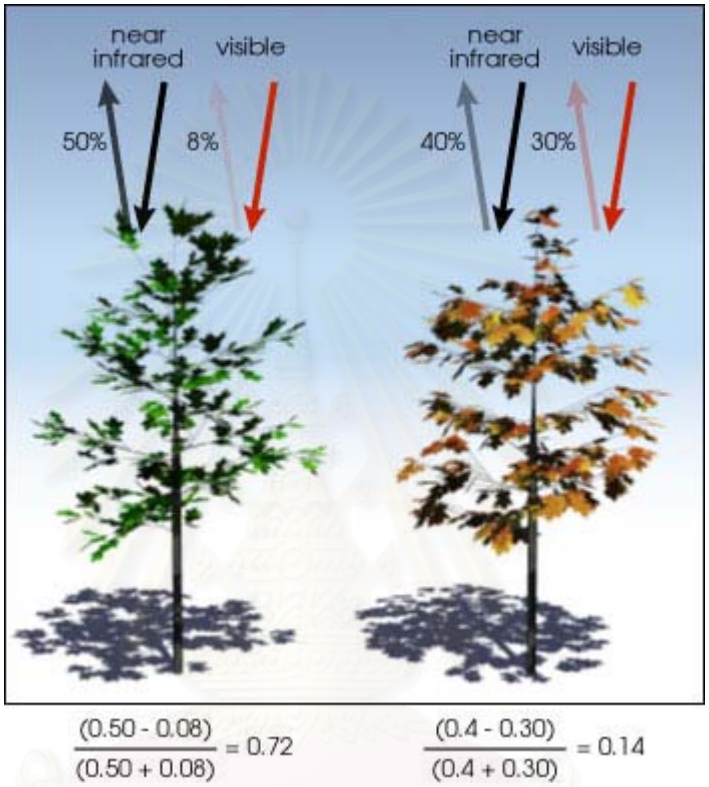

Fig 30 Comparison between NDVI of health tree (Left) and stress tree (Right) Source: (http://www.usgcrp.gov/ipcc/wg1spm.pdf)

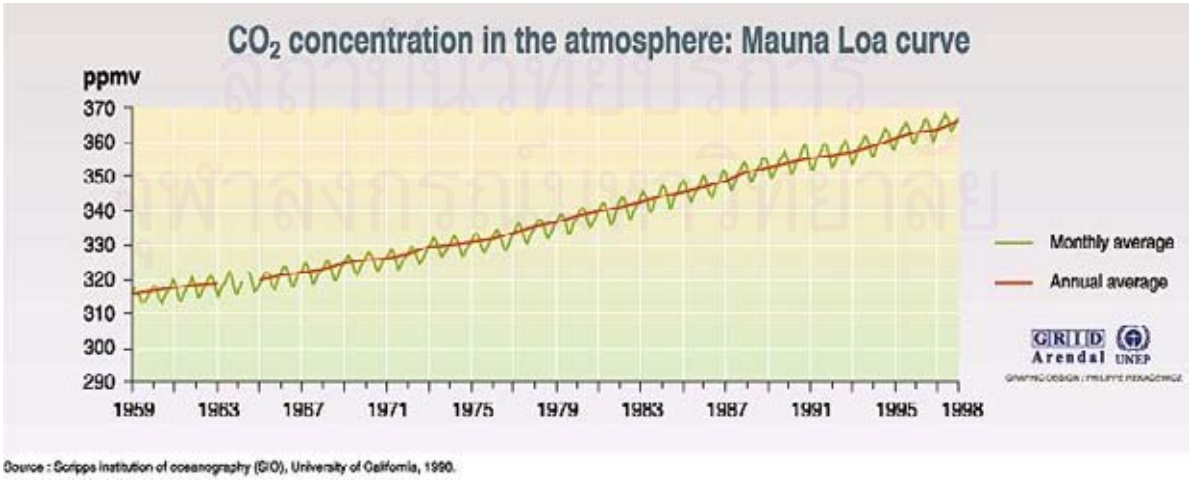

Fig.31. Trend of CO_2 concentration in the atmosphere at Mauna Loa Sattion.

Fig 32. Sampling area for study seasonal variation of NDVI. The box indicated for NDVI is extracted.

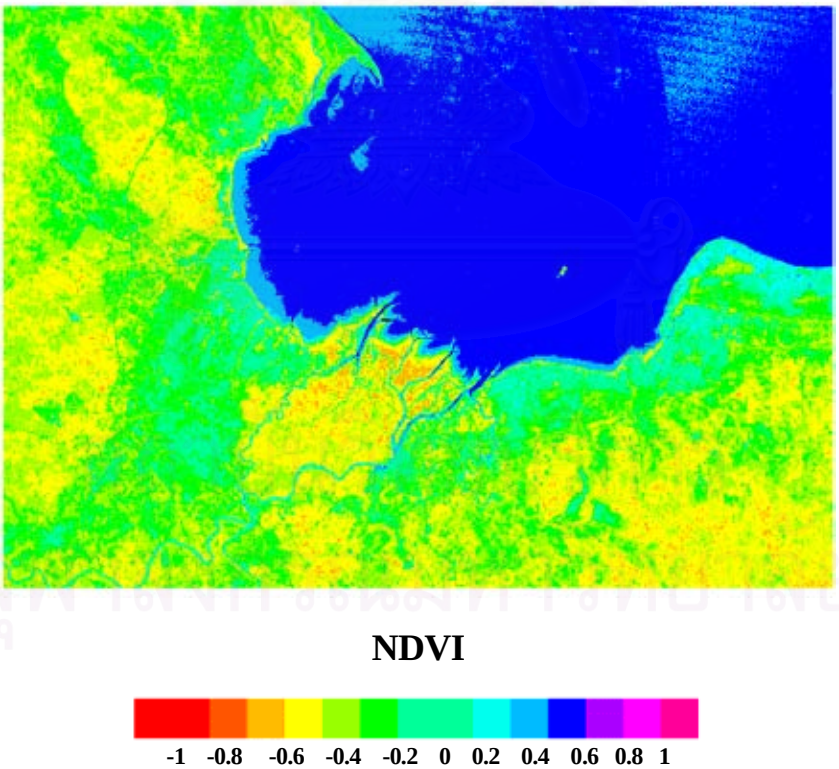

Fig. 33. Average NDVI.

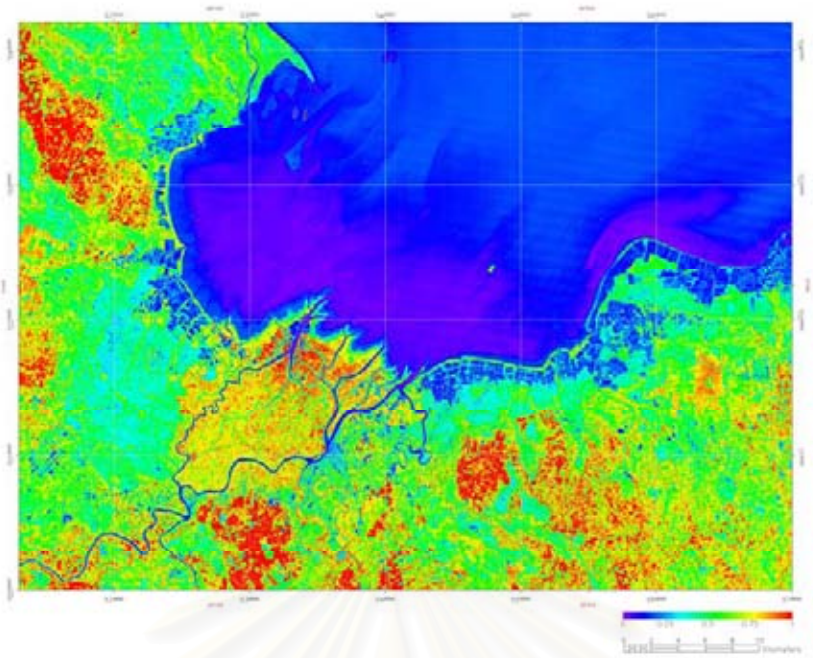

Fig.34a. NDVI on 28 March 1993 (El Niño)

Normally in March, rainfall is low (19.7 mm), air temperature is not very high (27.1^0 C) and low discharge(73.42 MCM). In 1993, air temperature, rainfall and runoff anomalies are plus.

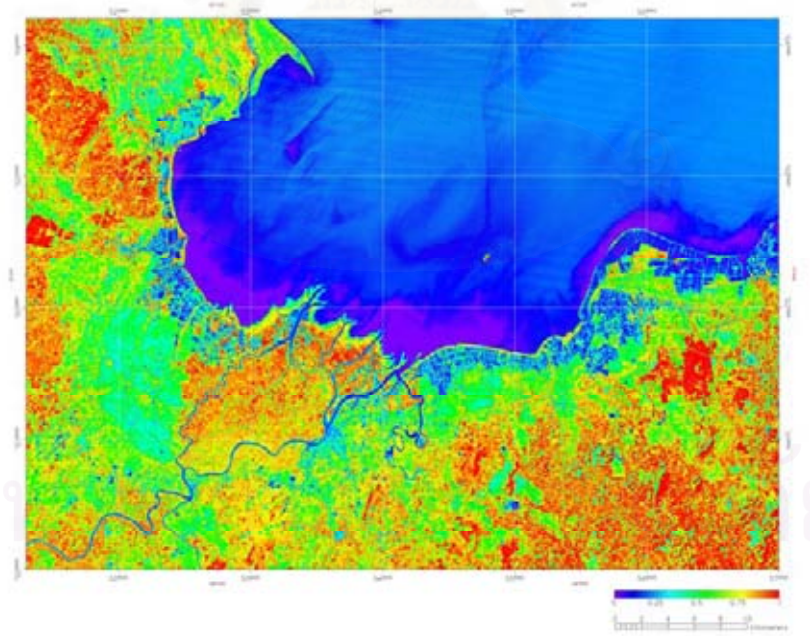

Fig.34b. NDVI on 12 December 1994 (El Niño).

Normally, in December, the air temperature is lowest in a year (25.2^0C), rainfall is rather low (152.9 mm) and river runoff is high (505.43 MCM), but this year is the El Niño year, the air temperature, rainfall and river runoff anomalies are plus.

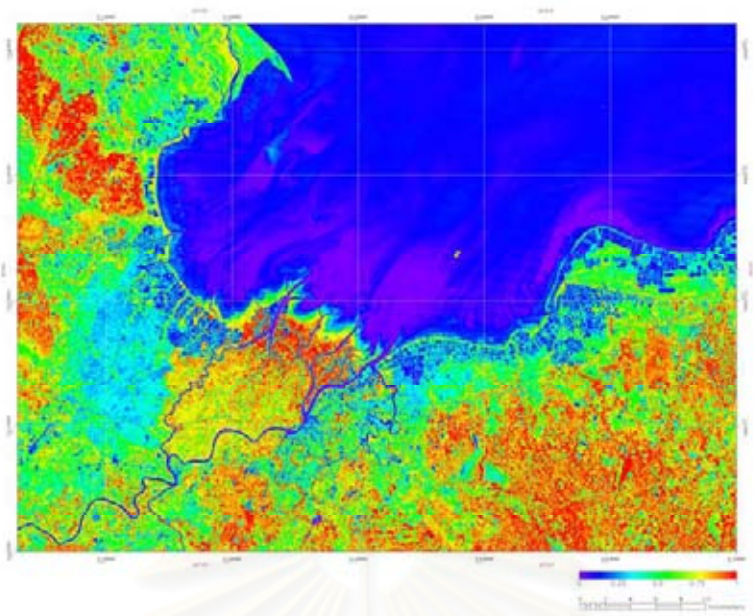

Fig. 34c. The NDVI on 11 June 1997 (El Niño).

Usually June is the month which the air temperature is lowering (27.1 ^{0}C), rainfall is increasing (138.1 mm) and river runoff is rising (208.77 MCM). In 1997, the air temperature and river runoff anomalies are plus, but rainfall anomaly is minus.

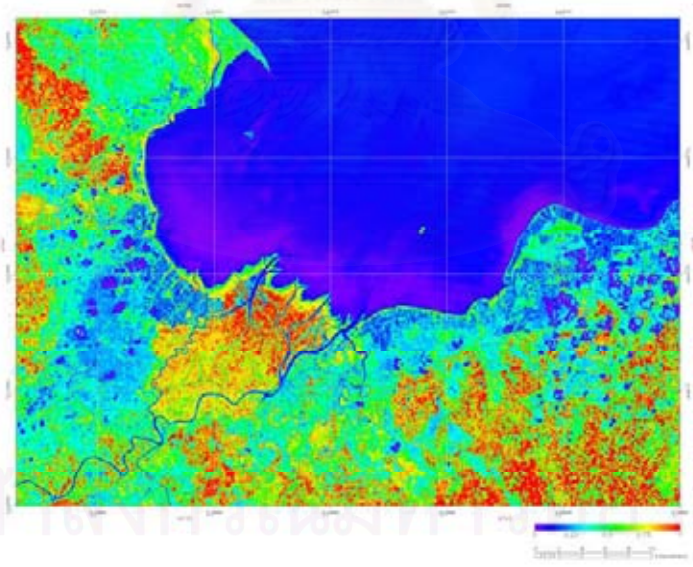

Fig..34d. The NDVI on 27 April 1998 (La Niña).

Normally, April is the hottest month in a year (28.0 ^{0}C), rainfall is low (60.4 mm) and river runoff is low (75.6 MCM). But 1998 is the La Niña year, the air temperature anomaly is much higher than normal, rainfall anomaly is minus and river runoff anomaly is a little higher than normal.

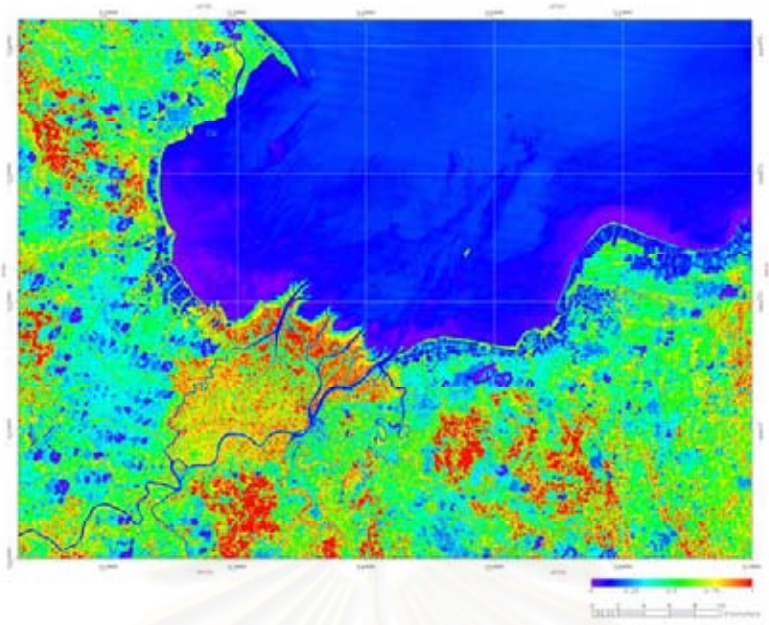

Fig.34e. The NDVI on 30 March 1988 (La Niña)

Usually in March, the air temperature is rising (27.1 ^{0}C), less rainfall (19.7 mm) and low river runoff (73.42 MCM), but this year is the La Niña year, the air temperature, rainfall and river runoff anomalies are higher than average.

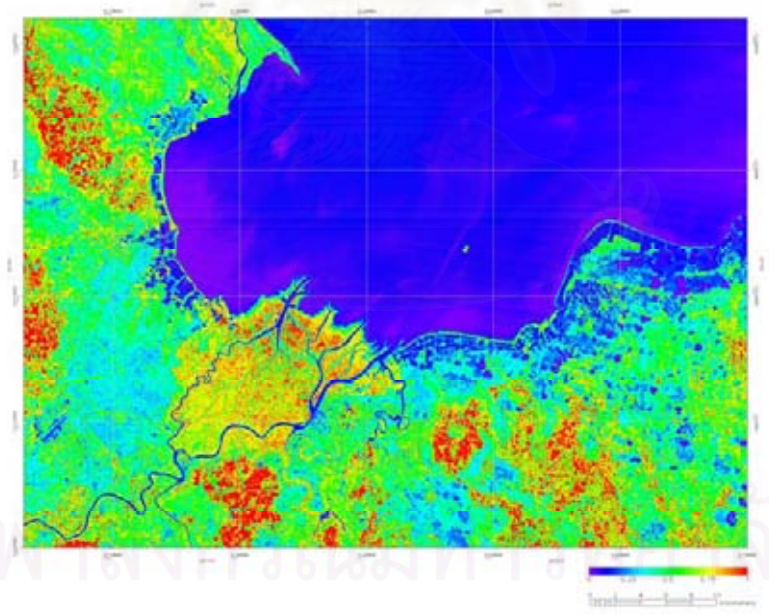

Fig.34f. The NDVI on 17 March 1989 (Normal).

Usually in March, the air temperature is rising (27.1 ^{0}C), less rainfall (19.7 mm) and low river runoff (73.42 MCM), but this year is the normal year, the air temperature anomaly is higher than average, but the rainfall and river runoff anomalies are less than average

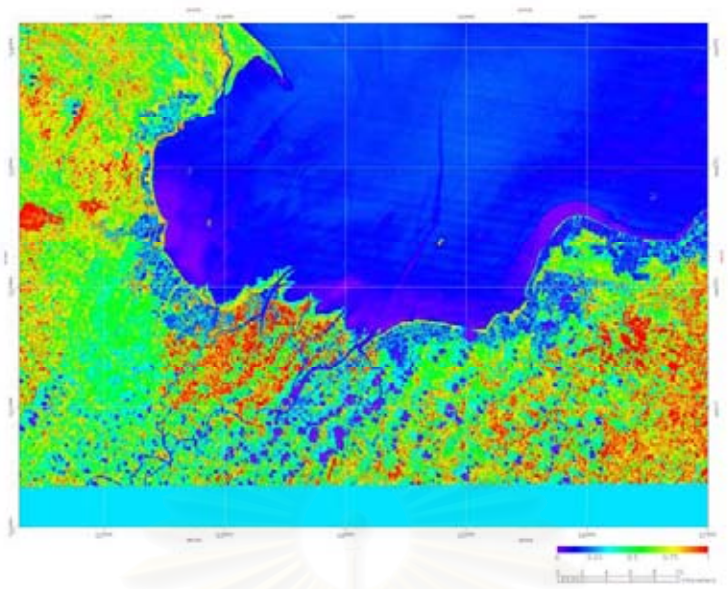

Fig.34g. The NDVI 17 February 1996 (Normal).

Usually, in this month, the air temperature is rising a little (26.0 C), least rainfall in a year (10.5 mm) and less river runoff (91.43 MCM), but for the normal year, the air temperature and rainfall anomalies are plus, but the river runoff anomaly is a little lower than average.

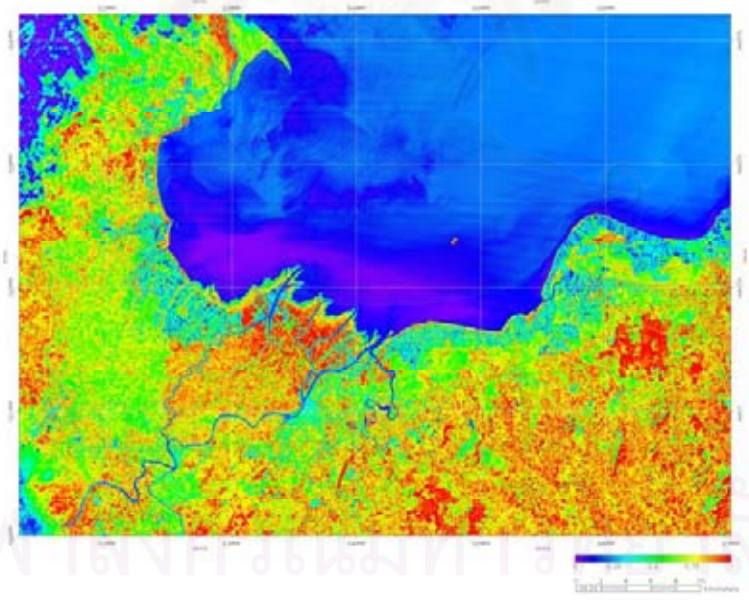

Fig.34h. The NDVI on 8 January 1999 (Normal).

Normally, in January, the air temperature is lowest in a year (25.2^0C), rainfall is low (50.9 mm) and river runoff is lowering (245.91 MCM). For this year as a normal year, the air temperature and rainfall anomalies are minus, but the river runoff anomaly is plus.

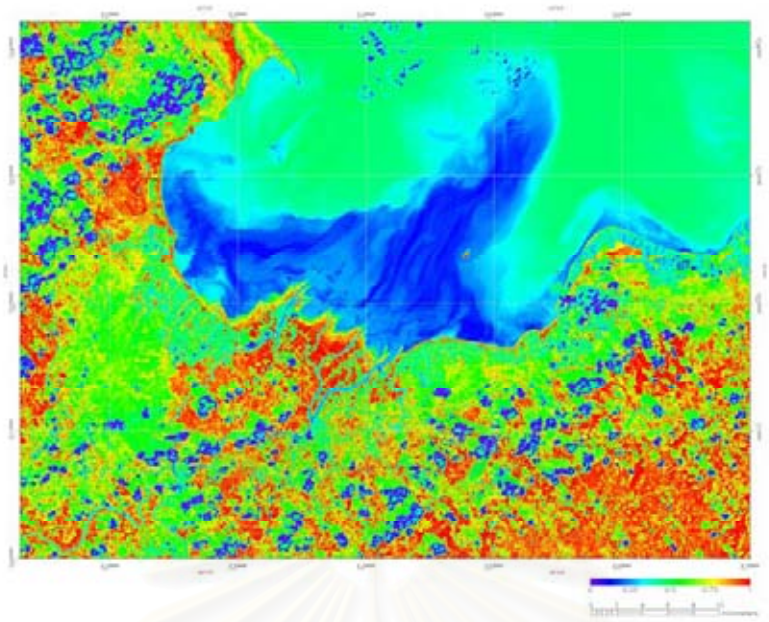

Fig.34i. The NDVI on 12 April 2000 (Strong La Niña).

Usually, April is the hottest month in a year (28.0 ^{0}C), rainfall is low (60.4 mm) and river runoff is low (75.6 MCM), but this year La Niña is very strong, the air temperature anomaly is plus and the river runoff anomaly is very high, but the rainfall is less than normal.

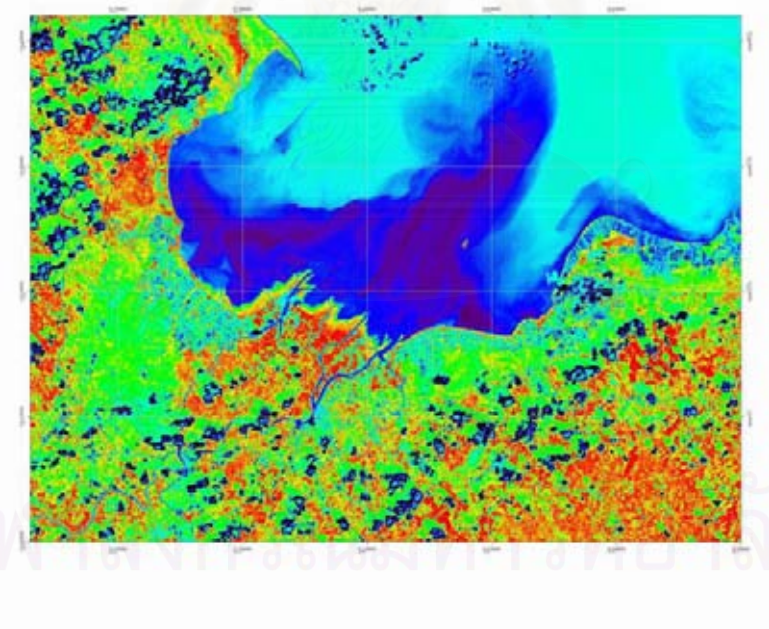

Fig. 34j. The NDVI on 4 December 2000 (Decline La Nina).

Usually, December is the coldest month in a year, as January (25.2 ^{0}C), but rainfall is higher than January (152.9 mm), the river runoff is low (245.91 MCM). In this year, the La Nina is declining, the air temperature is a little higher than normal, but the river runoff is much more higher than average, the rainfall is less than normal.

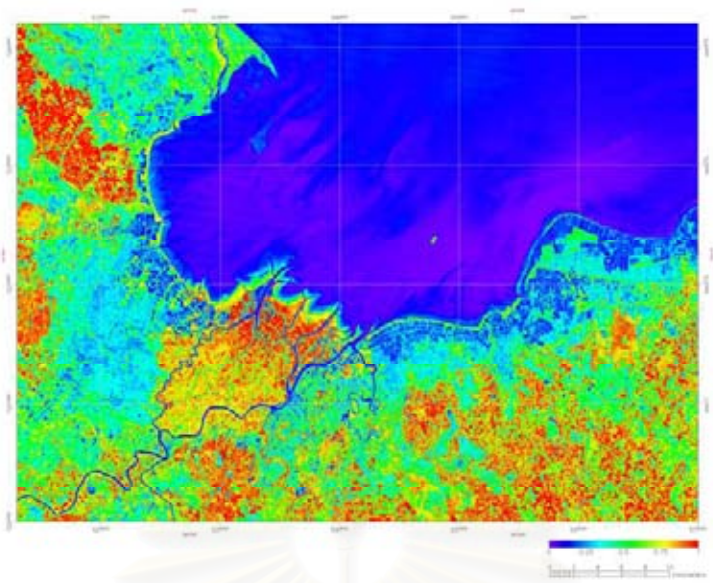

Fig.34k. The NDVI on 21 May 1995 (normal year).

Usually, in May, the air temperature is lower than(27.4^0 C) the hottest month of April, the rainfall increases (172.1 mm) and the river runoff is a little increase (145.4 MCM). In this normal year, the air temperature is higher than the average, but the rainfall and river runoff anomalies are less than the averages.

Comparison between color composite and NDVI Figs. 35 compared the false color composite and NDVI. We can see the meaning of vegetation condition in NDVI better than color composite.

Table 13 Computed statistic values of 11 NDVI classifications from Landsat imageries

Acquisition Date	NDVI Statistic Value			
	Minimum	Maximum	Average	S.D.
a) March 30, 1988	-1.000000	1.000000	-0.057823	0.437582
b) March 17, 1989	-0.866667	0.717647	-0.009657	0.365666
c) March 28, 1993	-1.000000	1.000000	-0.015477	0.425362
d) December 12, 1994	-1.000000	0.689655	0.014302	0.436832
e) February17, 1996	-1.000000	1.000000	0.000771	0.365594
f) June 11, 1997	-1.000000	1.000000	-0.073713	0.472504
g) April 27, 1998	-0.743590	0.690141	-0.016679	0.345569
h) January8, 1999	-1.000000	1.000000	0.002711	0.400699
i) April 12, 2000	-0.736842	0.579618	-0.158117	0.366898
j) December 4, 2000	-0.736842	0.579618	-0.158480	0.366796
k) January 6, 2002	-0.761905	0.628205	-0.076339	0.384647
Average	**-0.895077**	**0.807717**	**-0.049864**	**0.397104**

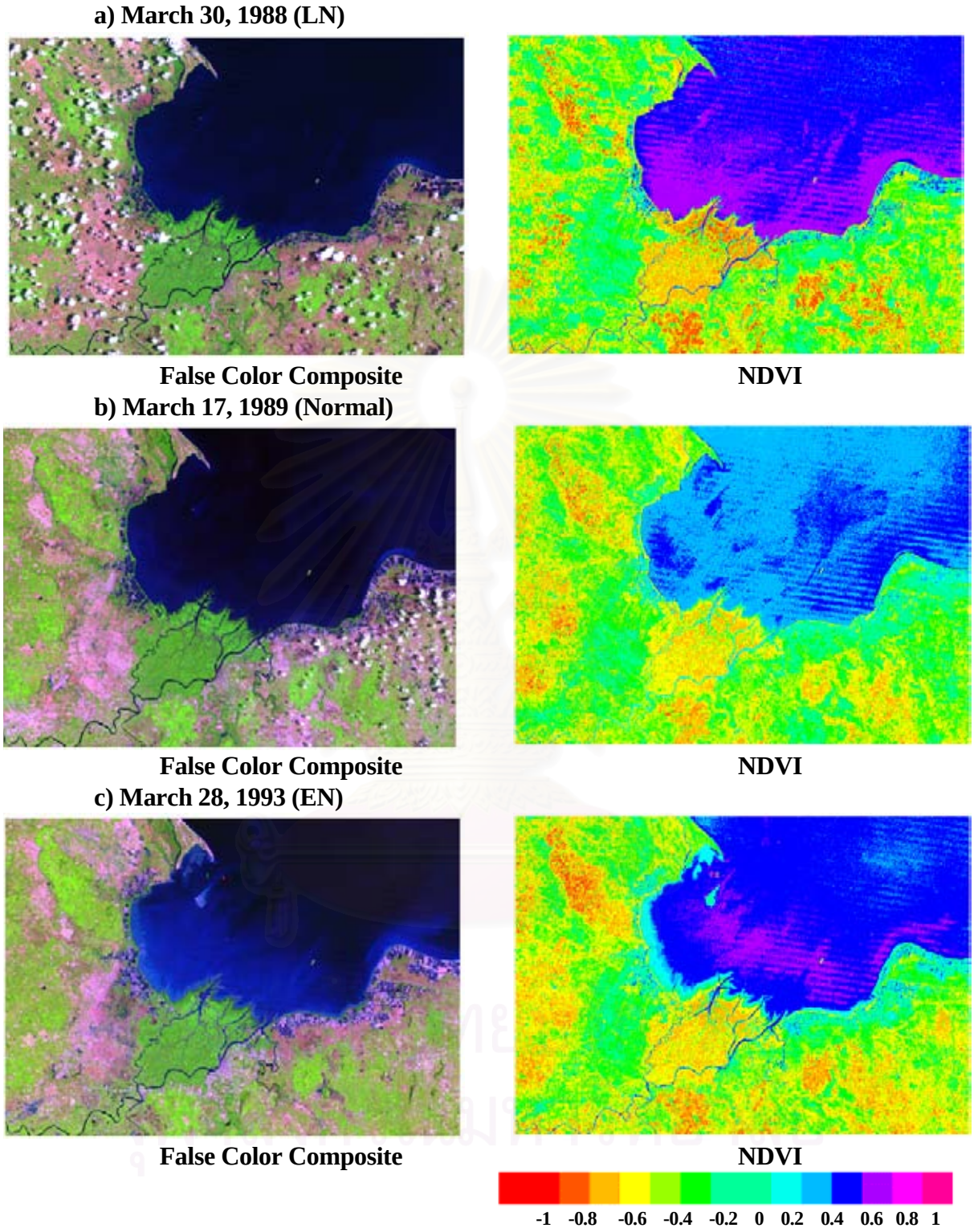

Fig. 35 Comparison between false color composite (Left) of Landsat imageries (RGB = 543) and Normalized Different Vegetation Index (NDVI) (Right)

d) December 12, 1994 (EN)

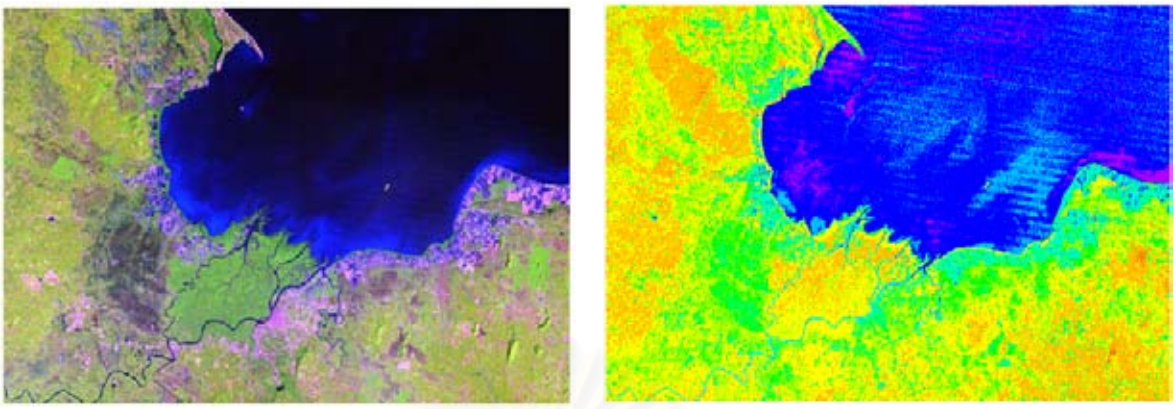

False Color Composite **NDVI**

e) February17, 1996 (Normal)

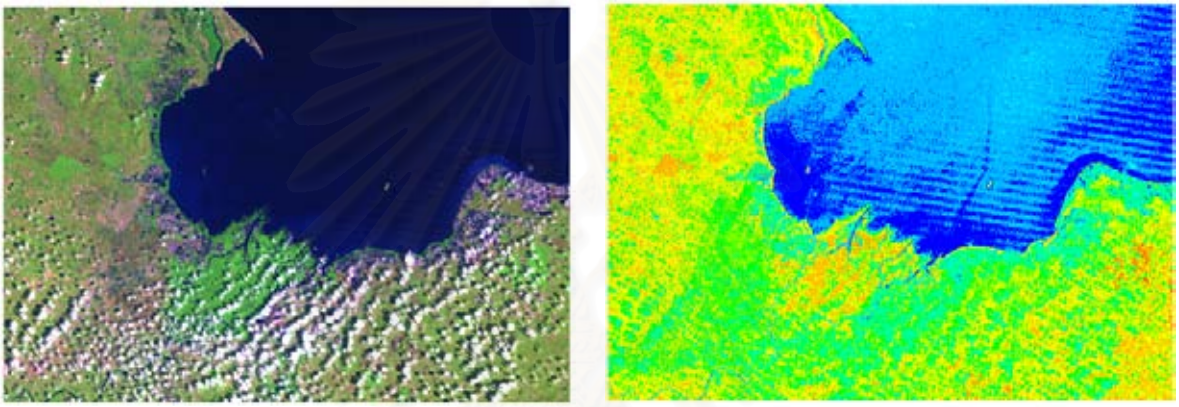

False Color Composite **NDVI**

f) June 11,1997 (EN)

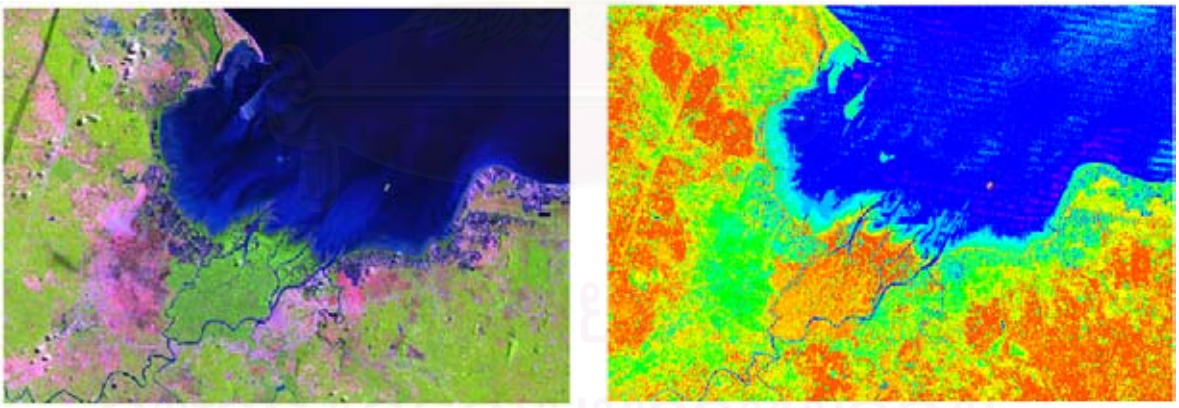

False Color Composite **NDVI**

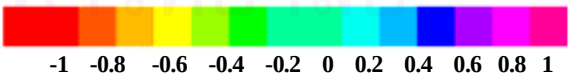

Fig.35 (Cont'd) Comparison between false color composite (Left) of Landsat imageries (RGB = 543) and Normalized Different Vegetation Index (NDVI) (Right)

g) April 27,1998 (LN)

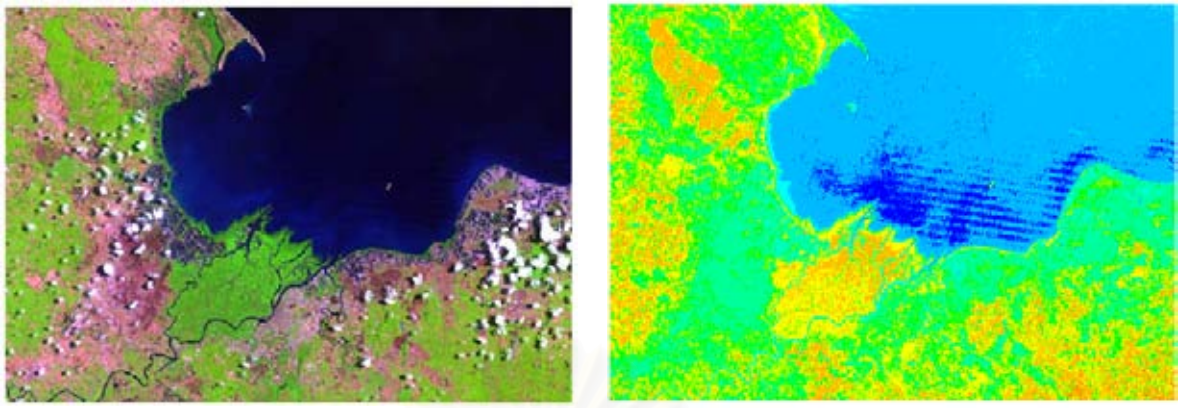

False Color Composite **NDVI**

h) January 8,1999 (Normal)

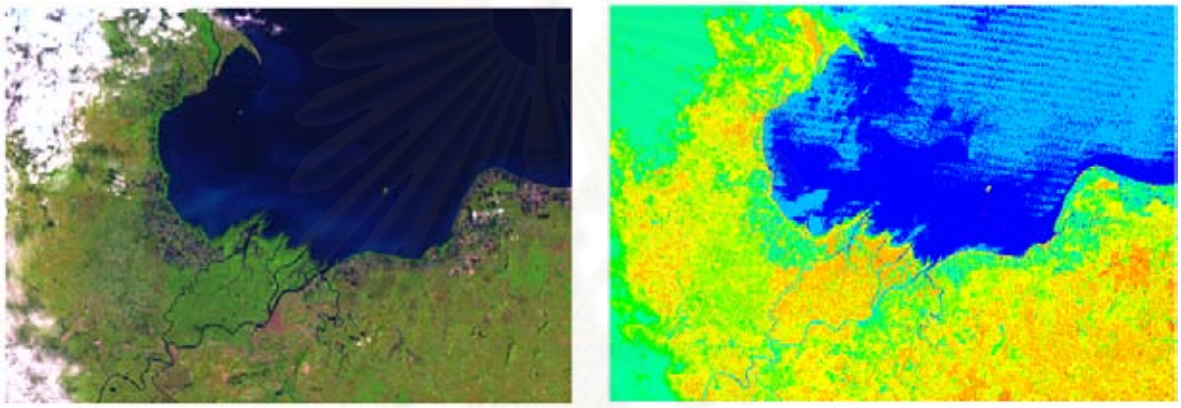

False Color Composite **NDVI**

i) April 12, 2000 (LN)

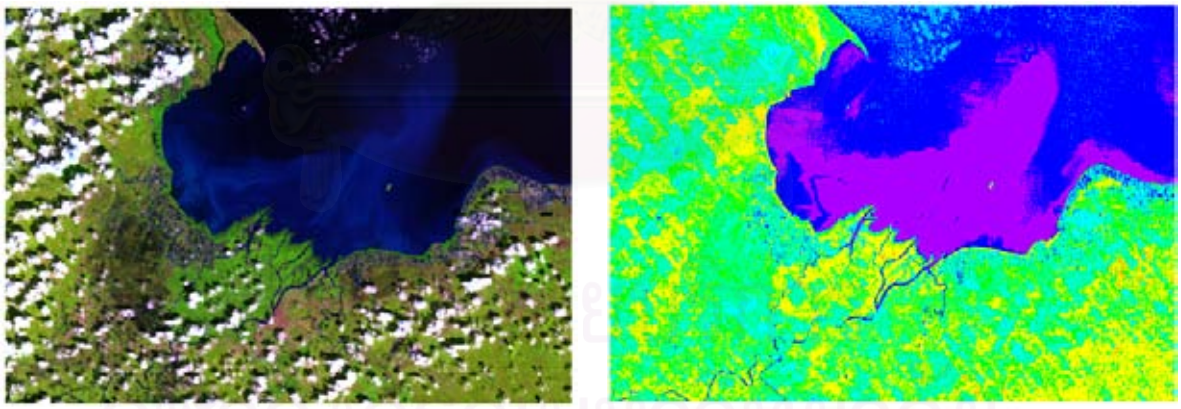

False Color Composite **NDVI**

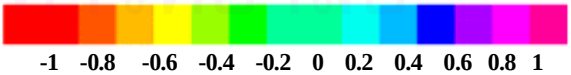

-1 -0.8 -0.6 -0.4 -0.2 0 0.2 0.4 0.6 0.8 1

Fig. 35 (Cont'd) Comparison between false color composite (Left) of Landsat imageries (RGB = 543) and Normalized Different Vegetation Index (NDVI) (Right)

j) December 4, 2000 (LN)

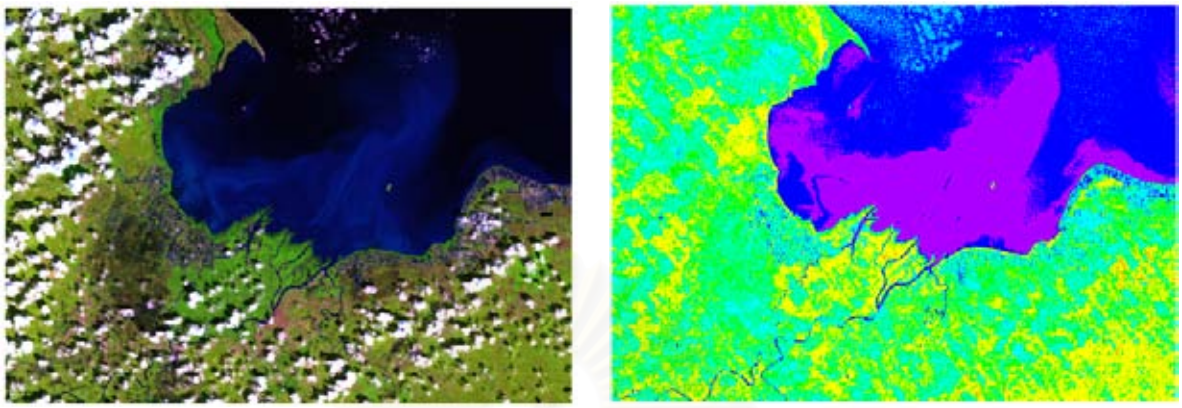

False Color Composite **NDVI**

k) January 6, 2002 (EN)

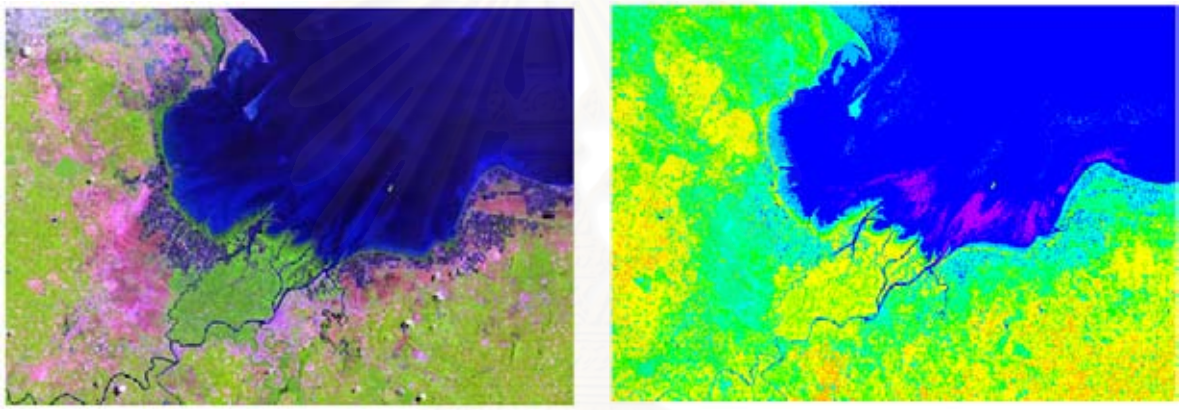

False Color Composite **NDVI**

-1 -0.8 -0.6 -0.4 -0.2 0 0.2 0.4 0.6 0.8 1

Fig. 35 (Cont'd) Comparison between false color composite (Left) of Landsat imageries (RGB = 543) and Normalized Different Vegetation Index (NDVI) (Right)

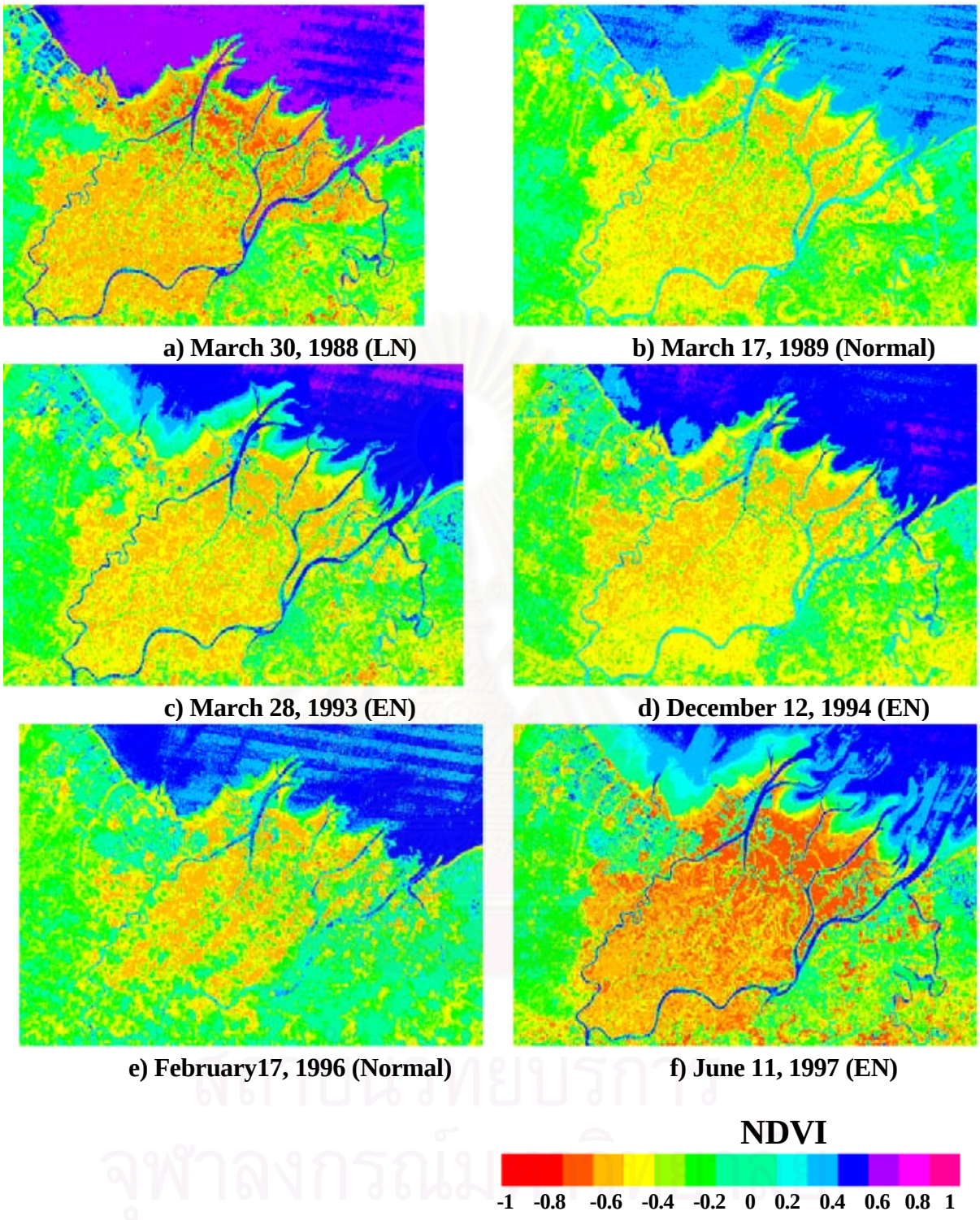

Fig. 36 NDVI from 1988-2002. Each panel is representative of NDVI. Missing value are shown as black area.

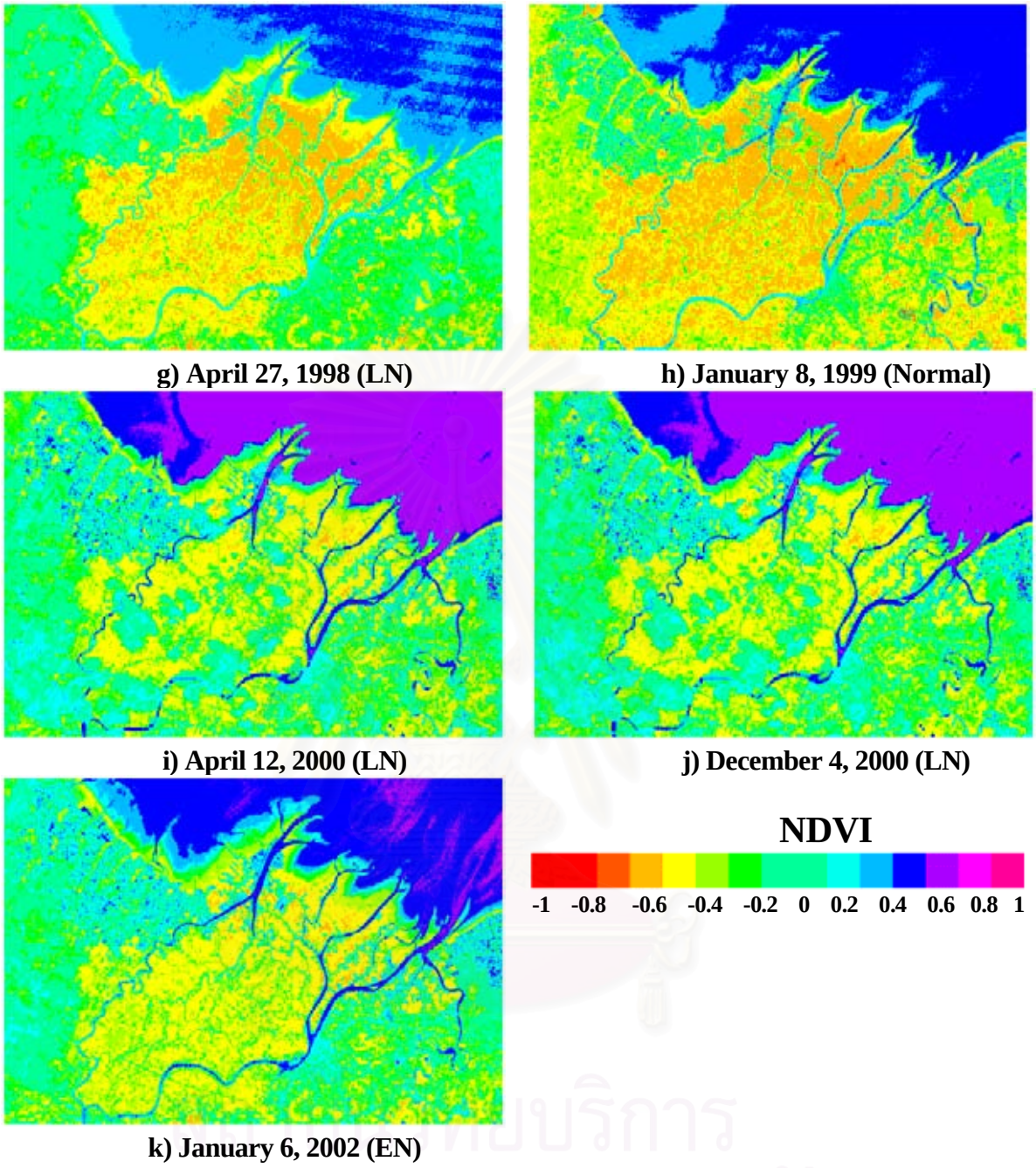

Fig. 36 (Cont'd) NDVI from 1988-2002. Each panel is representative of NDVI. Missing value are shown as black area.

3.2 Coastal Resources Aquaculture in Asia is the most contribution to the global aquaculture production in 1996 (Fig.37), in which Thailand contributed 14% (Fig.38). Thailand contributed 1.5% by quantity and 3.9% by value (Fig.39).

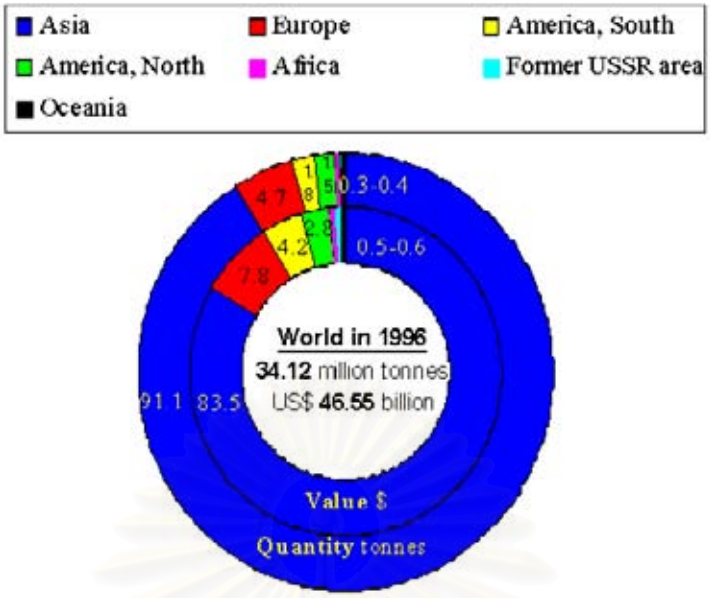

Fig. 37 Comparison of the Contribution (%) of Continents to Global Aquaculture Production in 1996.
http://www.fao.org/fi/trends/aqtrends/aqtrend.asp

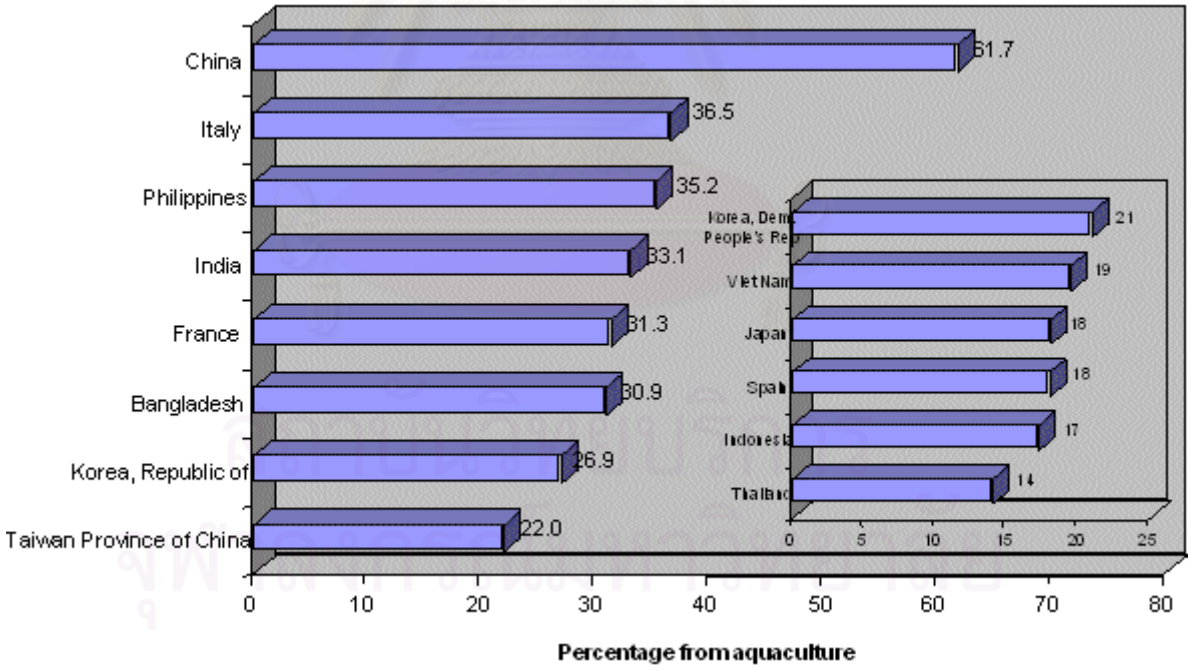

Fig. 38. Contribution (%) of Aquaculture to National Aquatic Production.

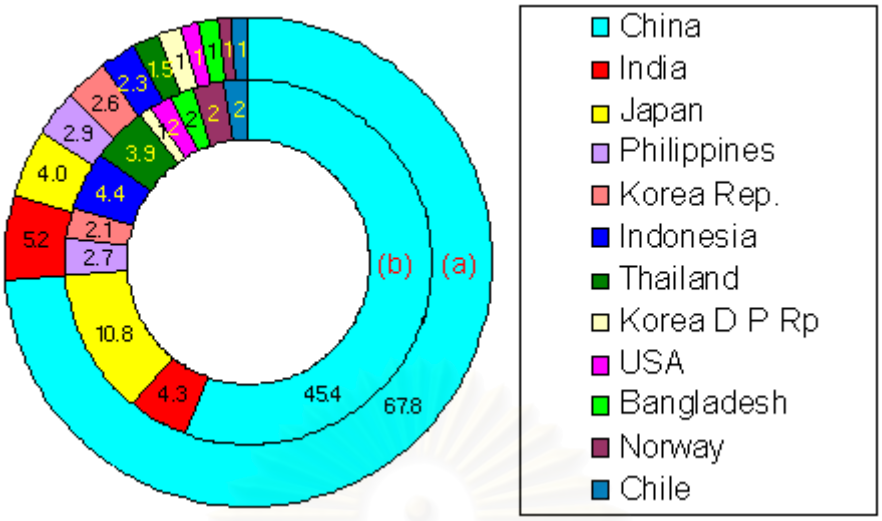

Fig. 39 Comparison of Aquaculture Production from Major Countries, by Quantity (a) and Value (b) in 1996.
Source: http://www.fao.org/fi/trends/aqtrends/aqtrend.asp

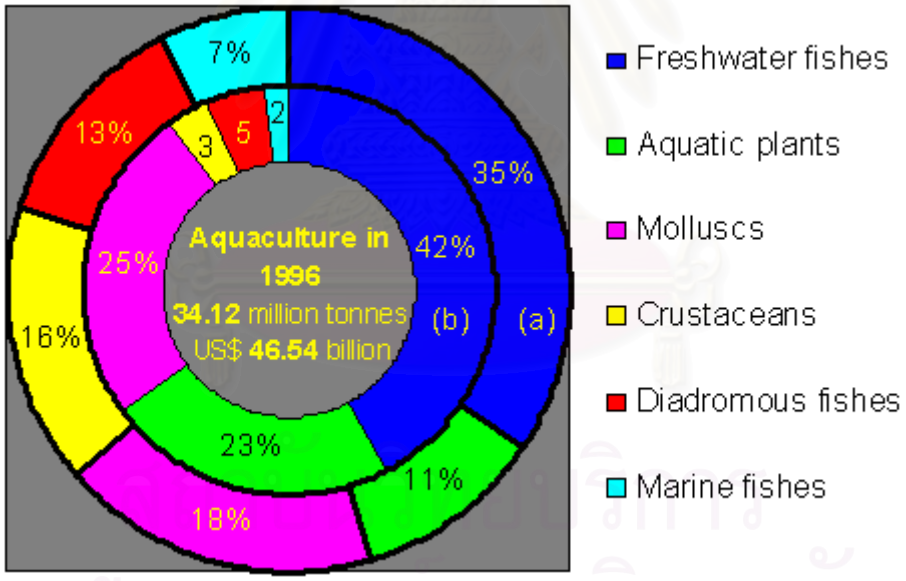

Fig. 40 Production in Value (a) and Tonnage (b) of Major Cultured Groups of Aquatic Organisms in 1996.
Source: http://www.fao.org/fi/trends/aqtrends/aqtrend.asp

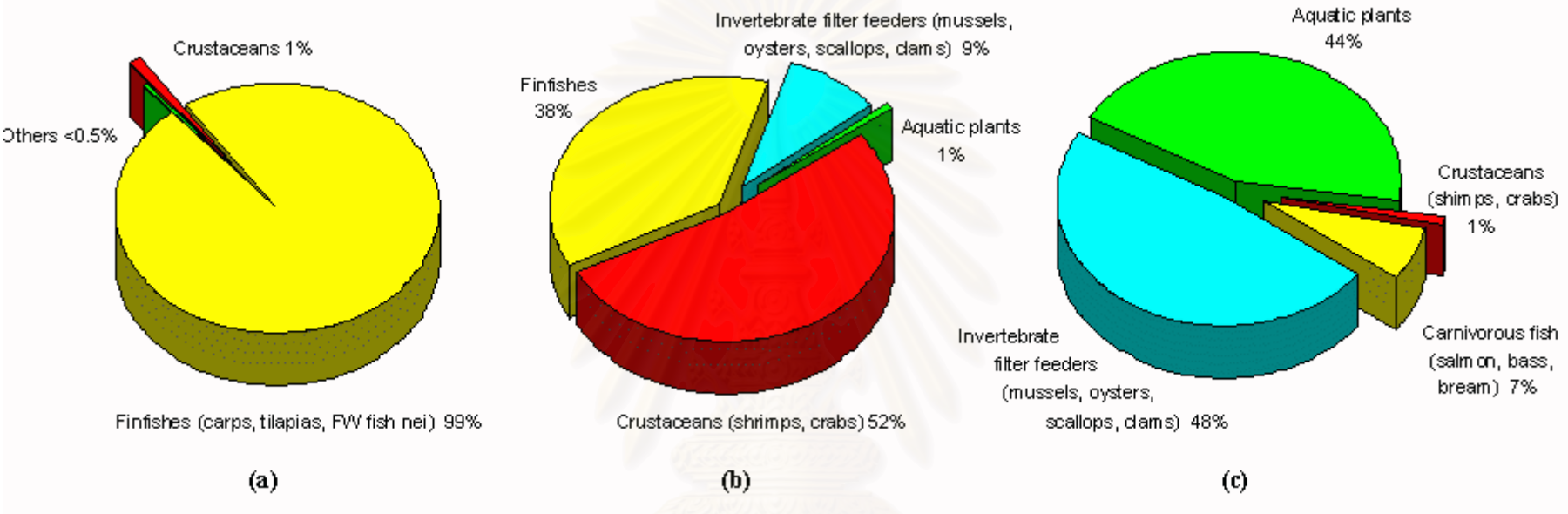

Fig. 41 Reported Global Total Aquaculture Production from (a) Freshwater (b) Brackish and (c) Marine Environments

Source: http://www.fao.org/fi/trends/aqtrends/aqtrend.asp

สถาบันวิทยบริการ
จุฬาลงกรณ์มหาวิทยาลัย

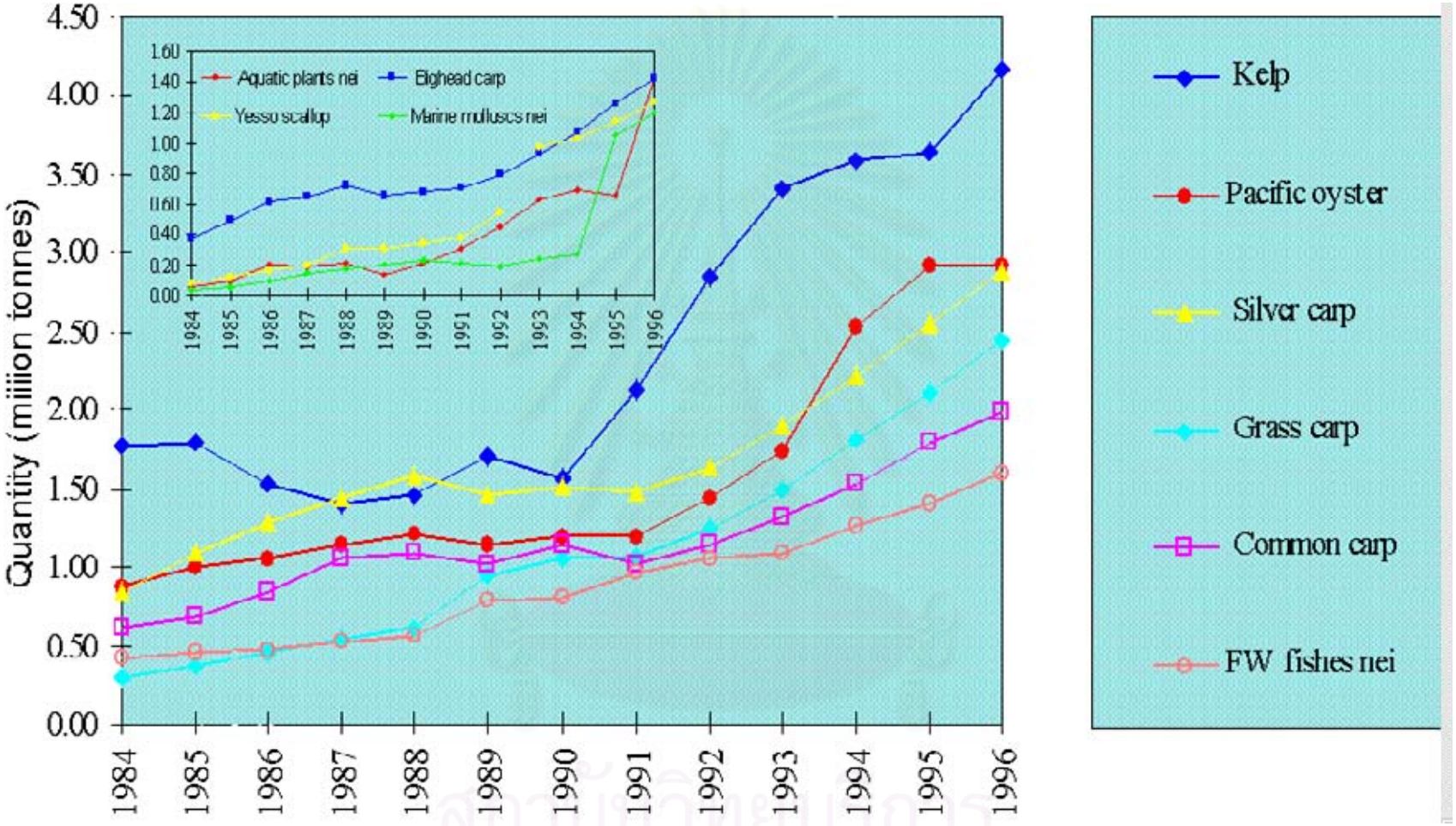

Fig. 42. Global Trends in Farmed Production of Top Ten Species and Species Groups.
Source: http://www.fao.org/fi/trends/aqtrends/aqtrend.a

Production of the freshwater Fish is the highest catch from Fig.40. Global Total Aquaculture Production from (a) Freshwater (b) Brackish and (c) Marine Environments can be estimated from Fig. 41. Global trends in farmed production of top ten species groups are in Fig.42.

For fisheries statistics at Surat Thani in Table 14, during El Niño years, the quantity of fish catch and the yields of aquacultures (shrimp and fish) were higher than average. During the La Niña years the same parameters were lower than average.

Table 14. Fisheries statistics of Surat Thani from 1987 to 2000 (from Fisheries Department).

Year	**ENSO**	**Fish Catch (Ton)**	**Aquaculture (Rai)**		**Yield(Ton)**		**Shrimp Area * (Rai)**
			Shrimp	**Fish**	**Shrimp**	**Fish**	
1987	EN	27,418	24,117.0	-	1,702.10	-	
1988	LN	18,128	41,550.0	-	3,268.69	-	37,694
1989	N	31,294	51,069.0	-	9,828.57	-	38,322
1990	N	33,314	55,030.0	0.88	14,400.00	-	
1991	EN	29,923	59,256.0	0.80	18,747.65	3.250	
1992	EN	5,780	59,540.0	1.70	20,046.99	5.250	
1993	EN	8,247	54,162.0	25.03	25,360.73	50.990	59,682
1994	EN	6,217	50,240.0	27.40	25,857.82	123.94	54,970
1995	N	6,699	41,098.0	28.29	22,220.77	142.99	
1996	N	4,363	42,892.0	44.94	21,226.00	62.490	46,803
1997	EN	4,130	34,398.0	47.68	12,338.11	54.650	55,284
1998	LN	3,822	38,019.3	41.14	13,796.96	139.00	37,694
1999	N or LN	-	-	46.07	-	-	59,211
2000	LN	-	19,480.0	32.44	16,122.35	-	60,860

Note * from Landsat.

EN = El Niño, LN = La Niña, N = Normal

3.2.1 **Forests** Natural and mangrove forests have been declined as shown in Table 15 which are the result of deforestation. The statistics were estimated from Landsat images by the Royal Forestry Department for the whole Surat Thani province and were classified (*) by the author. The increased figures are due to reforestation by various programs of Royal Forestry Department, Petroleum Authority of Thailand and Electricity Generation Agency of Thailand. For natural forest, RFD used the area of Surat Thani province as 12,891.47 km^2, while for mangrove forest, they used the area of Surat Thani province as 13,139.84 km^2 to compute the % of area of forest.

During the El Niño years, from Table 15, the areas of natural and mangroves were decreased,while during the La Niña years, the areas were increased.

Table 15 Areas of natural and mangrove forests at Surat Thani.

Year	ENSO	Forest Area* (km^2)	Surat Forest Area (km^2)	Surat Forest Area, %	Mangrove Area *(km^2)	Mangrove Area (km^2)	Mangrove Area (Rai)	Mangrove Area %
1961	N					256	160,000	1.948
1975	LN					37	23,125	0.281
1979	N					58.08	36,300	0.442
1986	N					42.84	26,774	0.326
1988*	LN	15.08	3,397	26.35	17.59			
1989*	N	12.56	3,388	26.28	18.85			
1991	EN		3,283	25.47		22.04	13,775	0.168
1993*	EN	12.56	3,166	24.56	14.57	31.64	19,775	0.241
1994*	EN	11.31			14.57			
1995	N		3,044	23.61				
1996*	N	11.31			14.07	31.338	19,586.25	0.238
1997*	EN	10.81			13.57			
1998*	LN	15.08	3,011	23.36	17.59			
1999	N	11.56			14.32			
2000*	LN	10.81			13.57			
2000*	LN	11.56	3,667.7	28.451	14.07	34.9	21,812.5	0.27
2002*	EN	10.30			13.82			

3.2.2 **Landuse** Table 16 is the area of landuse especially agricultural plantations as classified from the Landsat data. The changes of agricultural plantation were fluctuated owing to the social and economic problems. However, we can see that in normal years, the plants grew very well. During El Niño years, the areas of the plantations were decreased owing to the drier weather than normal. During the La Niña years, the areas were increased owing to the wetter weather than normal. The areas of shrimp ponds have been increased with the increasing population.

Table 16 The change of landuse areas (km^2) as classified from Landsat data.

Year	ENSO	Coconut	Rubber	Oil Palm	Paddy Field	Urban	Barren	Shrimp	Population
1988	LN	125.65	287.73	79.16	201.03	25.38	44.73	60.31	713,528
1989	N	150.78	319.14	80.41	206.06	27.64	304.32	61.32	725,643
1993	EN	113.08	371.16	87.95	259.08	31.41	499.82	95.49	802,073
1994	EN	110.57	405.08	85.44	251.29	32.67	415.89	87.95	815,444
1996	N	104.29	212.34	70.36	161.58	28.90	124.89	74.89	843,111
1997	EN	107.30	368.14	86.70	302.56	33.67	357.09	88.46	861,233
1998	LN	125.65	287.73	79.16	201.03	25.38	44.73	60.31	876,407
1999	N	111.83	388.00	85.69	258.08	30.91	87.95	94.74	886,979
2000	LN	109.06	363.12	86.95	247.27	31.16	150.52	97.25	
2001	LN	111.83	380.96	97.75	230.18	31.66	159.07	97.00	893,534
2002	EN	106.80	305.07	97.50	241.24	32.92	514.65	97.75	920,283

3.2.3 **Population** Table 17 is the total population of Surat Thani from 1968 to 2002. The population of Surat Thani has been increased every year.

Table 17 Population of Surat Thani from 1968 to 2002.

Year	ENSO	Population	Year	ENSO	Population
1968	N	433,961	1986	N	686,859
1969	EN	448,255	1987	EN	699,805
1970	LN	465,064	1988	LN	713,528
1971	LN	489,241	1989	N	725,643
1972	EN	502,547	1990	N	738,350
1973	LN	510,858	1991	EN	751,219
1974	LN	531,543	1992	EN	791,259
1975	LN	543,343	1993	EN	802,073
1976	EN	552,727	1994	EN	815,444
1977	EN	564,286	1995	N	831,376
1978	N	574,350	1996	N	843,111
1979	N	583,137	1997	EN	861,233
1980	N	593,095	1998	LN	876,407
1981	N	605,403	1999	N OR LN	886,979
1982	EN	615,649	2000	LN	893,534
1983	N	641,098	2001	N	907,612
1984	N	662,653	2002	EN	920,283
1985	N	677,602			

3.3 **Coastal Environment** The data on air temperature, rainfall, river runoff and mean sea level were analysed to see the linkage of ENSO on these environmental factors.

3.3.1 Air Temperature and Rainfall The yearly mean of air temperature and annual rainfall at Surat Thani from 1951 to 2001 were averaged using the baseline period from 1961 to 1990 as recommended by IPCC. The standard deviation of rainfall is 336.806 and of air temperature is 0.324. The baseline period for rainfall is 1635.55 mm and for air temperature is 26.4^0C. The anomaly was computed from $(x-x_{ave})/S.D.$

Table 18 Air temperature and rainfall with anomalies, Surat Thani.

Year	Rainfall	Anomaly	Temp	Anomaly	ENSO
1951	2182.1	1.62	26.3	-0.31	EN
1952	1898.9	0.78	26.6	0.62	N
1953	2076.2	1.31	27.0	1.85	EN
1954	1312.5	-0.96	26.3	-0.31	N
1955	1871.2	0.70	25.9	-1.54	LN
1956	2200.3	1.68	25.9	-1.54	LN
1957	922.9	-2.12	26.5	0.31	EN
1958	2033.2	1.18	26.8	1.23	N
1959	1593.3	-0.13	26.4	0.00	N
1960	1564.8	-0.21	26.2	-0.62	N
1961	1400.6	-0.70	26.2	-0.62	N
1962	1649.5	0.04	26.0	-1.23	N
1963	1772.3	0.41	26.2	-0.62	EN
1964	2164.0	1.57	26.2	-0.62	LN
1965	1641.2	0.02	26.1	-0.93	EN
1966	2169.3	1.58	26.4	0.00	N
1967	1740.9	0.31	26.1	-0.93	N
1968	1222.9	-1.23	27.0	1.85	N
1969	1660.4	0.07	26.8	1.23	EN
1970	2111.8	1.41	26.4	0.00	LN
1971	2002.5	1.09	25.9	-1.54	LN
1972	1375.8	-0.77	26.3	-0.31	EN
1973	1728.1	0.27	26.4	0.00	LN
1974	1555.2	-0.24	25.9	-1.54	LN
1975	2036.0	1.19	26.0	-1.23	LN
1976	1500.9	-0.40	25.9	-1.54	EN
1977	1671.5	0.11	26.3	-0.31	EN
1978	1434.2	-0.60	26.3	-0.31	N
1979	1398.1	-0.70	26.6	0.62	N
1980	1412.8	-0.66	26.6	0.62	N
1981	1311.7	-0.96	26.4	0.00	N
1982	1269.5	-1.09	26.4	0.00	EN
1983	1509.1	-0.38	26.8	1.23	N
1984	1480.4	-0.46	26.5	0.31	N
1985	1599.1	-0.11	26.5	0.31	N
1986	1902.2	0.79	26.5	0.31	N
1987	1325.7	-0.92	27.0	1.85	EN
1988	2163.1	1.57	26.7	0.93	LN
1989	1341.0	-0.87	26.5	0.31	N
1990	1515.5	-0.36	27.0	1.85	N
1991	1242.7	-1.17	26.8	1.23	EN
1992	1832.4	0.58	26.8	1.23	EN
1993	2362.5	2.16	26.6	0.62	EN
1994	1789.5	0.46	26.6	0.62	EN
1995	1558.9	-0.23	26.8	1.23	N
1996	2234.6	1.78	26.7	0.93	N
1997	1504.0	-0.39	27.1	2.16	EN
1998	1546.2	-0.27	27.4	3.09	LN
1999	1513.9	-0.36	26.4	0.00	LN
2000	1550	-0.25	26.5	0.31	LN

2001	1839.2	0.60	26.6	0.62	N

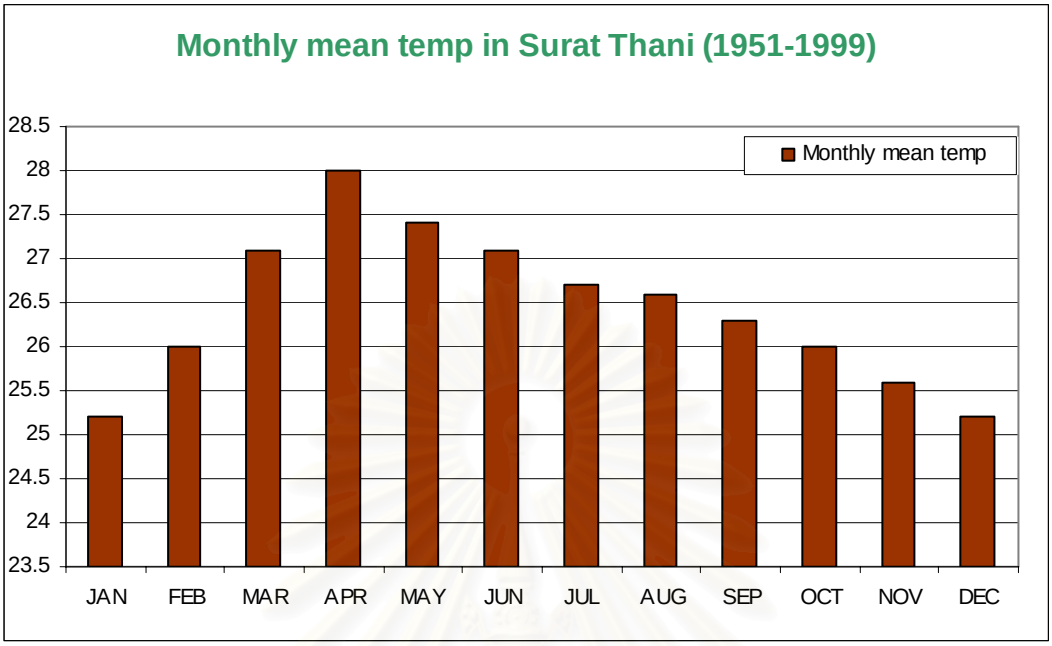

Fig.43 Monthly mean air temperature (^{0}C), Surat Thani, 1951-1999.

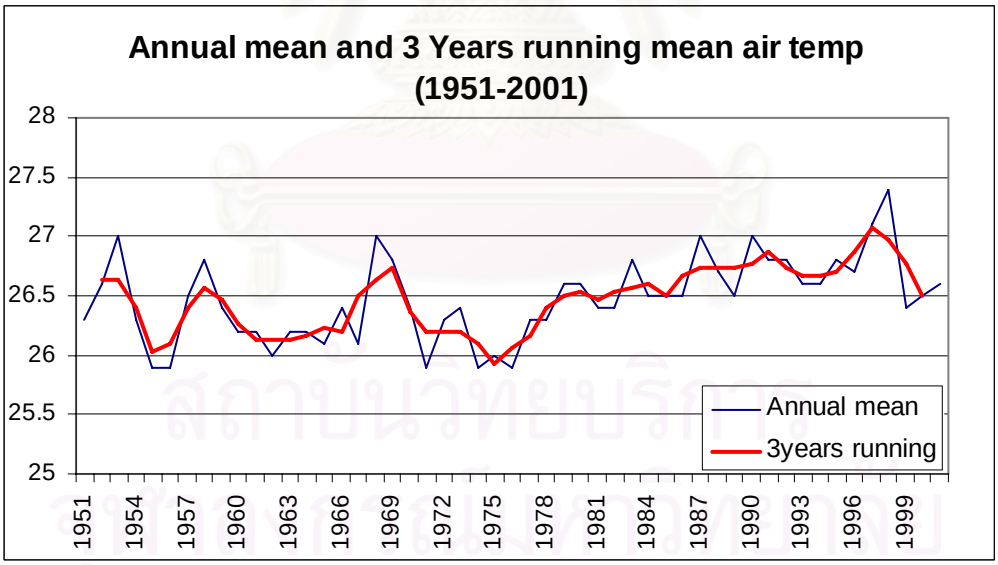

Fig. 44 Annual mean and 3 years running mean air temperature, Surat Thani, 1951-2001. The baseline period, 1961-1990 is 26.4^{0}C.

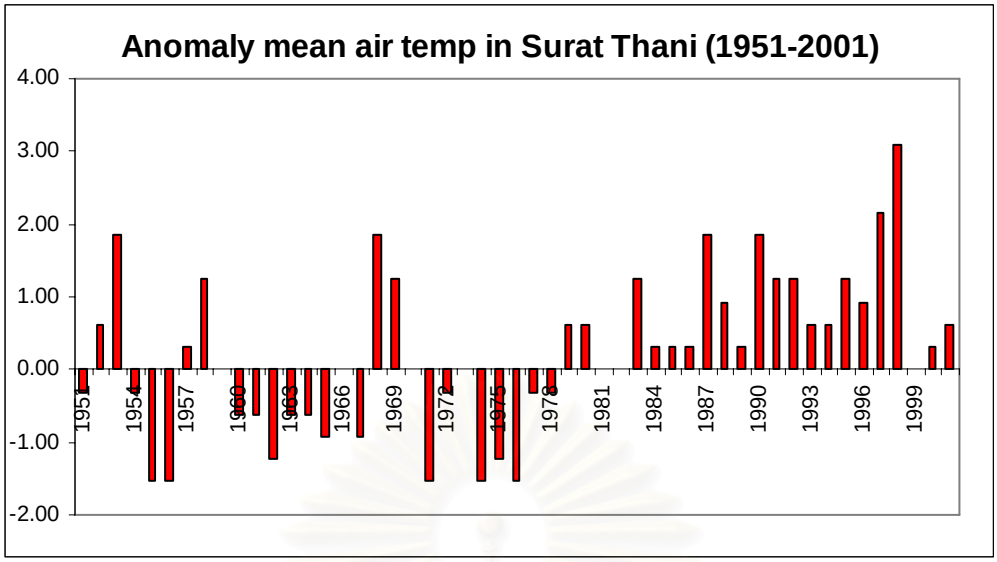

Fig.45 Anomaly mean air temperature, Surat Thani, 1951-2001.

The variations of the monthly mean air temperature at Surat Thani from 1951 to 2001 were shown in Fig.43. April is the hottest month (28^0C) and January is the coldest month (25.3^0C). The annual mean and 3-years running mean of annual mean air temperature were illustrated in Fig. 44. Since the mean air temperature from baseline periods is 26.4^0C, this figure shows that from 1951 to 1980 the mean air temperatures were lower than average but after 1980 to present, the trend is higher than normal. This means the warming of air temperature. The anomalies of annual mean air temperature were plotted in Fig. 45.

The linkage of ENSO was analysed from Fig.45 and Table 18. During El Niño, the air temperatures at Surat Thani have plus anomalies (higher than normal) 9 years and minus anomalies (lower than normal) 6 years. So we can conclude that El Niño causes the warm air temperature in most cases but not all. During La Niña, the air temperatures have plus anomalies 3 years and minus anomalies 6 times. Thus, La Niña causes the colder air temperature in most cases.

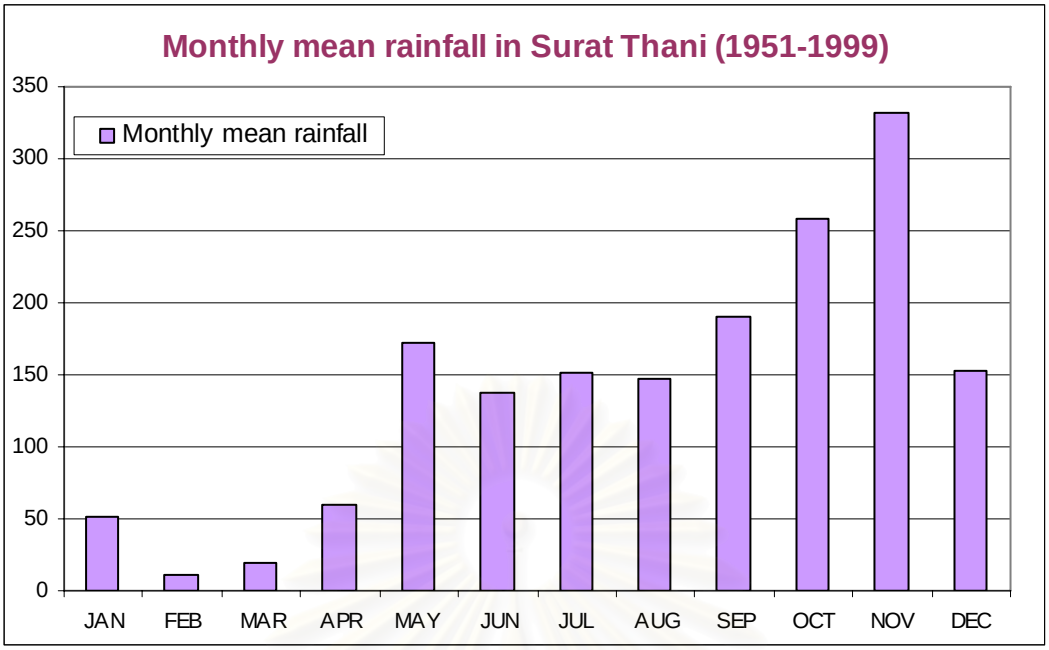

Fig.46 Monthly mean rainfall, Sura Thani, 1951-1999.

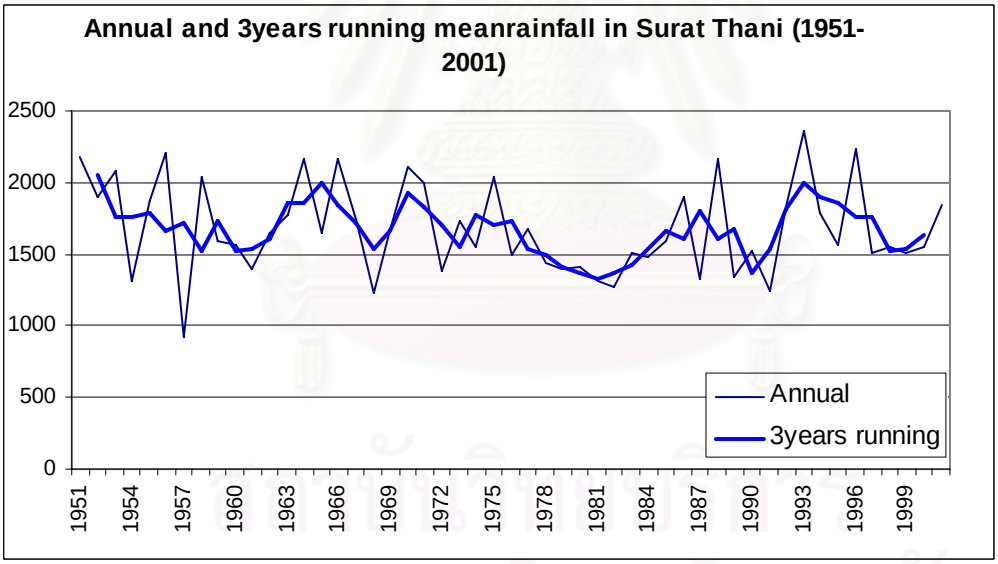

Fig. 47 Annual mean and 3 years running mean rainfall, Surat Thani, 1951-2001.

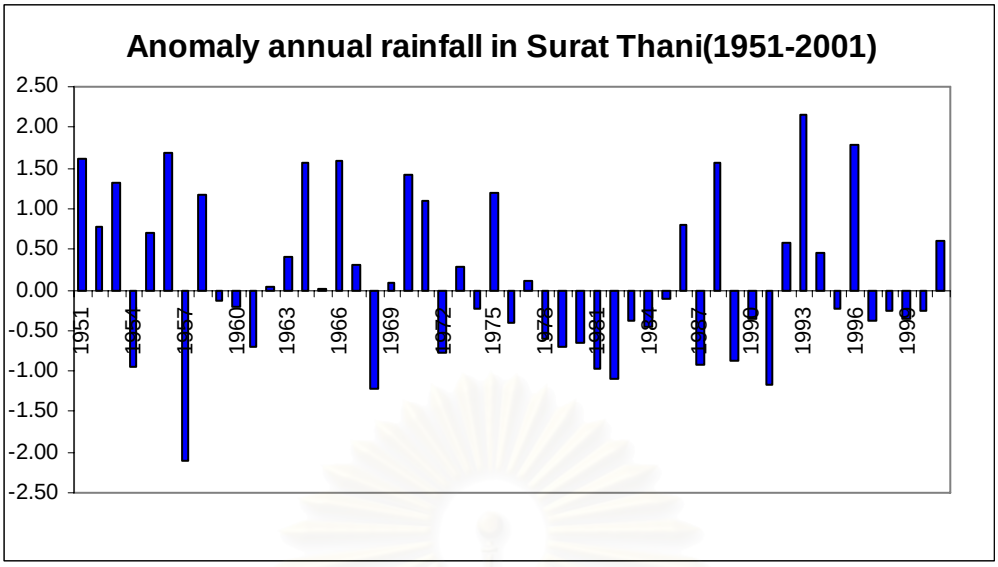

Fig.48 Anomaly annual rainfall, Surat Thani, 1951-2001.

The variations of the monthly rainfall a Surat Thani from 1951 to 1999 were shown in Fig.46. The peak rainfall occurred in November and least rainfall in February. The mean of rainfall averaged during baseline period from 1961 to 1990 is 1635.5 mm. Fig.47 which shows annual and 3-years running mean of rainfall has fluctuated patterns owing to other linkage such as monsoon and tropical cyclone rains.

The linkage of ENSO on rainfall was analysed from Table 18 and Fig. 48. During El Niño years, rainfall data show plus anomalies 9 years and minus anomalies 7 years. This means that El Niño caused higher rainfall than normal. During La Niña, rainfall data show plus anomalies 8 years and minus anomalies 4 years. La Niña also caused higher rainfall than normal. This result means that apart from ENSO, there must be other linkages as said to cause rainfall fluctuation.

สถาบันวิทยบริการ
จุฬาลงกรณ์มหาวิทยาลัย

3.3.2 Frequency of Tropical Cyclone Table 19 is the frequency of tropical cyclone passing Thailand from 1951 to 2002. October is the peak of tropical cyclone, which total of 48. January to March is a quite season. The linkage of ENSO and tropical cyclone can be seen from Table 19 and Fig. 49.

During El Niño years, the tropical cyclone frequencies are plus anomalies 5 years and minus anomalies 12 years. This means that El Niño caused higher frequency of tropical cyclone. During La Niña years, the tropical cyclone frequencies are plus anomalies 5 years and minus anomalies 7 years. This also means that La Niña also caused tropical cyclone but lesser than El Niño linkage.

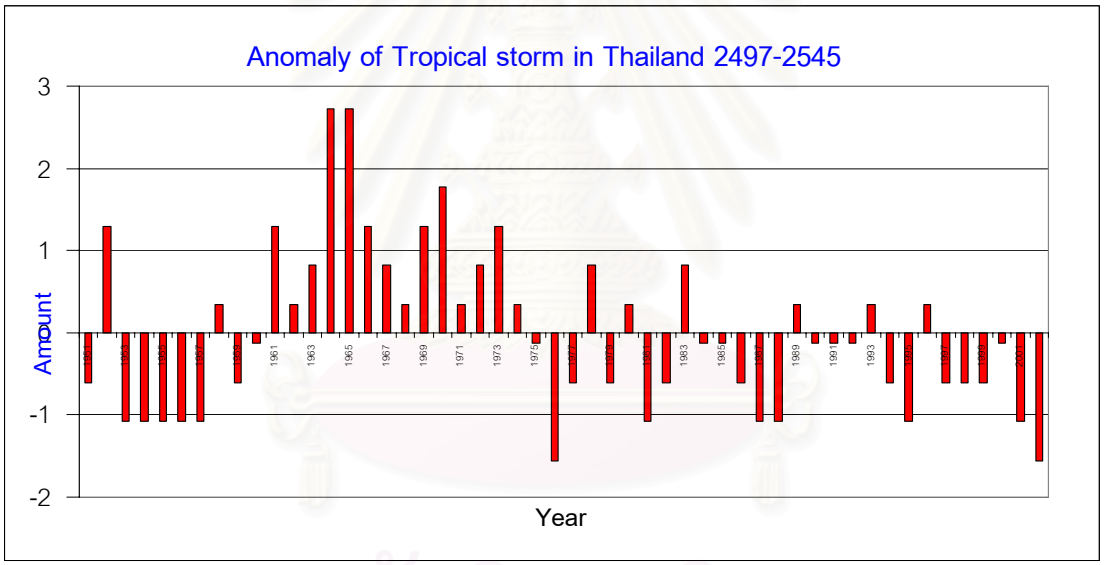

Fig. 49 Anomaly of tropical cyclone passing Thailand, 1951 to 2002.

Table 19. Frequency of tropical cyclone passing Thailand, 1951-2002.

Year	Jan	Feb	Mar	Apr	May	June	July	Aug	Sept	Oct	Nov	Dec	Total
1951							1		1				2
1952								1	1	4			6
1953						1							1
1954										1			1
1955									1				1
1956											1		1
1957										1			1
1958							1	1	1	1			4
1959									1	1			2
1960									1	1	1		3
1961				1	2			1		2			6
1962							1		1	1	1		4
1963							1		2	1	1		5
1964									2	4	2	1	9
1965								2	6			1	9
1966						1				2	2	1	6
1967									1	3	1		5
1968								2		1	1		4
1969						1	1		2	1	1		6
1970								1	2	2	2		7
1971							2		1	1			4
1972						1			2	1		1	5
1973							1	1	1	1	2		6
1974								1		1	1	1	4
1975					1				2				3
1976													0
1977									1		1		2

1978							1	1	2		1		5
1979								1	1				2
1980					1				2		1		4
1981										1			1
1982					1				1				2
1983						1				3	1		5
1984						1				1	1		3
1985									1	2			3
1986									1	1			2
1987								1					1
1988										1			1
1989					1					2	1		4
1990								1		2			3
1991								1	1	1			3
1992										2	1		3
1993							1	1			1	1	4
1994							1		1				2
1995								1					1
1996									1	1	2		4
1997									1		1		2
1998											1	1	2
1999										1		1	2
2000								1	1		1		3
2001								1					1
2002													0
Total	0	0	0	1	6	6	11	19	42	48	29	8	170
Ave				0.02	0.12	0.12	0.21	0.37	0.81	0.92	0.56	0.15	3.27
%				0.6	3.5	3.5	6.5	11.2	24.7	28.2	17.1	4.7	100

3.3.3 Mean Sea Level The monthly mean sea level data which were computed from tide gauge data from the Harbour Department at Thathong, Ban Don Bay from 1974 to 1991, with some missing year data are in Table 20. From the monthly mean data, February is the highest MSL (2.89 m) and the lowest MSLs of 2.11 m are in May, August and September.

Fig. 50 is the plot of anomalies of MSL data. The linkage of ENSO on MSL is not very clear owing to the small quantity of data. During El Niño years, the MSLs are plus anomalies for 3 years. During La Niña years, MSLs show plus and minus anomalies for one of each year. However, we may conclude that El Niño causes higher MSL than mean value (Table 21).

Table 20 Yearly mean sea level, Ban Don, 1974-1991.

M/Yrs	1974	1975	1976	1977	1978	1980	1990	1991	Mean
J	2.79	2.88	2.81	2.81	2.78	2.65	2.85	3.30	2.86
F	2.83	2.73	2.81	2.88	2.79	2.72	3.56	2.80	2.89
M	2.72	2.62	2.68	2.72	2.69	2.48	2.74	2.63	2.66
A	2.57	2.60	2.62	2.56	2.49	2.49	2.64	2.53	2.56
M	0	2.39	2.40	2.28	2.48	2.39	2.62	2.28	2.11
J	2.36	2.32	2.33	2.23	2.31	2.43	2.24	2.45	2.33
J	2.32	2.37	2.34	2.26	2.16	2.34	2.31	2.38	2.31
A	2.29	2.41	2.41	2.87	0	2.21	2.25	2.43	2.11
S	2.50	2.49	2.41	2.41	0	2.16	2.42	2.52	2.11
O	2.54	2.55	2.67	2.77	2.64	2.18	2.71	2.77	2.60
N	2.86	2.96	3.01	2.96	2.75	2.65	2.87	3.01	2.88
D	2.92	0	0	2.86	2.80	2.61	2.98	2.96	2.85
Mean	**1.62**	**2.57**	**2.59**	**2.63**	**2.59**	**2.44**	**2.68**	**2.67**	
compare with MSL	**-0.88**	**0.07**	**0.09**	**0.13**	**0.09**	**-0.06**	**0.18**	**0.17**	

Table 21 Annual and anomaly of mean sea level, Surat Thani, 1974-1991.

Year/ENSO	Annual Mean	X-(-0.03)	Anomaly
1974 LN	-0.88	-0.85	-2.43
1975 LN	0.07	0.1	0.29
1976 EN	0.09	0.12	0.34
1977 EN	0.13	0.16	0.46
1978 N	0.09	0.12	0.34
1980 N	-0.06	-0.03	-0.09
1990 N	0.18	0.21	0.60
1991 EN	0.17	0.2	0.57
Mean	-0.03		
R.sq=	0.3749		

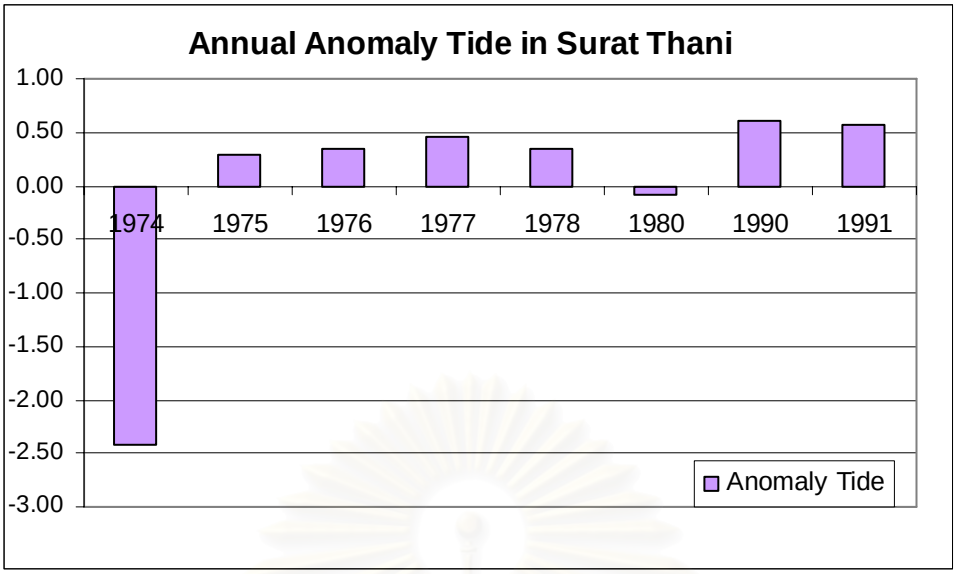

Fig.50 Annual anomaly tide, Surat Thani, 1974-1991.

3.3.4 River Runoff Table 22 is the Tapi river runoff from 1970 to 2001. The peak of Tapi river runoff is averaged 700.63 MCM in November and lowest 72.76 MCM in March, as illustrated in Fig.51. Fig.52 is the yearly mean and 3-years running mean of Tapi river runoff from 1970 to 2001. The trend of river runoff is increasing from 1994.

The anomalies of runoff were plotted in Fig.53. During El Niño years, the anomalies are plus for 4 years and minus for 6 years. This means that El Niño caused lower river runoff than normal. During La Niña years, the anomalies are plus for 6 years and minus for 3 years. Thus, La Niña caused higher runoff than normal.

สถาบันวิทยบริการ
จุฬาลงกรณ์มหาวิทยาลัย

Table 22 Runoff, Tapi River, 1970-2001. (From Royal Irrigation Department).

	Apr	May	Jun	Jul	Aug	Sep	Oct	Nov	Dec	Jan	Feb	Mar	Annual Runoff	Anomaly Annual Runoff
1970	53.14	74.56	154.83	249.78	459.04	417.31	569.55	678.59	433.38	189.13	58.49	83.2	3421.01	-0.52
1971	36.89	49.94	68.52	104.98	90.29	129.17	522.12	303.96	443.66	170.12	56.16	38.71	2014.5	-1.89
1972	61.78	64.2	71.11	96.34	117.5	341.28	594.09	600.48	574.73	134.96	54.86	40.35	2751.67	-1.17
1973	33.83	109.56	215.48	539.65	467.17	521.08	539.8	1051.4	752.37	212.72	81.13	62.04	4586.25	0.61
1974	51.2	150.9	154.5	182.3	296	377.1	576.9	955.7	617.2	2166.7	227.9	129.4	5986	1.96
1975	87.01	172.37	518.4	319.08	390.53	354.5	555.03	781.23	377.4	119.06	57.54	42.6	3774.73	-0.18
1976	53.31	195.7	212.11	164.16	272.17	513.73	465.35	604.11	482.98	164.07	65.32	48.04	3421.64	-0.52
1977	48.99	62.55	72.06	98.93	168.83	300.07	521.34	654.13	287.54	117.16	62.81	49.16	2443.57	-1.47
1978	78.07	190.23	271.48	424.17	409.16	506.01	516.53	427.35	263.14	103.51	56.03	46.28	3291.96	-0.65
1979	61.34	89.64	183.73	825.89	665.98	588.72	627.55	532.73	355.61	110.99	62.16	67.21	4171.55	0.20
1980	47.2	90.4	256.8	587.4	691.1	818.7	904.9	880.8	730.9	188	86.6	69.7	5352.5	1.35
1981	60.56	245.98	375.72	136.22	84.49	184.09	256.06	615.49	779.89	122.09	50.58	46.23	2957.4	-0.97
1982	80.05	216.02	337.78	723.7	549.07	484.84	640.99	669.58	274.41	105.05	43.17	23.74	4149.41	0.18
1983	24.37	72.83	219.54	275.42	453.33	527.29	779.03	634.3	240.69	131.73	124.9	61.19	3544.6	-0.40
1984	72.37	228.39	283.02	426.92	226.26	311.77	706.96	300.21	795.66	429.95	123.16	112.43	4017.09	0.05
1985	77.13	276.91	347.46	152.33	180.92	348.36	739.73	623.25	350.77	144.1	56.45	38.16	3335.56	-0.61
1986	38.6	192.4	180.8	366.5	593.6	1071.1	1192.1	846.8	461	161	77.2	57.4	5238.5	1.24
1987	40.98	87.43	167.94	59.77	377.41	382.76	464.12	585.95	847.87	210.84	96.32	55.94	3377.32	-0.57
1988	63.3	176.1	72.5	354.1	347.1	704	749.5	1416.1	668.2	192	82.6	63.6	4889	0.90
1989	72.61	139.13	140.02	215.02	309.34	410.51	752.13	551.03	115.7	56.84	33.14	32.39	2827.85	-1.10
1990	47.2	86.5	123.1	89.6	187.3	202.5	436.9	709.7	376.3	119.2	63.2	61.5	2502.9	-1.41
1991	34.16	103.82	248.95	327.03	516.36	708.06	618.98	437.73	272.33	216.25	70.6	43.01	3597.28	-0.35

1992	27.29	51.48	52.88	48.06	232.06	339.59	608.74	611.23	190.37	88.72	43.61	41.29	2335.32	-1.58
1993	56	67.4	71.6	203	209	477.1	848.7	625.2	1144.9	452.6	124.6	119.9	4400	0.42
1994	106.04	234.62	227.86	226.36	452.28	821.62	786.31	589.85	512	163.95	75.55	52.3	4527.75	0.55
1995	43.24	34.09	72.74	88.7	437.49	703.1	581.25	821.75	504.87	125.65	92.72	45.84	3551.44	-0.40
1996	76.3	127.93	188.31	254.42	298.3	483.75	603.9	621.34	813.36	198.51	110.69	67.49	3844.31	-0.11
1997	48	47.9	73.7	258	578.6	1005.7	908.3	630.1	354.3	107.8	44.3	26.6	4082.9	0.12
1998	28.2	29.5	160	204.7	435.5	771.5	1028.4	882.9	673.8	280.1	279.4	233.6	4647.6	0.66
1999	414.99	293.98	417.26	330.59	261.97	477.94	702	925.76	419.63	128.87	114.55	190.08	4677.6	0.69
2000	319.59	536.01	590.59	398.76	459.24	436.58	727.57	856.4	728.15	567.64	272.75	250.41	6146.67	2.12
2001	204.16	464.95	319.18	441.26	335.48	460.12	776.26	801.95	300.74	126.4	51.88	51.57	433.93	-3.42
Aver	79.62	155.38	212.22	291.91	358.59	522.47	670.42	700.63	499.23	242.29	90.23	72.76	3861.8	
													SD = 1031.45	

สถาบันวิทยบริการ
จุฬาลงกรณ์มหาวิทยาลัย

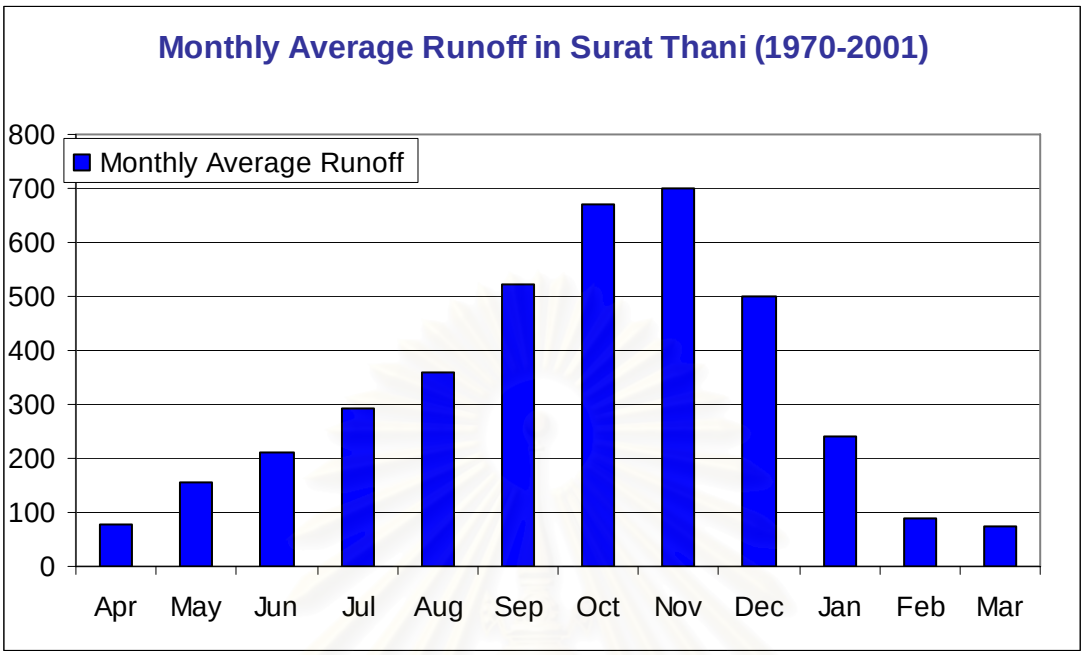

Fig.51 Monthly average runoff , Tapi River, 1970-2001.

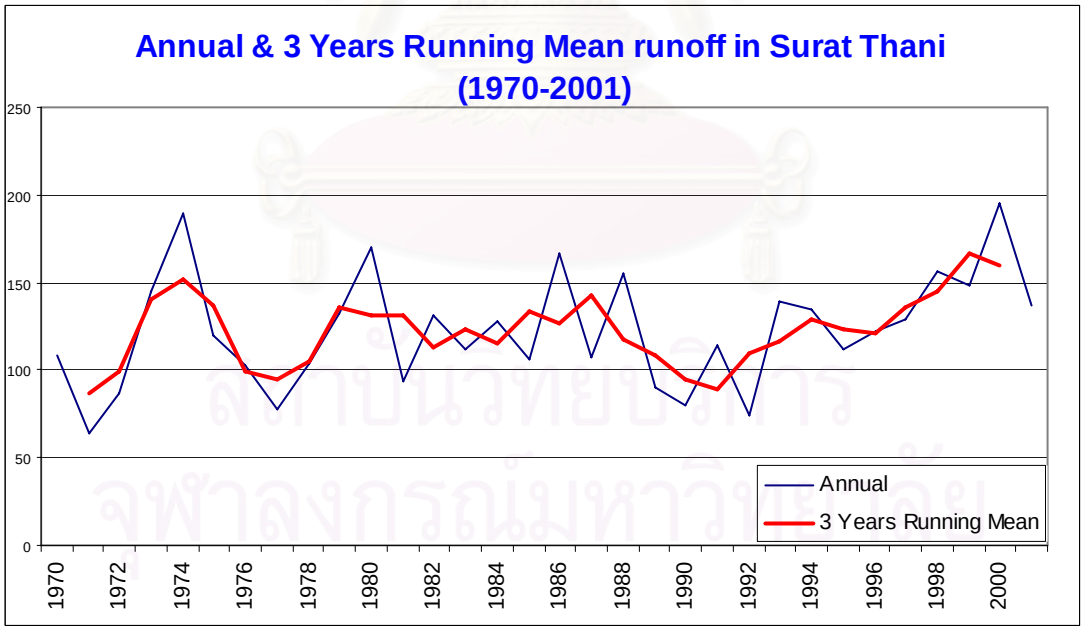

Fig.52 Annual and 3 years running mean runoff, Tapi River, 1970-2001.

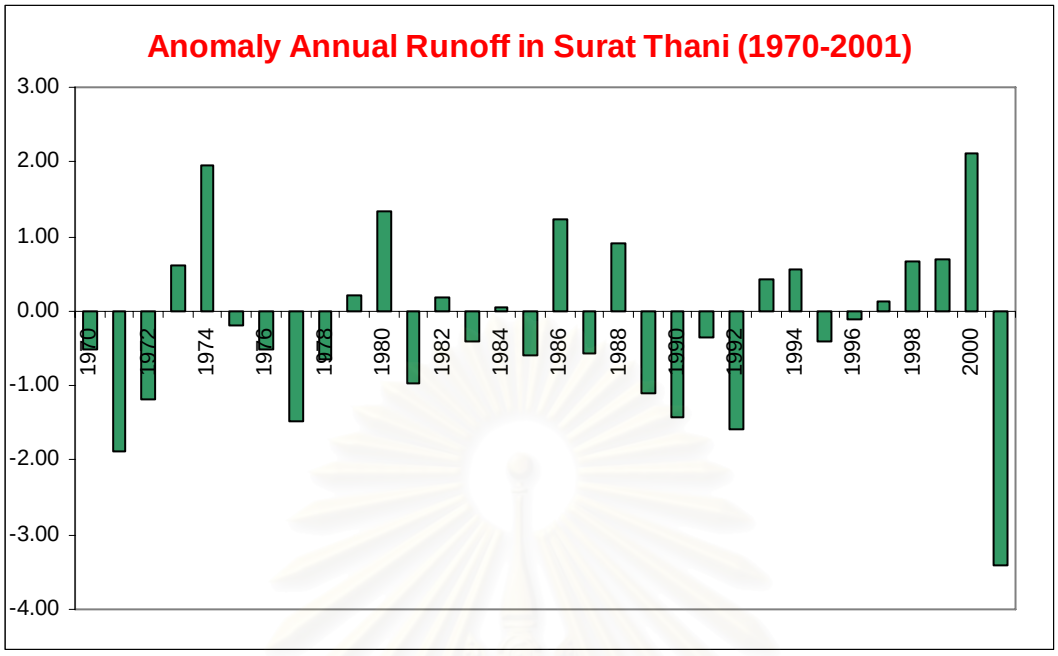

Fig.53 Anomaly annual runoff, Tapi River, 1970-2001.

3.4 Accuracy assessment A complete accuracy test of a classification map would be verification of the class of every pixel. Obviously this is impossible and indeed defeats the purpose of the image classification. Therefore, representative test areas must be used to estimate the map accuracy with as little error as possible. Classified image accuracy consists of the two accuracy types. First, overall accuracy which represents the accuracy of the entire product. Second, user's accuracy (or map accuracy) which a map user is interested in the reliability of the map in how well the map represents what is really on the ground.

As the collection of ground truth data is a time consuming and expensive, we decided to collect the ground truth data from the exciting land cover map described in previous paragraph, especially we consider that land cover categories do not change so much at a regional level. From the thematic data, we collected 69 ground truth regions which represent 12 land cover types.

To verify interpreted results, field surveys were conducted on October 12-13 2002 and March 26-27, 2003 to observe and collect information on land cover/land use classes. Figs. 21 to 28 are the photographs from different classes in the field.

The accuracy of the classification was determined by field surveys and comparing classified image with previous studies (e.g. Land-use map in year 1984 and 2000 produced by Land Development Department, Land-use map in 1993 produced by the Royal Forestry Department and

the National Mangrove Committee, National Research Council of Thailand). Detailed of field investigation describe in Table 10. While the overall accuracy of the classification is 0.82 the per class accuracy (for users) range from 0.71 to 0.92, the overall Kappa Statistic is 0.79 % and Overall Kappa Variance is 0.003 %.

Table 23 Ground survey locations

Category	Position		Category	Position	
	Easting (X)	Northing (Y)		Easting (X)	Northing (Y)
Urban and Built-up area	540 762	1 014 915	Paddy Field	546 747	1 013 944
	540 448	1 014 668		547 715	1 014 106
	540 567	1 011 663		548 924	1 014 590
	552 383	1 013 568		520 698	1 017 819
	552 494	1 018 136		521 263	1 014 106
	553 461	1 015 554		521 263	1 012 814
	565 216	1 024 434		521 666	1 009 828
	565 218	1 022 423		521 102	1 017 576
	565 265	1 024 543		520 618	1 019 433
	564 985	1 017 792		521 989	1 009 747
	565 143	1 024 468		523 198	1 017 576
				522 311	1 009 182
Shrimp Farm	555 254	1 016 194			
	555 258	1 016 311	Coconut	555 775	1 021 507
	564 327	1 024 284	Plantation	531 666	1 015 720
	564 365	1 024 333		530 053	1 012 169
	548 360	1 014 429		534 247	1 013 299
	546 182	1 016 043		537 392	1 014 186
	547 473	1 015 962		528 844	1 014 186
	527 392	1 018 222		530 537	1 015 478
	524 382	1 021 208			
	557 069	1 023 630	Barren land,	564 994	1 021 343
	555 940	1 016 204	bare soil or	564 950	1 021 345
	523 279	1 033 396	inundated	552 866	1 015 709
			area	549 973	1 014 671
Rubber	564 839	1 015 702		552 553	1 014 913
Plantation	564 778	1 015 693			
	575 096	1 029 736	Oil Palm	564 881	1 015 642
	562 504	1 011 528	Plantation	564 996	1 017 787
	564 792	1 013 353		552 957	1 015 155
	559 408	1 006 277			
	557 392	1 005 954	Mangrove	546 989	1 017 092
	514 166	1 011 927		542 503	1 015 670
	514 489	1 013 944		542 745	1 016 335
	551 344	1 008 214		547 261	1 017 022
	552 543	1 007 437		547 926	1 016 900
	547 382	1 006 892		537 765	1 017 647

Note: Sampling projection is UTM Zone 47 North with Indian 1975 datum

The confidential accuracy of mangrove classification is 0.97 and shrimp farm classification is 0.96. Table 24 shows results of classification accuracy assessment.

Table 24 Accuracy assessment of classification results.

Acquisition Date	**Type of Accuracy**	
	Overall	**User's**
March 30, 1988	0.74	0.77
March 17, 1989	0.88	0.76
March 28, 1993	0.83	0.81
December 12, 1994	0.82	0.79
February 17, 1996	0.88	0.76
June 11, 1997	0.82	0.79
April 27, 1998	0.81	0.88
January 8, 1999	0.86	0.84
April 12, 2000	0.88	0.85
December 4, 2000	0.82	0.88
January 6, 2002	0.80	0.84

3.5 <u>Conclusion and Recommendation</u> Supervised classification of land cover/land use pattern in Ban Don Bay coastal area was carried out using high altitude LANDSAT satellite in 11 periods. The El Niño years caused some less agricultural land areas due to the longer dry season and La Niña years caused some more productive land areas due to more wetter season.

The anomalies of air temperature, rainfall and river runoff are usually used to study the relationship of them to the ENSO phenomena. However, ENSO does not always occur all the year. It may extend to the next year. Sometimes, El Niño and La Niña occur in the same year. The yearly anomalies of these parameters can not always explain the erratic phenomena. Moreover, there are many causes of rainfall, therefore only ENSO can not explain solely the rainfall amount. The NDVI of Landsat data during the ENSO year and normal year can be better explained the different conditions of vegetation growing and their linkages with the ENSO phenomena. That is, during the El Nino year, the vegetation grows less than during the La Nina year, when the rainfall is higher, air temperature is lower and the river discharge is increased.

For fisheries statistics at Surat Thani during El Niño years, the quantity of fish catch and the yields of aquacultures (shrimp and fish) were higher than average. During the La Niña years the same parameters were lower than average The areas of shrimp ponds have been increased with the increasing population. The population of Surat Thani has been increased every year. During the El Niño years, the areas of natural and mangroves were decreased, while during the La Niña years, the areas were increased.

The variations of the monthly mean air temperature at Surat Thani from 1951 to 2001 showed that April is the hottest month (28^0C) and January is the coldest month (25.3^0C). Since the mean air temperature from baseline periods is 26.4^0C, this figure shows that from 1951 to 1980 the mean air temperatures were lower than average but after 1980 to present, the trend is higher than normal. This means the warming of air temperature. El Niño causes the warm air temperature in most cases but not all La Niña causes the colder air temperature in most cases.

The variations of the monthly rainfall a Surat Thani from 1951 to 1999 showed that the peak rainfall occurred in November and least rainfall in February. The mean of rainfall averaged during baseline period from 1961 to 1990 is 1635.5 mm. The annual and 3-years running mean of rainfall has fluctuated patterns owing to other linkage such as monsoon and tropical cyclone rains. El Niño caused higher rainfall than normal. La Niña also caused higher rainfall than normal. This result means that apart from ENSO, there must be other linkages as said to cause rainfall fluctuation.

El Niño caused higher frequency of tropical cyclone. La Niña also caused tropical cyclone but lesser than El Niño linkage. The linkage of ENSO on MSL is not very clear owing to the small quantity of data. During La Niña years, MSLs show plus and minus anomalies for one of each year. However, we may conclude that El Niño causes higher MSL than mean value. El Niño caused lower river runoff than normal. La Niña caused higher runoff than normal.

Land use/land cover changes in Ban Don Bay during 1988-2002 has been studied and found to be due to economic development, particularly agriculture and aquaculture. The depletion of mangrove forests in Ban Don Bay during 1973 -2002 was mainly due to coastal land development with the rate of depletion of about 68%. The depletion rate of mangrove area was much higher in the last five years. Conversion to aquaculture in particular shrimp farms was one of the major pressures in reducing the area of mangroves in Ban Don Bay. An attempt should be made to reduce further conversion or destruction to a minimum.

สถาบันวิทยบริการ
จุฬาลงกรณ์มหาวิทยาลัย

References

Allen, Robert J., 2000, ENSO and Climatic Variability in the Past 150 Years, in **El Niño and the Southern Oscillation, Multiscale Variability and Global and Regional Impacts**, (Eds.) Henry F. Diaz and Vera Markgraf, Cambridge University Press, Cambridge, pp. 3-55.

Anyamba, A. and Eastman, J. R. (1996) **Interannual Variability of NDVI Africa and its relation to El Niño / Southern Oscillation**. *International Journal of Remote Sensing*, **17**:2533-2548.

Anyamba, A. (1997) **Interannual Variations of NDVI over Africa and their relationship to ENSO: 1982-1995**. *Ph.D. Dissertation*, Clark University - Graduate School of Geography, Worcester, MA.

Buerman,W,,Wang,Y,Dong,J.,Zhou,L.,Zeng,X.,Dickinson,R.E.,Potte r, C.S. and Myneni, R.B. (2002) **Analysis of a Multiyear Global Vegetation Leaf Area Index Data Set**, Journal of Geophysical Research. (107) 14-1 – 14-16

Cane, M. A. (1986) **El Niño**. *Annual Review of Earth and Planetary Science*, **14**: 43-70.

Chagas, C. and Puppi, G. (1986) Summary and Conclusions. In C. Chagas and G. Puppi (Eds). **Persistent Meteo-Oceanographic Anomalies and Teleconnections.** Pontificia Academia Scientiaruum, Citte Del Vaticano. pp. 1-15.

Charuppat, T. and J. Charuppat (1997) **Application of LANDSAT-5 (TM) for Monitoring the Changes of Mangrove Forest Area in Thailand**. Proceedings of the 10th National Seminar on Mangroves, NRCT. 25-28 August, 1997, Songkhla, Thailand. Section I-9, pp. 1-8.

Cihlar, J., St.-Laurent, L. and Dyer, J. A. (1991) **The Relation Between Normalized Difference Vegetation Index and Ecological Variables**. *Remote Sensing of Environment*, 35:279-298.

Eastman, J.R., Anyamba, A., Ramachandran, M., 1996a, **The Spatial Manifestation of ENSO in Southern Africa**, Proceedings, *Conference on the Application of Remotely Sensed Data and Geographic Information Systems in Environmental and Natural Resources Assessment in Africa*, Harare, March 15-22, 269-281.

Eastman, J.R. and Anyamba, A. 1996 b, **Prototypical Patterns of ENSO-related drought and drought precursors in Southern Africa**, *The Thirteenth Pecora Symposium Proceedings*, August 20-22, 1996, Sioux Falls, South Dakota.

Evans, Cynthia A., Julie A. Robinson, M. Justin Wilkinson, Susan Runco, Patricia W. Dickerson, David L. Amsbury and Kamlesh P. Lulla, 2000, The 1997-1998 El Niño: Images of Floods and Drought, in **Dynamic Earth Environments, Remote Sensing Observations from**

Shuttle-Mir Missions, Kamlesh P. Lulla and Lev V. Dessinov (Eds).,John Wiley & Sons, Inc., N.Y., pp.61-76.

Glantz, M. (1991) Introduction: In M.H. Glantz, R.W. Katz, and N. Nicholls (Eds) **Teleconnections Linking World Wide Climate Anomalies: Scientific Basis and Societal Impact**, (Cambridge University Press, New York, pp. 1-12

Haemaprasit, N. and J. Paw (1988) **Fisheries and Aquaculture: Resource and Economics**. In: The Coastal Environmental Profile of Ban Don Bay and Phangnga Bay, Thailand. J.N. Paw, S. Bumpapong, A. White and M. Sadorra (editors), ICLARM, Technical Publication Series 2, 1988.

Havanond, S. (1997) **Progress on Mangrove Research and Development of Royal Forest Department**. Proceedings of the 10th National Seminar on Mangroves, NRCT. 25-28 August, 1997, Songkhla, Thailand. Section 11-11, pp. 1-10.

IPCC, 2001, **Climate Change 2001**: Synthesis Report, A Contribution of Working Groups I, II and III to the Third Assessment Report of the Intergovernmental Panel on Climate Change, R.T. Watson and Core Writing Team (Eds.), Cambridge University Press, Cambridge, U.K. & N.Y., USA, p.162.

Jawed, A. and A. Rangoonwala (1997) **Identification and Mapping of Mangrove Forest Along the Coast of Pakistan.** Proceedings of the International Symposium on Vegetation Monitoring. 29 - 31 August 1995, Chiba, Japan. S. Shindo and R. Tateihi (editors), pp. 304 - 307.

Justice, C. O, Holben, B. N. and Gwynne, M. D. (1986) **Monitoring East African Vegetation Using AVHRR Data**, *International Journal of Remote Sensing.* 7(11): 1453-1474.

Kiladis, G. N., and H. F. Diaz, 1989: **Global climatic anomalies associated with extremes in the Southern Oscillation**. *J. Climate*, **2**, 1069-1090.

Landsea, Christopher W., 2000, El Niño/Southern Oscillation and the Seasonal Predictability of tropical Cyclones, in **El Niño and the Southern Oscillation, Multiscale Variability and Global and Regional Impacts**, (Eds.) Henry F. Diaz and Vera Markgraf, Cambridge University Press, Cambridge, pp. 149-181.

Lentini, C.A.D., Podestá, C.G. Campos, E.J.D. and Olson, D.B. (2001) **Sea Surface Temperature Anomalies on the Western South Atlantic from 1982 to 1994**. Continental Shelf Research. (21) 89-112 pp.

Li, Z. and Kafatos, M. **Interannual Variability of Vegetation in the United States and Its Relation to El Niño/Southern Oscillation**. Remote Sensing of Environment. (71) 239-247 pp.

Lilesand, T. and Kiefer, R.W. (1994) **Remote Sensing and Image Interpretation**. 3rd edition, John Wiley & Sons, New York. 750 pp.

Mather, P.M. (1987) **Computer Processing of Remote-sensed Images: An introduction**, John Wiley & Sons, Chichester. 352 pp

Myneni, R. B., Los, S. O., and Tucker, C. J., 1996. **Satellite-based identification of linked vegetation index and sea surface temperature anomaly areas from 1982-1990 for Africa, Australia and South America**, *J. Geophysical Letter*s, 23:729-732.

Nicholson, S. E., Davenport, M. L., and Malo, A. R. (1990**) A comparison of vegetation response to rainfall in the Sahel and East Africa using the Normalized Difference Vegetation Index from NOAA AVHRR**. *Climate Change* 17: 209-241.

PCI. (1997) **Using PCI Software**: Volume I. Ontario, Canada. 272 pp.

Plisnier, P.D. Serneels, S and Lambin, E.F. **Impact of ENSO on East African Ecosystems: A Multivariate Analysis Based on Climate and Remote Sensing Data**. Global Ecology and Biogeography. (9) 481-497 pp.

Rasmusson, E.M. and T. Carpenter, 1982, **Variations in Tropical Sea Surface Temperature and Suface Wind Fields Associated with the Southern Oscillation/El Niño,** Monthly Weather Review, 110, pp.354-384.

Rasmusson, E. (1991) **Observational aspects of ENSO cycle teleconnections**. In M.H. Glantz, R.W. Katz, and N. Nicholls (Eds) *Teleconnections Linking World Wide Climate Anomalies: Scientific Basis and Societal Impact.* Cambridge University Press, New York, pp. 309-343.

Ropelewski, C. F. and Halpert, M. S. (1989) **Precipitation patterns associated with the high-index phase of the Southern Oscillation**. *Journal of Climate*, **2**: 268-284.

Sawangphol, Narumitr and Gullaya Wattayakorn, 1999**, Land Use Classification of Ban Don Bay Coastal Area, Surat Thani, Thailand**, UNESCO-MAB Regional Seminar for East and South-east Asian Countries, ECOTONE VIII: Enhancing Coastal Ecosystem Restoration for 21st Century, Ranong, Thailand, 23-28 May 1999, pp. 279-288.

Shabanov,N.V., Zhou, L., Knyazikhin,Y, Myneni, R.B. and Tucker, C.J. (2002) **Analysis of Interannual Changes in Northern Vegetation Activities Observed in AVHRR Data from 1981-1994**. IEEE Transaction on Geoscience and Remote Sensing. (40) January 2002. 115-130 pp.

Signormi,S,R, Murtugudde, R,G,, McClain, C,R,, Christian,J,R,, Picaut, J. and Busalacchi, A.J. (1999) **Biological and Physical Signatures in the Tropical and Subtropical Atlantic**. Journal of Geographic Research. Journal of Geographic Research. 1-22.

Siripong, Absornsuda, Wish Siripong and T. Sugimoto, 1996, **Landuse Changes at Suratthani, Southern Thailand from 1973 to 1993**, Proceedings of the SARCS/START/APN Global Change Science and policy Forum, Bangkok, Thailand, 27-28 March 1996, pp. 101-109.

Taunton, Susan, 2003, **Comparing NDVI and ENSO signals in southeastern Arizona between 1989 and 2001**, http://fp.arizona.edu/khirschboeck/climate/enso_rpt.htm .

Troup, A. J., 1965, **The Southern Oscillation**, Quarterly Jour. Of Royal Meteorol. Soc., 91, pp.490-506.

Tucker, C. J. Dregne, H. W. and Newcomb, W. W. (1991) **Expansion and contraction of the Sahara desert from 1980 to 1990**. *Science*, 233: 299-301

Tucker, C. J. (1979) **Red and photographic infrared linear combinations for monitoring vegetation**, *Remote Sensing of the Environment*, 8: 127-150.

Tucker, C. J. and Nicholson, S. E. (1999) **Variations in the Size of the Sahara Desert from 1980-1997**. Ambio 28: 587-591.

Walker, G.T., 1924, **Correlations in Seasonal Variations of Weather, I. A Further Study of World Weather**, Mem. Indian Meteorol. Dep., 24, pp. 275-332.

Wolter, K., 1987, **The Southern Oscillation in Surface Circulation and Climate Over the Tropical Atlantic, Eastern Pacific, and Indian Oceans as Captured by Cluster Analysis**. *J. Climate Appl. Meteor.*, **26**, 540-558.

Wolter, K., and M.S. Timlin, 1993, **Monitoring ENSO in COADS with a Seasonally Adjusted Principal Component Index**. *Proc. of the 17th Climate Diagnostics Workshop*, Norman, OK, NOAA/N MC/CAC, NSSL, Oklahoma Clim. Survey, CIMMS and the School of Meteor., Univ. of Oklahoma, 52-57.

Wolter, K., and M.S. Timlin, 1998, **Measuring the Strength of ENSO - How does 1997/98 rank?** *Weather*, **53**, 315-324.

Xiao,X., Braswell,B,, Zhang,Q. and Boles,S. (2003) **Sensitivity of Vegetation Indices to Atmospheric Aerosols: Continental Scale Observation in Northern Asia**. Remote Sensing of Environment.(84) 385-392 pp.

Yoshiaki, H. (1997) **Ground Truth Database for Vegetation Remote Sensing**. Proceedings of the International Symposium on Vegetation Monitoring. 29-31 August 1995, Chiba, Japan. S. Shindo and R. Tateihi (editors), pp.182 -185.

Zavala, C.A., Douglas, A.V. and Diaz, H.F**. Interannual Variability of NDVI in Northwest Mexico Associated Climatic Mechanism and Ecological Implication**. Remote Sensing of Environment. (82) 417-430 pp.

Zeng, N., Neeling,D.J., Lau,K.M. and Tucker, C.J. (1999) **Enhancement of Interdecadal Climate Variability in the Sehal by Vegetation Interaction**. Science. (286) November 1999. 1537-1540 pp.

สถาบันวิทยบริการ
จุฬาลงกรณ์มหาวิทยาลัย